Investigations of gas phase ion-molecule reactions at elevated pressures using ion mobility-mass spectrometry
by Kris E Sahlstrom

A thesis submitted in partial fulfillment of the requirements for the degree of Doctor of Philosophy in Chemistry
Montana State University

Abstract:
The field of gas phase ion chemistry has undergone rapid expansion during the last three decades. This has resulted in an increased need for experiments designed to elucidate the mechanisms, kinetics and thermochemistry of ion molecule reactions in the gas phase. Due to instrumental limitations, the vast majority of experimental methods operate under buffer gas pressures of less than a few Torr. Analytical methods operating at high pressures and support for theoretical models of ion-molecule reactivity are two areas that would benefit from the results from experimental methods operating under very high buffer gas pressure conditions. An Ion Mobility-Mass Spectrometer (IM-MS) has been constructed in our laboratory and has previously been applied to the study of simple substitution and clustering reactions. Modifications of the original IM-MS have increased the range of electric field strength and buffer gas pressure and have allowed the investigation of chemical systems between 300 and 1100 Torr. Rate constants for the thermal electron detachment of azulene" and for the reaction of chloride ion with methyl bromide have been measured over this pressure range. These investigations, and the reaction of chloride ion with isopropylbromide at atmospheric pressure, are the subject of this thesis work. Significant differences were observed in the behavior of these reactions when compared to results from experimental methods operating at lower buffer gas pressures. It has been determined that rate constants for the detachment of thermal electrons from azulene are inversely dependent on buffer gas pressure due to interaction of the anion with buffer gas molecules. Rate constants for the reaction of chloride ion with methylbromide were observed to increase with increased buffer gas pressure and the lifetime of the reaction intermediate was found to be in the low picosecond range. Investigations of the reaction of chloride ion with isopropylbromide revealed a change in mechanism on going from low to high buffer gas pressures. Direct bimolecular nucleophilic substitution is operative at low pressures while indirect unimolecular decomposition of the reaction intermediate was observed at high buffer gas pressures. The kinetic parameters and thermodynamic properties of this reaction at one atmosphere pressure were determined.

INVESTIGATIONS OF GAS PHASE ION-MOLECULE REACTIONS AT ELEVATED PRESSURES USING ION MOBILITY - MASS SPECTROMETRY

by

Kris E. Sahlstrom

A thesis submitted in partial fulfillment
of the requirements for the degree

of

Doctor of Philosophy

in

Chemistry

MONTANA STATE UNIVERSITY-BOZEMAN
Bozeman, Montana

July 1997

APPROVAL

of a thesis submitted by

Kris E. Sahlstrom

This thesis has been read by each member of the thesis committee and has been found to be satisfactory regarding content, English usage, format, citations, bibliographic style, and consistency, and is ready for submission to the College of Graduate Studies.

Eric P. Grimsrud _____ 8/8/97
Date

Approved for the Department of Chemistry

David M. Dooley _____ 8/11/97
Date

Approved for the College of Graduate Studies

Robert Brown _____ 8/11/97
Date

STATEMENT OF PERMISSION TO USE

In presenting this thesis in partial fulfillment of the requirements for a doctoral degree at Montana State University-Bozeman, I agree that the Library shall make it available to borrowers under rules of the Library. I further agree that copying of this thesis is allowable only for scholarly purposes, consistent with "fair use" as prescribed in the U.S. Copyright Law. Requests for extensive copying or reproduction of this thesis should be referred to University Microfilms International, 300 North Zeeb Road, Ann Arbor, Michigan 48106, to whom I have granted "the exclusive right to reproduce and distribute my dissertation in and from microform along with the non-exclusive right to reproduce and distribute my abstract in any format in whole or in part."

Signature 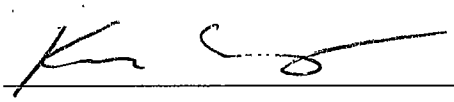

Date 8-11-97

ACKNOWLEDGMENT

I would like to thank the members of the research group for many hours of fruitful discussion and for their camaraderie and friendship. A particular note of appreciation goes to Dr. Berk Knighton for his invaluable technical assistance throughout this research project. The support and guidance of my research advisor, Dr. Eric Grimsrud, is gratefully acknowledged.

The successful completion of years of research, culminating in this doctoral dissertation, would not have been possible without the love and support of my family. The continued optimism and exuberance of my son, Josh, and daughter, Sabrina, provided the motivation to push ahead even in the dark nights of the Bozeman winter. I'm very thankful for the unflagging love and encouragement of my wife, Lynn, who had to contend with the sometimes onerous requirements an undertaking of this scope entailed. Finally, I'd like to thank my Mom for the spirit to pursue challenging goals in life and my Dad for the perseverance and discipline to see them through.

TABLE OF CONTENTS

TABLE OF CONTENTS - Continued

LIST OF TABLES

LIST OF FIGURES

LIST OF FIGURES - Continued

LIST OF FIGURES - Continued

LIST OF FIGURES - Continued

LIST OF FIGURES - Continued

LIST OF FIGURES - Continued

LIST OF FIGURES - Continued

ABSTRACT

The field of gas phase ion chemistry has undergone rapid expansion during the last three decades. This has resulted in an increased need for experiments designed to elucidate the mechanisms, kinetics and thermochemistry of ion molecule reactions in the gas phase. Due to instrumental limitations, the vast majority of experimental methods operate under buffer gas pressures of less than a few Torr. Analytical methods operating at high pressures and support for theoretical models of ion-molecule reactivity are two areas that would benefit from the results from experimental methods operating under very high buffer gas pressure conditions. An Ion Mobility-Mass Spectrometer (IM-MS) has been constructed in our laboratory and has previously been applied to the study of simple substitution and clustering reactions. Modifications of the original IM-MS have increased the range of electric field strength and buffer gas pressure and have allowed the investigation of chemical systems between 300 and 1100 Torr. Rate constants for the thermal electron detachment of azulene$^-$ and for the reaction of chloride ion with methyl bromide have been measured over this pressure range. These investigations, and the reaction of chloride ion with isopropylbromide at atmospheric pressure, are the subject of this thesis work. Significant differences were observed in the behavior of these reactions when compared to results from experimental methods operating at lower buffer gas pressures. It has been determined that rate constants for the detachment of thermal electrons from azulene$^-$ are inversely dependent on buffer gas pressure due to interaction of the anion with buffer gas molecules. Rate constants for the reaction of chloride ion with methylbromide were observed to increase with increased buffer gas pressure and the lifetime of the reaction intermediate was found to be in the low picosecond range. Investigations of the reaction of chloride ion with isopropylbromide revealed a change in mechanism on going from low to high buffer gas pressures. Direct bimolecular nucleophilic substitution is operative at low pressures while indirect unimolecular decomposition of the reaction intermediate was observed at high buffer gas pressures. The kinetic parameters and thermodynamic properties of this reaction at one atmosphere pressure were determined.

INTRODUCTION

The field of Gas Phase Ion Chemistry (GPIC) has undergone a period of very rapid growth in the past three decades (1-5). This has been the result of the ongoing and increasingly swift development of the electronic and vacuum technologies required for the instrumentation used in this field. This evolution has resulted in an unprecedented increase in the number of experiments and analytical applications based on processes occurring in the gas phase. Knowledge of the chemical and physical processes occurring in these gas phase environments is often essential in these applications. Thus, theoretical and experimental investigations to determine fundamental kinetic and thermochemical parameters for processes occurring in the gas phase are vital and have attended the rapid development of GPIC.

While literally thousands of papers have been published concerning ion-molecule (IM) reactions at low (< 5 Torr) buffer gas pressures, less than 20 papers have been published in which IM reactions have been investigated by instrumental methods that use buffer gases in the very high pressure (VHP) range (6 - 20). (For convenience, buffer gas pressure ranges will be divided into the low pressure (LP) range, between 10^{-7} and 10^{-5} Torr, the high pressure (HP) range, between 0.1 and 5 Torr and the very high pressure (VHP) range, between 100 Torr and 10 atmospheres buffer gas pressure). This is not due to a lack of interest in processes occurring at higher pressures, but rather due to instrumental difficulties encountered at these pressures. This lack of knowledge concerning IM reactions at VHP is an important motivation for developing new, reliable methods for investigating IM reactions under conditions of VHP.

In response to this need, a new instrumental method has been developed in our laboratory which incorporates the advantages of Ion Mobility Spectrometry (IMS) and Mass Spectrometry (MS) and which shall be referred to hereafter as Ion Mobility - Mass Spectrometry (IM-MS). This instrument has previously been successfully applied to the study of simple bimolecular reactions (10) and cluster equilibria (11). Modifications to the original IM-MS have since expanded its utility to include the investigation of IM reactions over the pressure range of 300 to 1100 Torr. Rate constants for the thermal electron detachment of azulene$^-$ (Az^-) and for the reaction of chloride ion with methyl bromide (Cl^-/CH_3Br) have both been measured over this pressure range. These investigations, and the reaction of chloride ion with isopropylbromide (Cl^-/*i*-PrBr), are the subject of this thesis work.

Motivations for Investigating Ion Molecule Reactions at Elevated Pressures

Important motivations for the study of GPIC at VHP are the establishment of a sound experimental foundation for theories of IM reactivity at very high pressures and for models of solvation and intrinsic structure-stability and structure-reactivity relationships. Also, some of the most sensitive analytical methods used in the environmental, forensic and biological sciences rely on processes occurring in the gas phase under very high buffer gas pressures (21 - 23). Clearly, it is vital that the chemical and physical processes occurring in VHP buffer gases be understood.

Experimental Support for Theoretical Models of Ion-Molecule Reactivity

The development of instrumental methods and the expansion of computing capabilities has helped catalyze the growth of theoretical models attempting to more accurately describe IM reactivity. One of the most significant theoretical advances in GPIC and one that underlies all gas-phase nucleophilic bimolecular substitution (S_N2) reactions is the "double well" description of an IM reaction coordinate proposed by Brauman et al. (24) and shown in Figure 1. This reaction coordinate was invoked to explain the inefficiency of exothermic S_N2 reactions having low or negative activation energies. A typical S_N2 reaction that exhibits this behavior is the Cl^-/CH_3Br reaction system given in detail below and also shown in Figure 1.

$$Cl^- + CH_3Br \underset{k_b}{\overset{k_c}{\rightleftharpoons}} Cl^-(CH_3Br)^* \xrightarrow{k_p} (Cl \cdot CH_3Br)^{\ddagger} \longrightarrow Br^-(CH_3Cl) \longrightarrow Br^- + CH_3Cl \qquad (1)$$

k_b', $k_q[M]$, k_p'

$Cl^-(CH_3Br)$

Even though the activation barrier for this reaction is ~ -2.0 kcal mol^{-1} below the energy of the reactants, the reaction proceeds to products with only about 1% efficiency, i.e. only about 1 out of every 100 collisions results in the formation of products. The reason for this inefficiency, and the motivation for studying reactions such as these at higher buffer gas pressures, can be understood by following the progress of this reaction along the reaction coordinate in Figure 1.

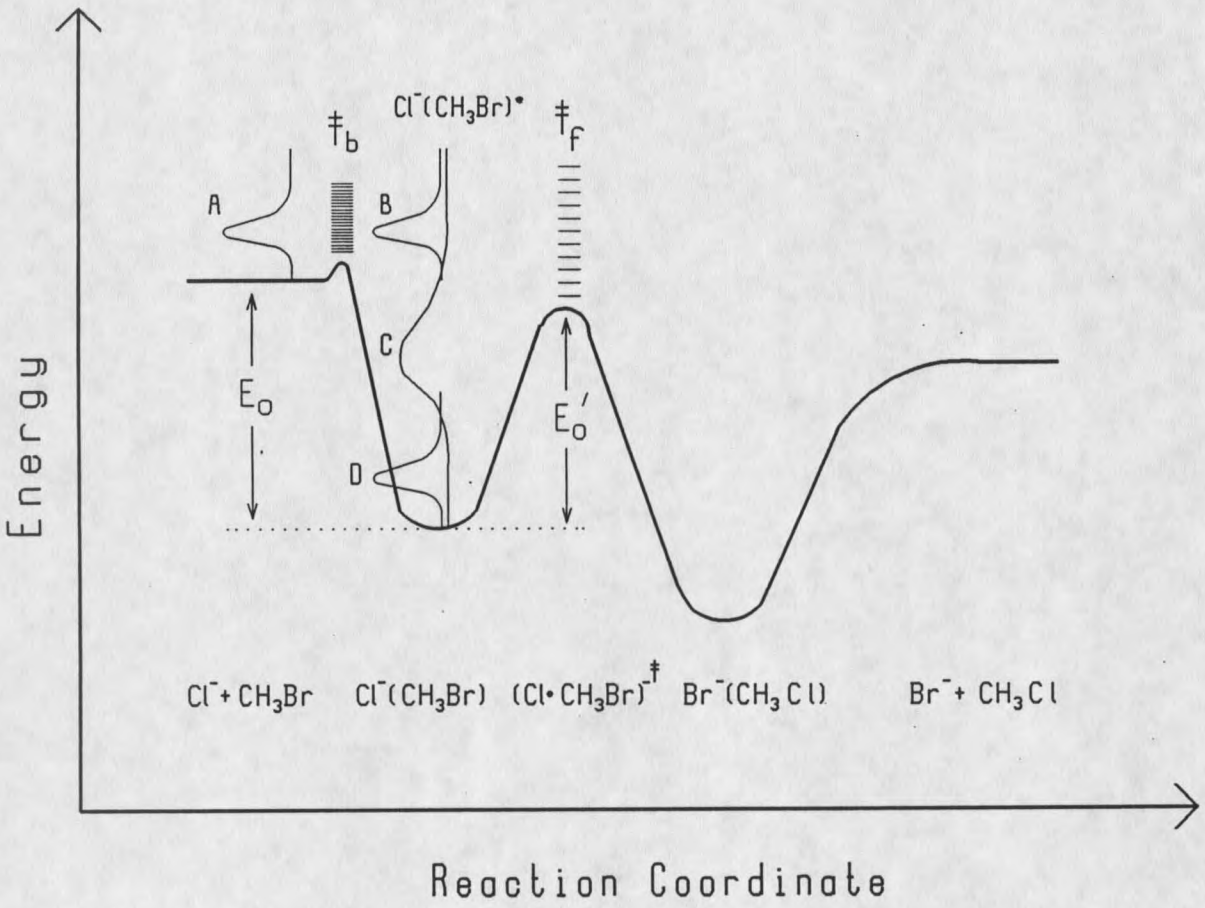

Figure 1. Reaction coordinate diagram for a typical gas phase S_N2 nucleophilic displacement reaction. Curve A represents the energy distribution function for the reactants in thermal equilibrium with the buffer gas. Curve B represents the distribution function for entrance-channel complexes at low pressure, curve C for an incompletely thermalized ensemble of complexes and curve D for the ion complexes at high pressure (completely thermalized). Other major points are discussed in the text.

The reactants, with a total energy distribution represented by curve A in Figure 1, come together with a collisional rate, k_c, described by conventional ADO theory (1), and form entrance channel ion-complexes, $Cl^-(CH_3Br)$. This interaction involves an energy barrier due to the centrifugal forces in the $Cl^-(CH_3Br)$ rotating ion complex, represented in Figure 1 by the first transition state, $\neq_b$. The inefficiency of the reaction is a result of competition between passage over the transition state ($\neq_f$) to products and dissociation back over the centrifugal barrier to form reactants. The observed rate constant for reaction sequence 1 depends on the magnitude of the rate constants for these two reaction pathways as shown in equation 2.

$$k_{observed} = k_c\left(\frac{k_p}{k_b + k_p}\right) \qquad (2)$$

where k_p and k_b also represent $k_{p'}$ or $k_{b'}$ in reaction sequence 1. The expression in parenthesis, $k_p/(k_b + k_p)$, describes the efficiency of reaction; i.e., any reaction where k_p is large, (k_b can be ignored) is limited by the collisional rate constant, k_c. Conversely, any reaction where k_p is small is limited by the isomerization of entrance channel complexes over the transition state to form exit channel ion-complexes. The magnitude of the unimolecular rate constants in reaction sequence 1 is a function of the energy of the entrance channel ion-complexes. The ion complexes are initially formed with an excess internal energy equal to the exothermicity of the association reaction, represented by the species $Cl^-(CH_3Br)^*$ in Figure 1 (curve B), and are said to be chemically activated. These chemically activated complexes can dissociate backwards to reactants, k_b, isomerize over the transition state to form exit channel ion-products, k_p, or

collisions with the buffer gas can remove the excess internal energy to form the ion-complex represented by the species $Cl^-(CH_3Br)$. These species, referred to as thermalized ion-complexes (having thermal energy), can also form reactants or products with rates characterized by the different rate constants, k_b' and k_f'.

Whether an S_N2 reaction proceeds through chemically activated or thermal-energy ion-complexes depends on the average lifetime of the ion-complex and on the pressure of the surrounding buffer gas. If the average lifetime of the ion-complex is much shorter than the average time between collisions of buffer gas molecules (low buffer gas pressure), then the ion-complexes will retain much of their chemical activation energy, characterized by rate constants k_i. A chemical system operating under these conditions is said to be in its low pressure limit (LPL) of kinetic behavior. If the average ion-complex lifetime approaches that of the time between collisions (intermediate buffer gas pressure), then a fraction of the ion-complexes will lose their excess energy by collisions with the buffer gas molecules. The total energy distribution of the ion-complexes under these conditions might be expected to resemble curve C in Figure 1. Finally, if the average ion-complex lifetime is very long relative to the time between collisions with buffer gas molecules (very high buffer gas pressure), all of their chemical activation energy will be quenched by the buffer gas. The total energy distribution of these thermal-energy ion-complexes will then be determined by the temperature of the buffer gas, represented by the Boltzman distribution curve D in Figure 1. Under these conditions, reaction sequence 1 will proceed through the thermal-energy ion-complexes characterized by rate constants k_b' and k_p'. A reaction is said to be operating in its high pressure limit (HPL) of

kinetic behavior if the pressure of the buffer gas is high enough (or the lifetime of the ion-complex is long enough) to effectively thermalize all the ion complexes.

There are two fundamental theories for determining rate constants (k_i) for the chemically activated and thermal-energy entrance channel ion-complexes (25 - 27). The theory treating the unimolecular dissociation of the chemically activated species is referred to as RRKM (Rice, Ramsperger, Kassel and Marcus) and that for the thermal-energy species is the Transition State Theory (TST). The general expression for the unimolecular rate constant of a system in its LPL of kinetic behavior is given by equation 3

$$\text{RRKM:} \qquad k(E) = G(E - E_0) / hN(E) \tag{3}$$

where $G(E - E_0)$ is the sum of the vibrational and internal rotational quantum states for the transition state (forward or backward) in the energy range $E - E_0$ and $N(E)$ is the density of states for the entrance channel ion-complex. At a specific energy level (Figure 1), the ratio of the forward and backward rate constants is given by

$$\text{RRKM:} \qquad \frac{k_p}{k_b} = \frac{G'(E - E_0' - \Delta E_{rot})}{G(E - E_0)} \tag{4}$$

where ΔE_{rot} is a correction for the internal energy of the forward transition state to allow for conservation of angular momentum. The rate constants given here are micro-rate constants characteristic of a specific energy level; equation 4 must be integrated over an appropriate energy distribution function (i.e. ref. 25, p 240) to arrive at the overall ratio of rate constants for chemically activated reaction 1. The inefficiency of reaction 1 ($k_p/k_b < 1$) is due to the

greater number of states in the entropically favored (loose) reverse direction (dissociation) as compared to isomerization over the entropically less-favored (tight) forward transition state (Figure 1).

When an IM reaction is brought to its HPL of kinetic behavior, the unimolecular rate constant for dissociation of the ion-complex can be determined by TST, shown in Equation 5.

$$\text{TST:} \qquad k = f \frac{kT}{h} \frac{Q^{\ddagger}}{Q_A Q_B} e^{-E_0/RT} \tag{5}$$

Here, $Q^{\ddagger}$, Q_A, Q_B are the partition functions (electronic, vibrational, translational and rotational) of the activated complex and of reactants A and B, respectively, T is the temperature of the buffer gas and f is the transmission coefficient. The transmission coefficient is introduced to allow for the possibility of exit-channel complexes isomerizing back over the transition state and re-forming entrance channel ion-complexes. It is essentially that fraction of species crossing the transition state that go on to form products and is assumed to be unity under conditions of high buffer gas pressure (26).

While statistical methods (RRKM) of interpreting the kinetics of some reactions have been very successful (28, 29), recent theoretical and experimental evidence have indicated non-statistical (non-RRKM) behavior for some simple IM reactions. Theoretical calculations have revealed such non-statistical behavior as vibrational mode-specific rate enhancements (30 - 31), de-coupling of intra-molecular ion-complex vibrational modes (33), translational versus internal reactant energy rate differences (34) and vibrational excitation of reaction products (35).

These theoretical results have also found support in recent experiments. Graul and Bowers (36 - 37), using Mass Spectrometer based methods (~ 0.1 Torr), measured the kinetic energy distribution of the $Cl^-(CH_3Br)^*$ ion-complex dissociation products and found vibrationally excited products. Viggiano, et al. (38), using a selected ion flow tube (~ 0.5 Torr), found that the rate constant for reaction sequence 1 did not depend on reactant internal energy, implying a de-coupling of the vibrational modes in the ion-complex. These theoretical and experimental results imply that statistical theories might not adequately describe some chemical systems. These uncertainties could be eliminated, and the kinetics of reaction could be reliably interpreted, if such systems could be brought to their HPL of kinetic behavior. Also, the interpretation of IM reaction kinetic data is simplified if the reaction can be brought to its HPL of kinetic behavior. In the HPL, theoretical analysis of the kinetic data requires only knowledge of the reactants and the forward, rate-determining transition state, no knowledge of entrance channel complexes or of the reverse transition state is required.

Well-established instrumental methods for investigating IM reactions, such as Ion Cyclotron Resonance and Mass Spectrometry, operate at low buffer gas pressures. Under these conditions, the ion-complexes are not expected to undergo collisions with the buffer gas and so are in their LPL of kinetic behavior. Other instrumental methods operate at high buffer gas pressures (Flowing Afterglow and Selected Ion Flow Tube) where it is difficult to predict whether or not an IM reaction is in the LPL or HPL of kinetic behavior. The IM-MS was developed in response to the need for instruments operating at very high buffer gas pressures that could force a reaction to its HPL of kinetic behavior. Also, by comparison with reaction

kinetics obtained using lower pressure methods, techniques at very high pressures could indicate whether an IM reaction was at or approaching its HPL of kinetic behavior.

Determinations of Intrinsic Chemical Behavior: Support for Models of Solvation

Theorists and physical organic chemists are interested in experimental methods that can reproduce, in the gas phase, reactions of interest in solution, so that the effects of solvation and ion-pairing on the intrinsic properties of the species involved can be determined. Two reviews of the use of GPIC as a tool for elucidating information about reactions in solution can be found written by Speranza (39) and by Bartmess (40). For this application of GPIC experiments to be valid, they must study isolated ions that have the same distribution of internal energy as in solution phase, i.e. a thermal distribution, which can be guaranteed only with complete thermalization of reacting species. While many experimental methods operating at buffer gas pressures less than about 5 Torr, such as the selected-ion flow tube (SIFT), ion cyclotron resonance (ICR) and the pulsed electron high pressure mass spectrometer (PHPMS) provide valuable information about the structure and stability of ionic intermediates, they may provide only phenomenological rate and mechanistic information rather than information characteristic of thermal (as in solution phase) species.

The effect of solvation on the reaction coordinate for a typical S_N2 reaction can be seen in the three curves in Figure 2, reproduced from Speranza (39). Curve A in Figure 2 is similar to that in Figure 1, discussed earlier, while curves B and C show the effects of increased solvation. The dramatic change in the rates of some IM reactions occurring in solution phase

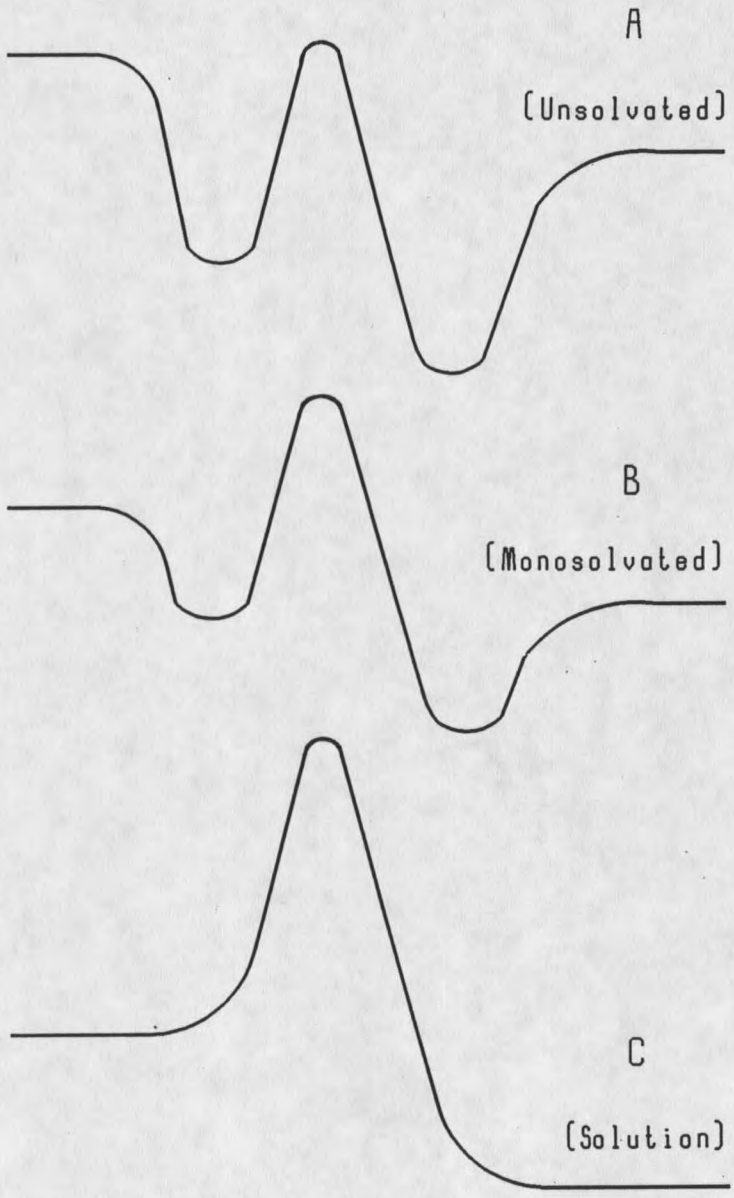

Figure 2. Reaction coordinate diagrams for the same reaction carried out in the gas phase with an unsolvated (curve A) or monosolvated (curve B) ionic reactant, or carried out in solution (curve C).

compared to the same reaction in the gas phase can be traced to the large change in the central barriers shown in Figure 2. It should be noted that large differences in reaction rates in gas phase compared to solution phase have been found only in the case of ionic (IM) reactions. For example, the rate constant for the Diels-Alder dimerization of cyclopentadiene is essentially the same in hexane or ethanol and is only three times larger than in the gas phase (41). However, it has been found that the simple S_N2 reaction, reaction 1, proceeds 15 orders of magnitude faster in the gas phase than in methanol (42).

Experiments carried out in the gas phase have also supported theories of reaction mechanisms determined from solution phase experiments. For example, it was long believed that the higher reactivity of the iodide ion relative to other halide ions in nucleophilic S_N2 reactions in solution was a consequence of the increased ability of the more polarizable iodide ion to more readily supply electron density near the substrate (24). However, studies in aproptic solvents and more recently in the gas phase have shown that the higher reactivity of the iodide ion is due to its lower degree of solvation (lower central barrier), rather than to effects caused by its higher polarizability.

The effects of solvation on the kinetics of IM reactions have been investigated by Bohme et al. (43) in their study of the reaction of F^- with CH_3Br and CH_3Cl and of Cl^- with CH_3Br. They found that the rate constant for the bare (unsolvated) anion (near collisional for F^- and $\approx$ 1% collisional for Cl^-) was decreased by three orders of magnitude with the addition of just one solvent molecule to the anion and was too slow to measure with the addition of two or more solvent molecules. In aqueous solution, the rate constant for these reactions is slower by

another 15 to 16 orders of magnitude. It was also noted that the rate constant for the reaction of Cl^- with CH_3Br in the gas phase measured using their flowing afterglow apparatus (~ 5 Torr buffer gas pressure) was approximately twice the rate constant of the same reaction also measured in the gas phase, but using instead a pulsed ICR operating at much lower buffer gas pressures (~ 1×10^{-5} Torr). Recent measurements by Giles and Grimsrud (10) using IM-MS (640 Torr pressure) have resulted in a rate constant for this reaction which is higher than that obtained using the flowing afterglow method. Thus, it is evident that the rate constants for IM reactions are not only different in solution and in gas phase, but are also dependent on the buffer gas pressure.

Furthering our understanding of the theory of IM reactions and providing support for models of solvation are important uses of VHP instrumental methods. Perhaps a more practical application of this technology, and an increasingly vital one, is the need to develop a better understanding of IM processes underlying some of the most sensitive analytical methods in use today.

Support for Sensitive Analytical Methods

Analytical methods operating in the VHP range can be extremely sensitive and find widespread use in the detection of trace quantities of explosives, narcotics, environmental pollutants, and for characterizing biological samples. They include Ion Mobility Spectrometry (IMS), Atmospheric Pressure Ionization Mass Spectrometry (APIMS) and Electron Capture Detection (ECD) for use with Gas Chromatography (GC). As discussed in the preceding sections, the rate constants obtained from investigations of IM reactions under low pressure

conditions are not necessarily applicable when applied to ionic reactions operating at high pressures. For example, work carried out by Knighton et al. (45) has shown that the APIMS spectra of C_7F_{14} were significantly altered by the addition of water or methanol at partial pressures that may also be found in the buffer gases used in the detection methods mentioned above. The APIMS spectra were altered by the formation of molecular anions clustered with the added water or methanol. It is expected that the formation of clustered species at higher pressures, particularly at low temperatures, would significantly effect the response in these detection schemes to the analyte due to the change in stability of the clustered anion. In addition, work by Mock et al. (46) in which the rate constant of thermal electron detachment of the azulene molecular anion, Az^-, was measured using the Photo-Detachment Modulated-ECD (PDM-ECD) at two atmospheres pressure yielded a rate constant three times lower than that measured by Kebarle et al. (47) using a PHPMS at 5 Torr pressure. Further measurements of the rate constants of Az^- thermal electron detachment have been carried out and reported herein using IM-MS. The results of this work revealed that the rate constants of thermal electron detachment at ~ one atmosphere pressure are higher than that reported by Mock but lower than that measured by Kebarle. This implies that increased buffer gas pressures might result in a larger equilibrium concentration of azulene adducts that are more stable than the unclustered anion. The effects and implications of azulene electron detachment using IM-MS will be discussed in more detail later.

The formation of adducts and dimers at the very high buffer gas pressures in IMS has been observed to significantly alter ion mobility spectra. Eiceman et al. (48) reported peak

distortion and baseline perturbations in the ion mobility spectra of butyl acetate isomers. Fragmentation of the iso-, tert- and sec- butyl acetate isomers and declustering of the n-butyl acetate isomer from the dimer to the monomer ions was observed at high (160 °C) temperatures. Preston et al. (49) observed the change in reduced ion mobility as a function of neutral reagent concentration in the ion mobility spectra of DPM/acetone (DPM = 3-(3-methoxypropoxy)propanol (dipropylene glycol monomethyl ether), acetone/water and pyridine/water. A decrease in the reduced mobility (longer observed drift times) as the neutral reagent (acetone or water) concentration was increased was attributed to the establishment of a clustering equilibrium in the drift tube. It was also possible to determine the thermodynamic constants for these clustering reactions by measuring the change in reduced mobility as a function of neutral reagent. Thermodynamic constants for the dimerization of pyridine were determined in this manner. Investigations of this type reveal the uncertainties inherent in the interpretations of ion mobility spectra. Clearly, these complicating effects of VHP buffer gases need to be investigated and understood.

Instrumental Methods for Investigating IM Reactions in the Gas Phase

The temperature and pressure ranges used in IM-MS and in other instrumental methods in GPIC are illustrated in Figure 3 (39). It is evident from Figure 3 that most techniques for investigating IM use low to high buffer gas pressures where chemically activated, rather than thermalized, ion-complexes are likely. A brief review of the instrumental methods illustrated in Figure 3 will reveal some of the advantages and disadvantages of methods operating under low and high buffer gas pressures.

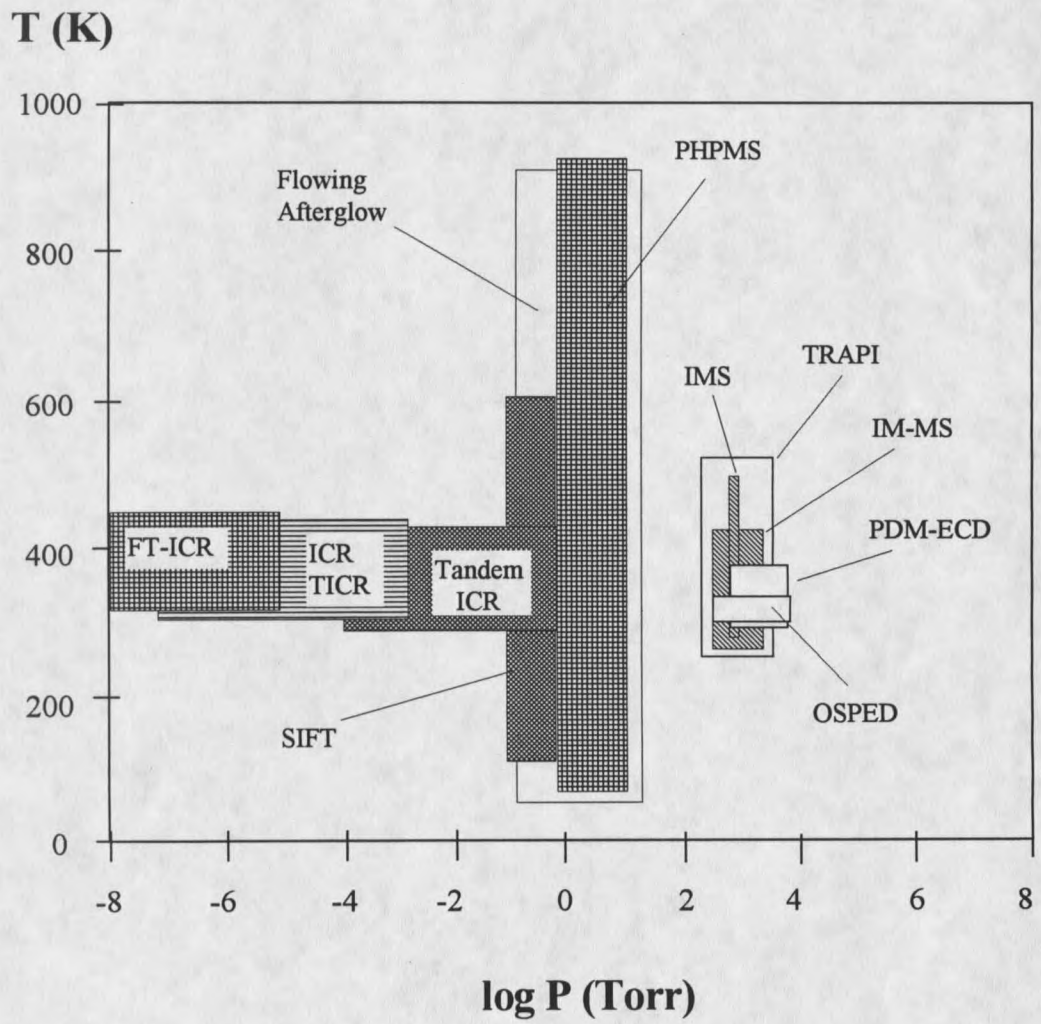

Figure 3. Illustration of the various methods available for investigation of gas phase ion-molecule reactions. Limiting operating conditions of temperature and pressure are indicated.

Instrumental Methods in the LP and HP Range

It is evident in Figure 3 that the major instrumental methods in use in the low pressure regime are based on various configurations of Ion Cyclotron Resonance (ICR). A review of ICR, Trapped ICR (TICR) and Tandem ICR has been published by Bowers and Kemper (50) and includes an historical perspective, instrumental overviews and discussions of ICR as a method for studying IM reactions. A similar review by Freiser (51) covers these aspects of ICR as applied in Fourier Transform ICR (FT-ICR). ICR-based techniques have been responsible for measurements of a wide variety of IM reaction rate constants (52, 24). However, the low pressures used limits its use in the study of equilibrium processes. One of the main advantages of ICR methods is the ability to investigate (reaction) kinetic energy effects. Examples include the determination of IM reaction product distributions as a function of reactant ion kinetic energy and measurements of released kinetic energy in dissociation reactions (53 - 57). However, with the exception of some experiments using TICR and FT-ICR, this advantage comes at the price of a non-thermal distribution of reactant ion translational energy. Instrumental methods that operate in the high pressure (HP) range, such as Flowing Afterglow (FA), Selected Ion Flow Tube (SIFT) and the Pulsed High Pressure Mass Spectrometer (PHPMS), can be used to investigate IM reactions under conditions at which the reactant ion kinetic energy is thermal.

The Flowing Afterglow technique (58) works by first ionizing a high velocity (10^4 cm s^{-1}) carrier gas (usually He) either by a microwave discharge, electron impact or DC discharge source, creating a gaseous plasma. A small fraction of suprathermal ions and electrons flow out of the source (an "afterglow") and are collisionally thermalized by the carrier gas. Most of

these ions are pumped out of the flow tube by a high capacity mechanical pump while a small fraction leaks through a pinhole orifice into a differentially pumped mass spectrometer. Ion molecule and ion-ion recombination reactions can be studied by selectively introducing known concentrations of ion source gas either upstream or downstream of the ion source. The primary ions thus created react with neutral reagents introduced farther downstream in the flow tube. The measured loss of primary ion as a function of reactant gas concentration leads to determinations of IM reaction rate constants. Flowing afterglow instruments are usually constructed of stainless steel and are able to operate over a wide temperature range (80 - 900 K) and over a pressure range from about 0.1 to a few Torr (Figure 3). Some of the disadvantages of the FA are the creation of many ionic species in addition to the primary ion and the existence of energetic ionic species in the afterglow. In spite of these complications, FA has resulted in numerous rate constant determinations and a wealth of chemical information and is still useful in many analytical applications.

The Selected Ion Flow Tube (58) is similar to the FA with the exception that of all the ions generated in the source region, only the primary ions of interest are transmitted by a quadrupole mass filter before being injected into the flow tube. This results in a much lower ion density in the tube, but eliminates other ions, metastable species and photons that can be problematic in the FA. The ability to create negative and positive ions in a source separate from the flow tube over a wide range of temperature (80 - 600 K) and over a pressure range of 0.1 to a few Torr has allowed the study of a wider range of reactions than in the FA. Again, IM investigations using SIFT are too numerous to list here, but references can be found in two

review articles (59, 60). The SIFT instrument has been successfully applied to the measurements of IM reaction rates as a function of reactant kinetic energy (61, 62). The kinetic energy of the primary ions is made suprathermal by passage of the selected ions through a drift tube inserted into the flow tube. An electric field is generated in the drift tube, imparting excess energy to the ions prior to reaction with the neutral reagent molecules.

The final HP instrumental method to be briefly discussed is the Pulsed High Pressure Mass Spectrometer (63). Inspection of Figure 3 shows that this method operates within the same general pressure and temperature range as the FA and SIFT methods. However, the PHPMS is considered to be a method primarily for investigating IM equilibria, although observations of the approach to equilibrium can also provide much information regarding IM kinetics. The PHPMS consists of a pulsed electron beam gun, an ion source and a differentially pumped mass spectrometer. The ion source typically contains about 0.5 to 5 Torr of buffer gas (usually CH_4) and a few millitorr of one or several reagent gases. A short burst (~10 μsec) of electrons ionizes the buffer gas to form secondary electrons which are effectively thermalized by collisions with the buffer gas. Molecules of high electron affinity capture these thermal secondary electrons and are subsequently thermalized by collisions with the buffer gas molecules. Electron transfer between these two species occur as the molecules diffuse through the buffer gas to an exit aperture for sampling by an attached mass spectrometer. Measurements of the logarithmic decay of these ions over time allow for the determination of the forward rate constant and the equilibrium constant. Measurements such as these, reported

in numerous publications (64 - 68), have allowed for determinations of the kinetics and the thermochemical properties of a very wide range of reactions.

Instrumental Methods in the VHP Range

As mentioned previously, less than 20 papers have been published pertaining to the study of gas-phase IM reactions in the VHP range. The instrumental methods used in these investigations are the Time-Resolved Atmospheric Pressure Ionization Mass Spectrometer (TRAPI), Optical Spectroscopy in a Pulsed Electrical Discharge (OSPED), the Ion Mobility Spectrometer (IMS), the Photodetachment-Modulated Electron Capture Detector (PDM-ECD) and the Ion Mobility - Mass Spectrometer (IM-MS).

The TRAPI method, developed by Matsuoka et al. (15 - 19), is similar in operation to a PHPMS except that ions are produced by an X-ray pulse in an atmospheric pressure source, rather than by a pulse of high energy electrons in an ion source with about 5 Torr pressure. The products of selected IM reactions occurring within the TRAPI source volume flow by convection (rather than by diffusion as in PHPMS) and are leaked through an aperture to an associated mass spectrometer; reaction rates are determined by measuring the intensity of selected ions over time. While the rate constants of about a dozen IM reactions have been measured using this technique, there is some question as to their accuracy due to uncertainties in the ion concentration uniformity in the source, collisional rate effects near the aperture and possible cooling in the adiabatic expansion out of the aperture (69).

Uncertainties associated with the transport of ions to a detector are eliminated with the use of the OSPED technique. Collins et al. (6-8) have measured IM reaction rates (charge

transfer reactions) using OSPED over a pressure range from 0.4 to 2.0 atmospheres. The ion source in this technique consists of a reaction cell with two quartz windows at either end with a 25 μm thick titanium window on one side. A high current electron beam is passed through this titanium window, creating ions in the cell for subsequent IM reactions. The rate constants of IM reactions are determined by recording the absorption spectrum of a selected excited species as a function of time after the electron pulse. This method has to date been limited to charge transfer reactions involving relatively small atomic and diatomic species.

Strode et al. (13) have measured the rate constants of about 20 IM reactions at two atmospheres pressure utilizing the PDM-ECD. This method relies on the differential response of a modified ECD (window installed on one side to allow light pulses to enter) between pulses of light selectable between 250 and 1200 nm (to allow for the photodissociation of the product anion of interest). This method was also utilized for the analysis of fast unimolecular reactions. The rate constants for the thermal electron detachment of Az^- were measured using this method and the results will be discussed in greater detail later.

Two other techniques for investigating IM reactions at VHP are the radiolytic and nuclear decay methods. However, these are based on chemical, rather than instrumental, methods and so are not reviewed here. Information about kinetic investigations utilizing these methods can be found in publications by Cacace (70) and Speranza (71).

The final instrumental methods listed in Figure 3 are the closely related Ion Mobility Spectrometry (IMS) and Ion Mobility - Mass Spectrometry (IM-MS). Ion Mobility-Mass Spectrometry, its design and use in IM investigations, is the subject of this thesis work and will

be discussed in detail later. Ion Mobility Spectrometry has been utilized over the last three decades mainly as an ultra-sensitive analytical device for detecting trace quantities of explosives, illicit drugs, and atmospheric pollutants, while also finding application in the biological and forensic sciences (72 - 85). Although IMS is used primarily as a combination separation and detection tool, it has also been used as a stand alone detector following other separation methods such as GC, supercritical fluid GC and liquid chromatography (86 - 92). Briefly, IMS works by first ionizing an analyte in a ^{63}Ni radioactive source followed by separation based on size (mass *and* structure) in an atmospheric pressure drift tube under the influence of an applied electric field with subsequent time-resolved detection at a Faraday plate. Various modifications of this basic technique have been developed, such as using photoemissive and laser ionization sources and compact tube designs and detection schemes to exploit its relatively simple mechanical design (93 - 102). Excellent review articles have been published describing the use of IMS as an analytical technique (22, 103 - 107). While a number of authors have investigated IM reactions using IMS, with the exception of two mentioned previously, these studies have been limited to the chemistry occurring in the ion source (mostly charge transfer reactions) prior to injection into the drift tube region (108 - 110). It is rather surprising that over the relatively long history of IMS only two publications have dealt with IM reactions occurring in the drift tube region.

The Ion Mobility - Mass Spectrometer (IM-MS) is based on the same operating principles as IMS. These operating principles and the application of IM-MS to the study of IM reactions is the subject of this thesis work. It is expected that much of the knowledge gained in

these experiments should be directly beneficial to those working in the field of IMS. As mentioned (briefly) previously, the IM-MS has already been used to successfully measure rate constants for a series of simple S_N2 reactions (10) and to measure the equilibria and reactivity of the cluster ions $Cl^-(CHCl_3)_{0-2}$ with CH_3Br and CH_3I (11) at 640 Torr. Following a detailed description of the design and operation of the IM-MS, a discussion of the study of three additional chemical systems will be presented. These systems are the thermal electron detachment of azulene (Az^-), the pressure dependence of the S_N2 reaction $Cl^- + CH_3Br \rightarrow Br^- + CH_3Cl$ and the complex S_N2 reaction of Cl^- with *i*-PrBr at atmospheric pressure.

INSTRUMENTAL DESIGN AND PRINCIPLES OF OPERATION

A detailed description of the original IM-MS instrument and basic operating principles has been published previously by Giles and Grimsrud (10). This design has since been extensively modified to accommodate the need for improved control of and extended range of temperature, pressure, gas flow and electric field strength. This warrants a somewhat detailed review of the layout described by Giles and Grimsrud. These modifications have increased the utility of IM-MS as a means of investigating gas phase ion molecule reactions at very high buffer gas pressures.

Instrumental Design

The IM-MS consists of three major components as shown in Figure 4: An Ion Mobility Spectrometer (IMS), a Mass Spectrometer (MS) and a Gas Handling Plant (GHP). An expanded view of the source and detector ends of the IMS is given in Figure 5.

Ion Mobility Spectrometer

The Ion Mobility Spectrometer (IMS) is composed of a source assembly and a Faraday plate detector located inside of a 40 cm long by 9 cm diameter Pyrex tube with ends terminating in glass-to-metal seals and stainless steel conflat flanges. Nineteen electrodes (stainless steel hose clamps) are attached to the outside of the tube and are electrically connected in series through 1MW resistors. The electrode nearest the Faraday plate is connected to a ± 5000V power supply (Model 205B-05R Bertan Assoc, Inc., Hicksville, NY).

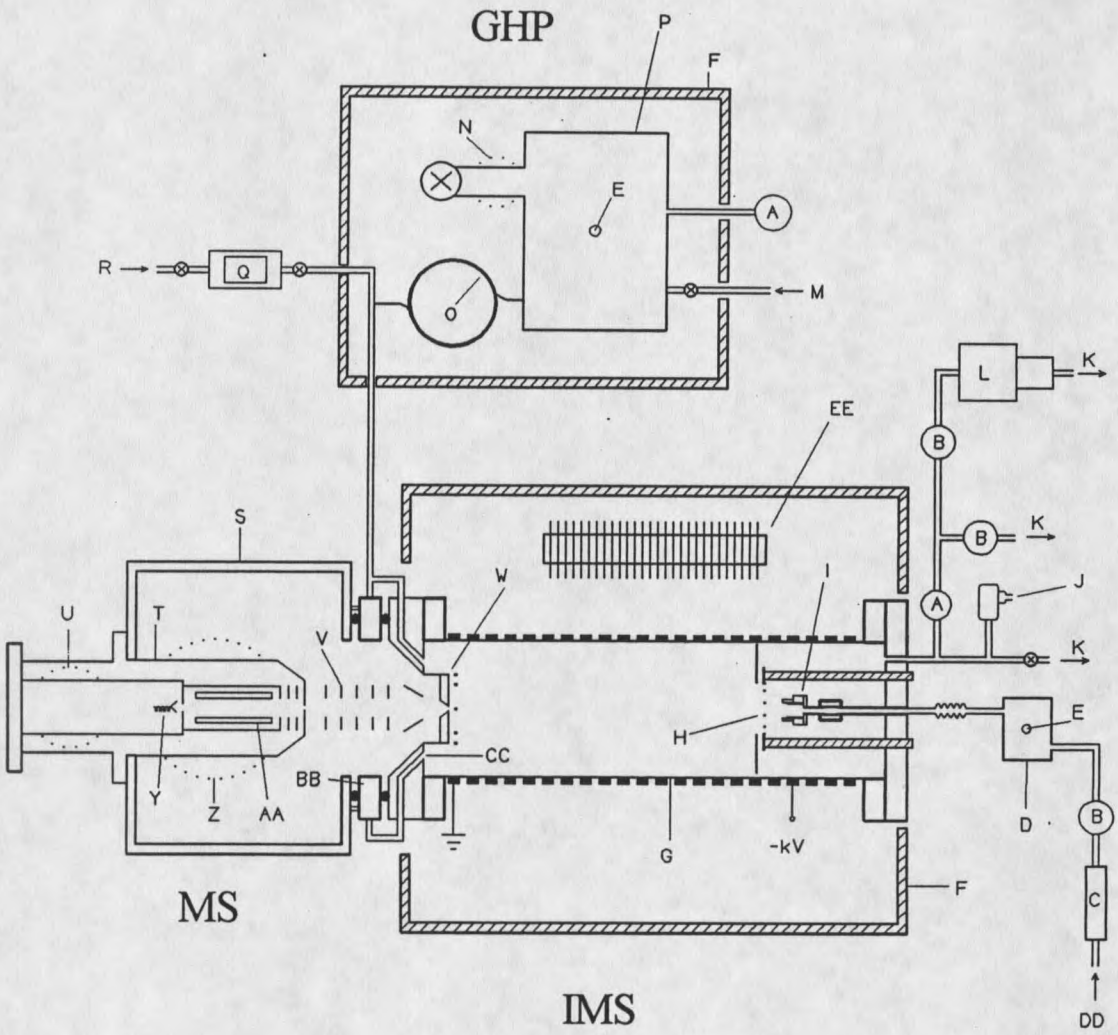

Figure 4. Diagram of the IM-MS apparatus: (A) pressure transducer, (B) needle valve, (C) rotameter, (D) source volume, (E) septum inlet, (F) insulated box, (G) Pyrex drift tube, (H) BN grid, (I) ion source, (J) pressure release valve, (K) source and drift gas exhaust, (L) mechanical vacuum pump, (M) N_2 GHP gas supply, (N) 3 inch diffusion pump, (O) fused silica capillary, (P) 4 liter stainless steel volume, (Q) mass flow controller, (R) N_2 drift gas supply, (S) first vacuum envelope, (T) second vacuum envelope, (U) 4 inch diffusion pump, (V) electrostatic lens elements, (W) Faraday plate/MS aperture, (X) on/off valve, (Y) channeltron electron multiplier, (Z) 6 inch diffusion pump, (AA) quadrupole mass filter, (BB) universal joint, (CC) drift gas inlet, (DD) N_2 source gas supply, (EE) water cooled heat exchanger (optional).

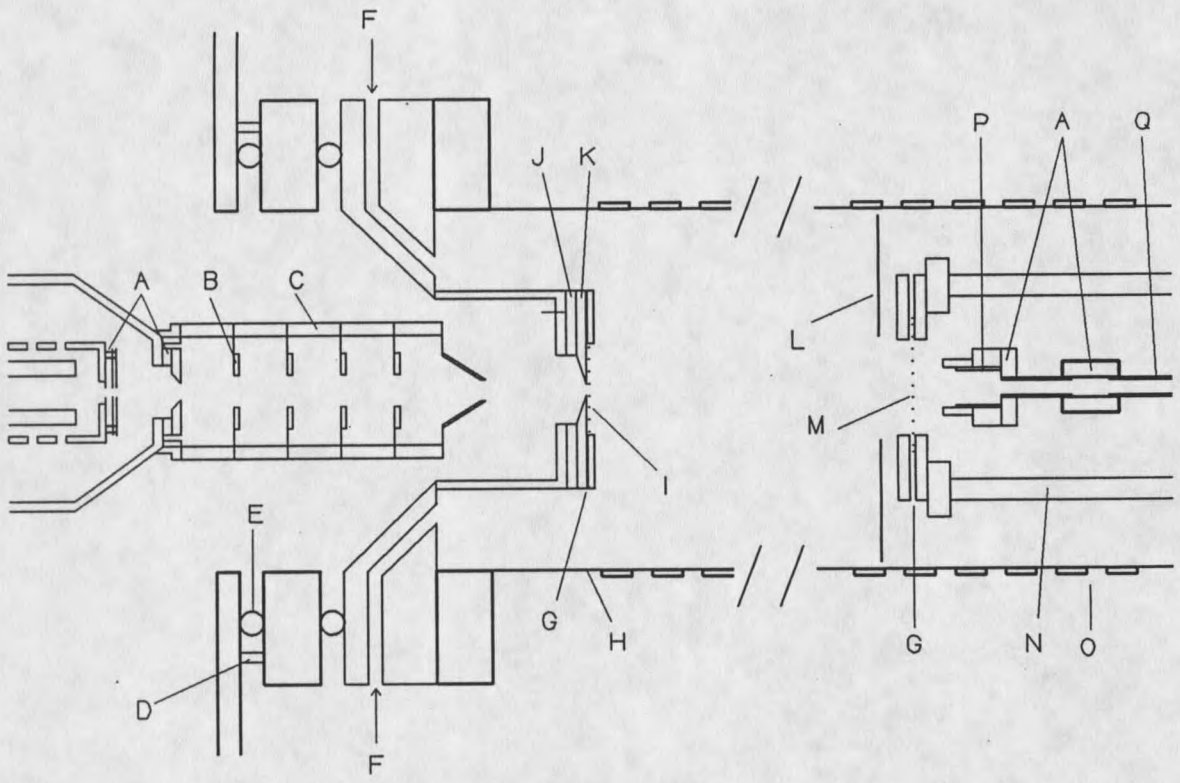

Figure 5. Expanded view of the source and detector ends of the drift tube: (A) ceramic insulators, (B) electrostatic lens elements, (C) ceramic support posts, (D) stainless steel spacer post, (E) Viton O-ring, (F) drift gas entrance port, (G) Teflon washer, (H) Pyrex glass tube, (I) screen grid, (J) macor washer, (K) Faraday plate, (L) annular drift gas deflector plate, (M) BN grid, (N) drift field ring, (O) 15 mCi ^{63}Ni foil, (P) stainless steel tube.

Any electrodes located behind the source are "floating" at the same potential as that applied at the source while those between the source and the Faraday plate (ground potential) are at incrementally decreasing potentials due to the 1MΩ series resistors.

A buffer gas, also referred to as the drift gas, is introduced into the drift tube through two ports located in the IMS-MS interface flange at a nominal flow rate of 350 ml min^{-1}. The flow rate of the drift gas was controlled by a mass flow controller (Type 1179A, MKS Instruments, Inc., Andover, MA) and an associated single channel readout (Type 246B, MKS Instruments, Inc., Andover, MA). A carrier was directed into the other end of the drift tube through a metering valve, rotameter and source volume and then into the source through a port in the source flange at a nominal flow rate of 50 ml min^{-1}. Both the drift gas and the carrier gas flow out of the drift tube through an exhaust port in the source flange.

The drift and carrier gases were usually regular grade nitrogen although other gases have been used depending on the nature of the investigation. The nitrogen drift gas was purified by first passing it through a high capacity gas purifier (Model 2-3800, Supelco, Inc., Bellefonte, PA) and then through a second indicating gas purifier (Model OMI-1, 2-3900, Supelco, Inc., Bellefonte, PA). This purification scheme was used for all inert and noble gases, however, methane gas was incompatible with the Supelco 2-3800 purifier mentioned above and was purified with standard oxygen and water traps (Alltech Associates, Inc., Deerfield, Ill) followed by the second OMI-1 indicating purifier. The carrier gas, inert or methane, was purified in the same manner as described for the methane drift gas, above.

Because the drift gas flow is usually much greater than the carrier gas flow, the carrier gas is swept with the drift gas out the exhaust port and is not expected to penetrate very far into the drift tube region. The exhaust port leads to a manifold consisting of 1) a mechanical pump for low tube pressure operation, 2) a simple toggle valve for ambient tube pressure operation, 3) to a flow restrictor (three meters of 1/16" SS tubing) for high tube pressure operation (later changed to a needle valve) and, 4) to a 10 psi pressure release valve to protect the tube from dangerous overpressure. The pressure in the drift tube was monitored using a pressure transducer (Barocel, Edwards High Vacuum Int'l., Inc.) and associated readout (Model 1505, Edwards High Vacuum Int'l.). The exhaust gas flow rate was measured using a standard bubble flow meter. All electronic flow measurements were verified by manual measurements using a bubble-type flow meter.

The entire IMS assembly is located inside an insulated, thermostated aluminum box which is temperature variable from below ambient to 200 °C. The oven was heated by two 1550 watt finned strip heaters and a temperature controller (Model CN9000A, Omega Engineering, Inc., Stamford CT) and, when necessary, was cooled by passing tap water through a heat exchanger mounted on the inside wall of the oven (Figure 4). The drift and carrier gases were heated by heater tapes prior to their entry into the drift tube and are monitored by type J thermocouples. Two additional Type J thermocouples are located inside the drift tube, one next to the source and the other next to the detector, for increased control of IMS tube temperature.

The IMS Source and Detector

The source and detector ends of the IMS (Figure 5) are composed of a source for generating ions, a gating mechanism to periodically allow these ions into the drift region and a Faraday plate to detect their arrival.

The ion source consists of a 15 mCi ^{63}Ni-on-Pt radioactive foil (New England Nuclear, Boston, MA) that is mounted on the inside edge of a 1 cm^3 stainless steel cylindrical volume. This volume is attached to, and electrically isolated from, 1/4" stainless steel carrier gas tubing by two ceramic insulators and is held at the same electrical potential as the ring electrode located immediately over the source on the outside of the tube. The other end of the source is located about 0.5 cm behind a Bradbury-Nielsen (BN) grid assembly (Figure 5).

The BN grid is the "gate" by which ions formed in the radioactive source are periodically released into the drift tube. It is composed of an interdigitated co-planar vertical array of wires glued with non-conductive epoxy onto a stainless steel annular ring with a 3 cm circular opening. The wires are 0.001 cm in diameter and are spaced approximately 100 μM apart. The array is arranged such that every other wire is connected to one of two circuits; one circuit maintains half of the array at the potential appropriate for the position of the array in the external field, and the other circuit periodically applies a voltage in excess of this potential (typically 20 volts) to the other half of the array. The BN gate is "open" when no voltage is applied such that all wires are at the same potential and any ions can pass between the wires under the influence of the external electric field. The gate is "closed" when 20 volts are applied to half the array; the resulting electric field between the wires causes any ions moving

towards the gate to be collected on the wires biased opposite the charge on the ion, no ions can thus get through the array. The entire BN gate assembly is held in position about 0.5 cm in front of the source by ceramic support posts. Electrical power is brought to the wire arrays and to the source by three 15 kV (de-rated from atmospheric to vacuum) coaxial feedthroughs in the source conflat flange.

The detector is located at the end of the drift tube opposite the source and is composed of a Faraday plate and a screen grid. The Faraday detector is a stainless steel plate approximately 6 cm in diameter and is located 25 cm from the BN gate. The ion current at the Faraday plate is amplified by an attached electrometer (Keithly Model 428) nominally set to a gain of 10^9 V/A and is then sent to a digital signal averager (Nicolet Model 370). If the BN gate is set to pulsed mode and the digital signal averager is set to trigger on each pulse, an ion arrival time spectrum (ion mobility spectrum) can be obtained. Resolution of the ion peaks is enhanced by a 3 cm diameter, 0.025 μm thick gold-plated stainless steel screen grid (Graseby Electronics, Watford, UK) attached to the front of the Faraday plate. This grid is electrically isolated from the Faraday plate by a Teflon washer and is maintained at a slightly higher potential appropriate for its position in the electric field. The grid capacitively decouples the Faraday plate from the approaching ion cloud, thereby reducing the magnitude of image charges. The Faraday plate is mounted on the nose cone of an attached mass spectrometer and is electrically isolated from it by a macor washer. There are two viton O-rings on either side of this washer to provide a vacuum tight seal between the IMS tube and the high vacuum environment of the attached mass spectrometer. A 50 μm aperture plate (Optimation, Inc.,

Salem, NH) is attached to the middle of the Faraday plate with conductive epoxy which allows small amounts of the contents in the VHP drift tube to be leaked into the LP mass spectrometer for mass analysis and identification of IMS analyte peaks.

The Mass Spectrometer

The Mass Spectrometer (MS) is attached to the detector end of the IMS by two thick viton O-rings on either side of an aluminum flange which provides a leak tight seal to prevent contamination in the drift tube and which also reduces stress on the IMS Pyrex drift tube. The mass spectrometer has two vacuum chambers; the first chamber houses the quadrupole lens elements and is kept at a pressure of approximately 4×10^{-4} Torr against the leak in the Faraday plate aperture by a 6 inch diffusion pump. There are six quadrupole lens elements, the last of which is attached to, but electrically isolated from, a nose cone which leads to a second vacuum chamber. In this vacuum chamber, maintained in the 10^{-6} Torr range by a 3 inch diffusion pump, ions are focused into a quadrupole mass filter and detected by a channeltron electron multiplier (Model 4039, Galileo Electro Optics Corp., Sturbridge, MA) operated in the pulse counting mode. These pulses are amplified using a pre-amplifier (Model F-100T, Modern Instrumentation Technology, Inc., Boulder, CO) and then sent to a rate meter (Model TC 525, Tennelec/Nucleus, Inc., Oak Ridge, TN). The quadrupole has been adapted from a used GC/MS system (Model 3200, Finnigan, Inc.,) and is controlled by an MS data system (Vector One, Teknivent, Maryland Heights, MO) and a computer (486DX2, Digital Equipment Co.).

The Gas Handling Plant

The final component of the IM-MS is a gas handling plant (GHP) which is used to introduce neutral reagents into the drift tube. This consists of a 4.084 liter stainless steel volume housed inside a thermostated and insulated aluminum box heated by two 1250 watt finned strip heaters and a temperature controller (Model CN9000A, Omega Engineering, Inc., Stamford CT). When in use, the GHP volume is pressurized to approximately 2500 Torr with purified nitrogen (using the same purifying methods discussed previously for the nitrogen carrier gas) which is allowed to leak out into the drift gas stream through a 3 meter, 100 μm internal diameter fused silica capillary tubing. Accurately known concentrations of neutral reagent, from a few parts-per-billion to tens of parts-per-million, can be created in the drift tube region by injecting known volumes of neutral reagent (gas or liquid) through a septum and into the pressurized GHP volume. The injected material is diluted with the nitrogen in the GHP and undergoes a second dilution as it enters the drift gas stream and is carried into the drift tube. The flow rate through the capillary was determined by monitoring the pressure drop in the GHP volume over time. The pressure in the GHP volume was measured using a pressure transducer (Barocel, Edwards, Inc.) and associated readout (Model 1505, Edwards High Vacuum Int'l). An attached 3 inch diffusion pump and mechanical backing pump allow for evacuation of the GHP volume after each series of experiments.

Principles of Operation

The use of IM-MS for characterizing a simple S_N2 reaction and also for investigating complex cluster equilibria and reactivity has been demonstrated previously by Giles and Grimsrud (10, 11). A review of the basic procedures underlying all applications of the IM-MS will serve to integrate functions of the instrumental components detailed above and will provide a groundwork to appreciate the overall utility of the IM-MS method. All of the basic operating principles, data acquisition and analysis can be demonstrated by describing the experimental procedures involved in investigating the S_N2 reaction given in reaction 6.

$$Cl^- + i-PrBr \xrightarrow{k_2} Br^- + i-PrCl \qquad (6)$$

Typical operating conditions for this type of investigation are listed in Table 1.

Table 1.

Typical operating conditions used in IM-MS

Parameter	Setting
IMS tube temperature	150 °C
GHP temperature	100 °C
Source gas flow	50 ml min^{-1}
Drift gas flow	350 ml min^{-1}
Electric field strength	144 V cm^{-1}
BN gate pulse width	0.5 ms
Sweeps per IM spectrum	500
Sweeps per MAIM spectrum	5000 to 16,000
Tube pressure	300 - 1100 Torr
Room pressure	640 Torr

To determine the kinetics of reaction 6 using IM-MS, it is required only to measure the amount of Br^- produced as a function of neutral (*i*-PrBr) and reagent anion (Cl^-) concentrations under controlled conditions of reaction time and temperature.

Generation of Reagent Ions and Ionic Dynamics in the Drift Tube

Reagent ions, (chloride ions in this case) are generated in the ^{63}Ni source by dissociative electron capture to carbon tetrachloride (CCl_4). The CCl_4 is carried into the source by injecting CCl_4 vapor (nominally 10 µl headspace vapor) into the source volume where it is swept with the nitrogen carrier gas into the source. The radioactive ^{63}Ni produces high energy β^- particles (average energy ≈ 19 kev) which are rapidly thermalized by the nitrogen carrier gas, producing approximately 500 thermal electron/positive ion pairs per β^- particle. Carbon tetrachloride dissociatively captures these thermal electrons, resulting in a steady-state concentration of Cl^- ions in the source region. Due to the nature of radioactive sources, other ions are also created in the source such as various $Cl^-(X)$ adduct ions, where X can be H_2O, HCl, HBr or some other impurity. While these ions are undesirable, as long as they are unreactive and remain at relatively low levels, they can safely be ignored. Because the source and the ring electrode on the tube at the same location is at a high negative potential, nominally -3600 V, these anions tend to migrate down the electric field toward the BN gate while the positive ions move away from the gate.

Packets of Cl^- anions, as well as any other anions, are periodically released out of the source and into the drift region by pulsing the BN gate as described in the previous section.

Once the packet is outside of the source, it will move under the influence of the electric field toward the Faraday plate detector with a velocity given by

$$v_d = KE \tag{7}$$

where E is the electric field strength and K is the ion mobility given by:

$$K = \frac{3}{16}\frac{q}{N}\left(\frac{1}{m}+\frac{1}{M}\right)^{1/2}\left(\frac{2\pi}{k_b T}\right)^{1/2}\frac{1}{\Omega_D} \tag{8}$$

where q is the charge on the ion, N is the drift gas number density, m is the mass of the ion, M is the mass of the drift gas molecule, T is the drift tube temperature, k_b is Boltzman's constant and Ω_D is the ion-buffer gas interaction cross section (111).

The initial shape of the ion packet is determined by the characteristics of the BN gate; how fast it opens and closes and how long it stays open (duration of the pulse width). The opening and closing rate is fast relative to the pulse width and so the ion packet is expected to be in the shape of a flat circular disk. However, as this packet moves down the drift tube, its shape changes due to ion diffusion and to ion-ion coulombic repulsion if the ion density is high enough. The diameter of the initial ion packet is $\approx$ 0.4 cm and has been shown (111) to increase isotropically due to diffusion and ion-ion repulsion by about 75% during transport through the drift tube. A significant loss of ion signal can result if the electric field strength is reduced. Due to increased ion drift times, radial diffusion can increase to the extent that the ion packet extends past the outer diameter of the Faraday plate. While the attendant loss of ion signal can be detrimental (decreased signal to noise ratio), it is important to note that this loss

of signal is *non-mass selective* due to the fact that smaller ions with a high rate of diffusion are also characterized by a high mobility and low drift time, t_d, resulting in the same rate of loss as heavier ions.

An important aspect of experiments carried out using IM-MS is that all of the ions in the drift tube are thermalized. For example, the average kinetic energy is determined by the temperature of the drift tube and is equal to 3/2 kT. The kinetic energy imparted to the ions by the electric field is given as 1/2 mv_d^2, and in randomized motion, given as 1/2 Mv_d^2, where v_d is the drift velocity, m is the mass of the ion and M is the mass of the buffer gas molecules. The average total kinetic energy of the ion, E_{ion}, is given by

$$E_{ion} = \frac{3}{2}kT + \frac{1}{2}mv_d^2 + \frac{1}{2}Mv_d^2 \qquad (9)$$

Evaluation of equation 9 (also known as the Wannier equation) using the mass of Cl^-, the mass of nitrogen, the temperature of the drift tube (Table 1) and the drift velocity of a Cl^- ion (1000 cm s^{-1} under the conditions in Table 1) gives a total energy of 50.3 meV. The last two terms on the right hand side of equation 9 (drift field terms) account for only 0.3 meV of the total which indicates that the energy of the ion is almost all thermal kinetic energy. It should be noted that this result is true only under conditions of relatively low electric field strength. Higher field strength increases v_d and could result in ion energies substantially greater than thermal which would complicate interpretations of reaction rates measured under these conditions. It can be deduced from equations 8 and 9 that v_d depends only on $qE/N\Omega_D$, thus, if Ω_D is a constant (hard spheres), Revercomb and Mason (111) have established a criterion for

low field behavior which requires E/N to be ≤ 2 Td. (1 Td = 1 Townsend = 1 x 10^{-17} V cm^2). All experiments reported in this thesis have been carried out under low field conditions as defined by this criterion.

Ion-Molecule Reactions in the Drift Tube

The current due to the arrival of the packet of chloride ions is detected by the Faraday plate, converted to a voltage (nominally 10^9 V/A) and sent to a digital signal averager. A complete ion arrival time spectrum is obtained by synchronizing the triggering of the digital signal averager with the opening of the BN gate. Such a spectrum, referred to as an Ion Mobilty Spectrum (IMS), or as an ion mobility waveform, is given in Figure 6 for the Cl^- ions in reaction 6 under the conditions in Table 1 and where no *i*-PrBr has yet been added to the drift tube. The identity of the ions comprising the overall IMS can be determined by use of the attached mass spectrometer (MS). The MS can characterize the contents of the drift tube leaking through the 50 um aperture in the Faraday plate by scanning over a range of m/z values (typically 0 to 400 amu) with the BN gate in the continuously open mode. The results of this type of analysis carried out under the same experimental conditions as the Cl^- ion mobility spectrum is also given in Figure 6. It can be seen that a simple mass spectrum is obtained with the $^{35}Cl^-$ and $^{37}Cl^-$ isotopes being the only major ions detected. The mass spectrometer can then be tuned to monitor a single ion and, with the MS rate meter output sent to the digital signal averager and synchronized with the BN gate, the ion arrival time spectrum of this single ion can be obtained. Such a spectrum, called a Mass Selected Ion

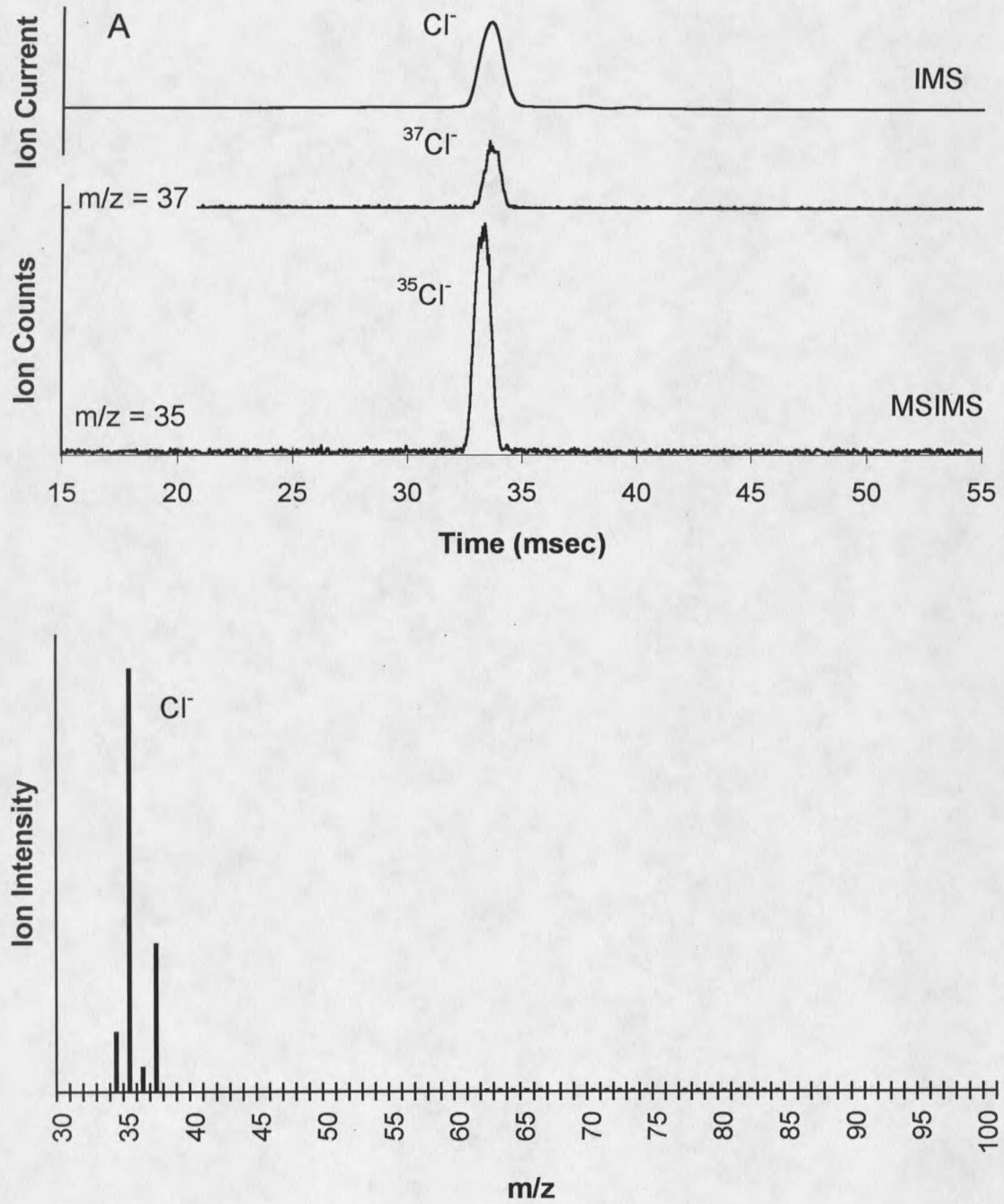

Figure 6. A. Ion Mobility Spectrum (IMS) and Mass Selected Ion Mobility Spectrum (MSIMS) obtained for reaction 6 with no *i*-PrBr yet added to the drift tube. MS tuned to isotopes $^{35}Cl^-$ and $^{37}Cl^-$ in the MSIMS, showing that the Cl^- peak in the IMS is composed of these isotopes. B. Total mass spectrum of the contents in the drift tube obtained under the same conditions in which the Cl^- ion mobilty spectrum was acquired.

Mobility Spectrum (MSIMS) is shown in Figure 6. It is evident from the MSIMS data in Figure 6 that the overall IMS is a sum of the ion arrival time spectra of the isotopes of Cl^-.

Figure 7 shows the ion mobility spectra obtained with increasing concentrations of *i*-PrBr in the drift tube. It can be seen how the original Cl^- peak is reduced and another, broader peak, identified as Br^-, is formed near the Cl^- peak at a somewhat longer drift time. Also, it is evident that the ratio of the Cl^- peak area to the second peak area decreases with increasing concentrations of *i*-PrBr in the drift tube. The coincidence of increasing area of the second peak with increasing concentrations of *i*-PrBr implies that this second peak is formed by a reaction involving *i*-PrBr with Cl^- in which ions are formed with a slightly greater drift time than Cl^- ions. Knowledge of basic reaction mechanisms would lead to the further assumption that the reagents involved in this reaction are likely to participate in an S_N2 reaction which would result in the formation of Br^- ions and *i*-PrCl. Investigation and verification of these assumptions is possible by once again analyzing the contents of the drift tube and by obtaining a MSIMS of each significant ion using the attached MS.

Figure 8A shows the results of the mass analyses carried out under the experimental conditions in Table 1 and with a concentration of *i*-PrBr in the drift tube of 4.38×10^{13} molec cm^{-3} corresponding to ion mobility waveform C in Figure 7. It is evident that the major ions in the drift tube are the isotopes of Cl^- and Br^-, The Cl^- and Br^- MSIMS in Figure 8B, positioned under the IMS spectrum, shows that the second peak is composed of Br^- ions with drift times ranging from coincidental with the drift time of Cl^- to a peak at a drift time of ~ 35 ms. The existence and shape of the Br^- MSIMS verifies the assumption of an S_N2 reaction occurring

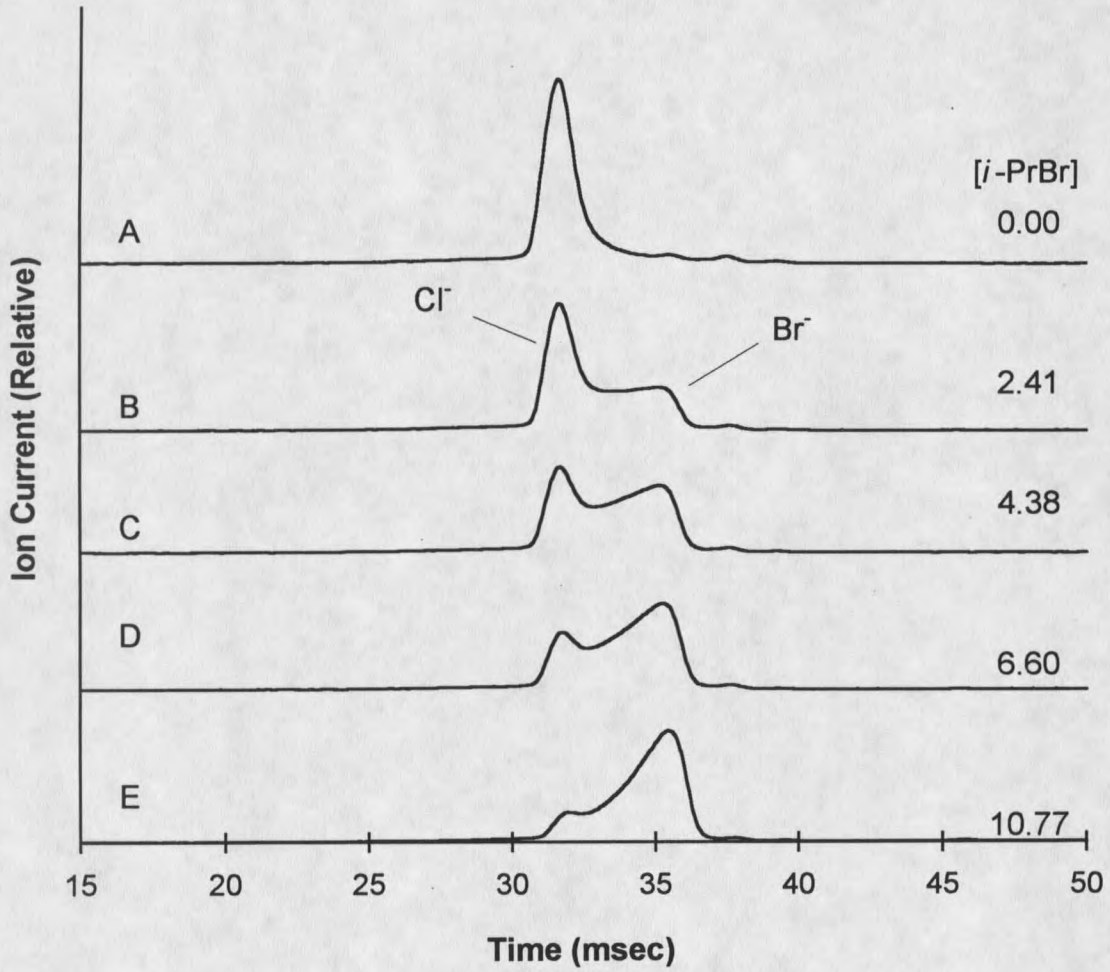

Figure 7. Ion Mobility Spectra obtained over the course of reaction 6. Concentrations of *i*-PrBr in the drift tube are: A = 0.00, B = 2.41, C = 4.38, D = 6.60 and E = 10.77 ($x10^{13}$ molec. cm^{-3}).

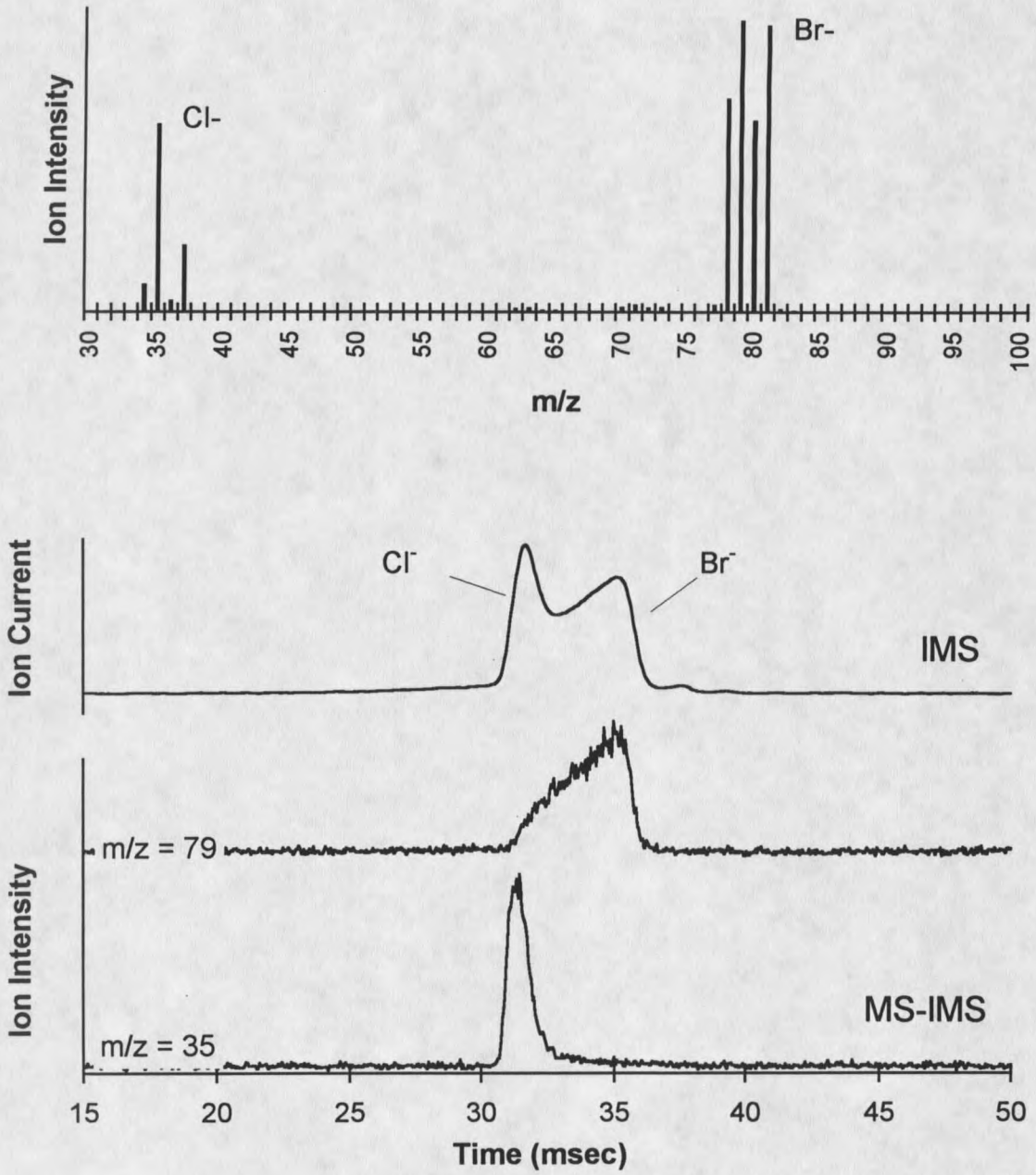

Figure 8. A. Total mass spectrum obtained by analyzing the contents of the drift tube under the conditions in which spectrum C in Figure 7 was obtained. Peaks at 78 and 80 amu due to the low resolution of the mass spectrometer. B. Ion mobility spectrum C from Figure 7 and associated MSIMS for the ions Cl^- and Br^-. It can be seen that the ion mobility waveform is composed of the Cl^- and Br^- ion as indicated.

between Cl^- and *i*-PrBr. Bromide ions are produced by reaction of the Cl^- ion packet as it moves through the drift tube which has a homogeneous concentration of *i*-PrBr in atmospheric nitrogen all along its length. The wide range of Br^- drift times is due to this reaction occurring at all points along the drift tube. Bromide ions produced just outside of the source must traverse a longer distance than those produced by reaction at intermediate distances down the tube or those produced just before the Faraday plate. The slope of the Br^- peak is due to the decreasing concentration of Cl^- ions as the packet is depleted by reaction in transit through the tube. Finally, it can be seen in Figure 9 how combining the two MSIMS spectra of Cl^- and Br^- results in a waveform virtually identical to the overall IMS waveform shown in Figure 8. These IMS waveforms, obtained under conditions of varying concentrations of *i*-PrBr, contain sufficient information to allow elucidation of the second-order rate constant for reaction 6.

Determination of Reaction Rate Constants

Second order rate constants, k_2, for bimolecular reactions can be obtained by analysis of IMS waveforms over the course of a reaction as either the concentration of neutral reagent, [*i*-PrBr], or as the reaction time is varied. A review of the waveforms in Figure 7 shows the dynamic nature of an IMS waveform as increasing the concentration of *i*-PrBr in the drift tube increases the extent of reaction 6. The pseudo-first order reaction rate constant, $\alpha = k_2[i\text{-PrBr}]$, for this bimolecular reaction is given by

$$\alpha = \frac{1}{t_d} \ln\left(\frac{A(Cl^-) + A(Br^-)}{A(Cl^-)}\right) = k_2\,[i - PrBr] \qquad (10)$$

where $A(Cl^-)$ and $A(Br^-)$ are the areas under the peaks containing the Cl^- and Br^- ions, respectively, and t_d is the drift time (reaction time) of the Cl^- reagent ions. The areas under the Cl^- and Br^- containing peaks can be obtained by analyzing the waveforms as shown in Figure 9 (IMS C in Figure 7 used for illustration). Line 1 is the background ion intensity determined far from the analyte peaks (baseline). Lines 2 and 6 indicate the beginning of the arrival of Cl^- reactant ions and the end of the arrival of Br^- product ions, respectively. The product ion arrival time data between points 4 and 5 are fit to an exponential curve using least squares, extrapolated to point 3 and then linearly extrapolated to the intersection of lines 1 and 2. The peak area above lines 2, 3 and 4 is due to Cl^- reactant ions and that below lines 2, 3, 4 and 5 and bounded by line 6 is due to Br^- product ions. A turbo-basic program has been written to facilitate measurement of peak areas using the boundary conditions outlined above. Knowledge of these areas and of the reaction time, t_d, is sufficient to obtain the pseudo-first order reaction rate constant, α, for reaction 6. This procedure is repeated over a series of injections of *i*-PrBr into the GHP (increasing the homogeneous concentration of *i*-PrBr in the drift tube). A plot of the resulting pseudo-first order rate constants versus concentration of *i*-PrBr in the drift tube is shown in Figure 10. It can be seen how the points at higher concentrations fall below the least squares line. This is due to the negative error associated with the difficulty of measuring small reactant ion peak areas. Determination of the slope of the least squares line obtained using points in the linear range results in a good estimate of the second order rate constant, k_2, for reaction 6.

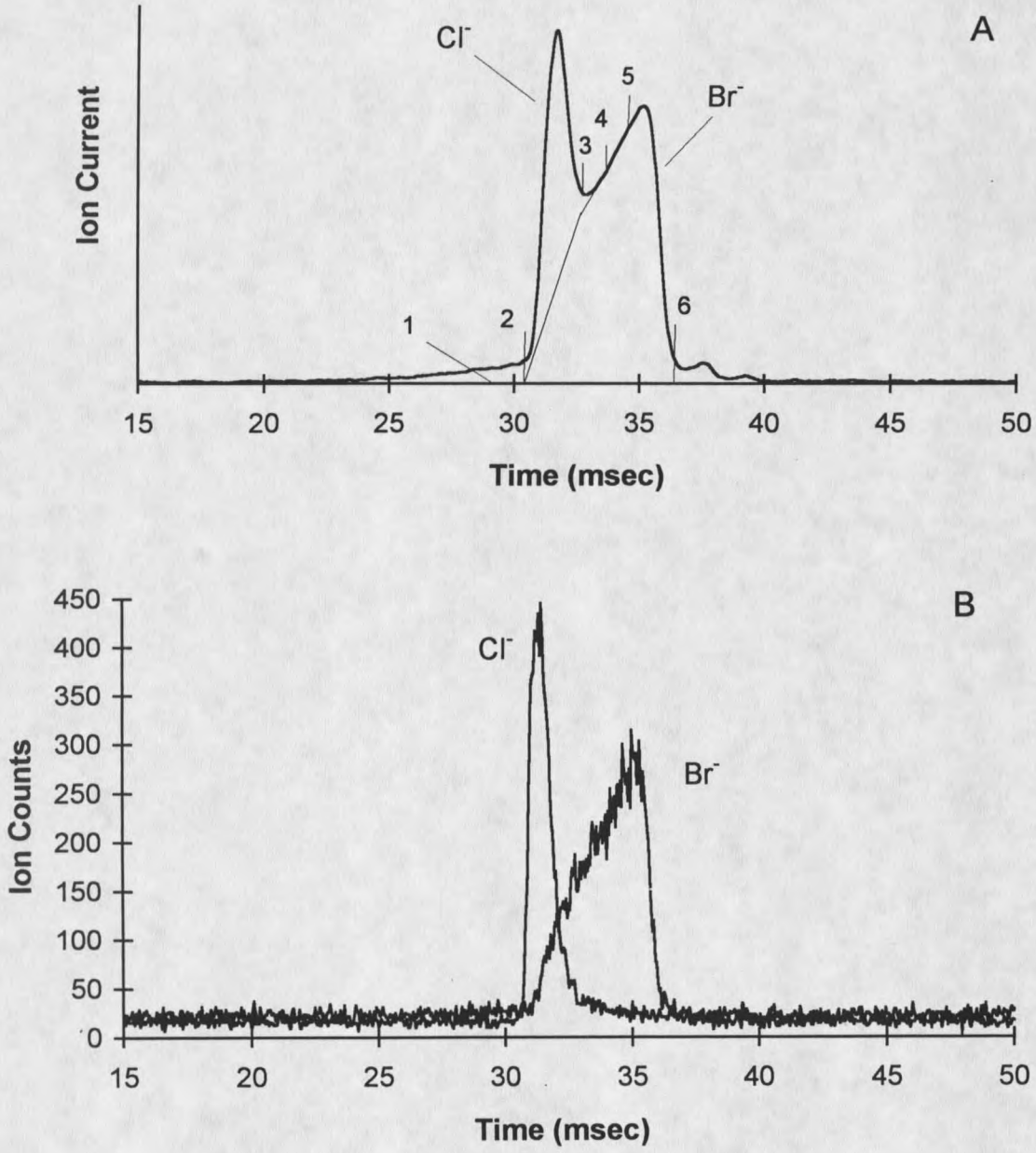

Figure 9. A. Reaction modified ion mobility waveform with 4.38 x 10^{13} *i*-PrBr molec. cm^{-3} in the drift tube. Numbered lines used for determining k_2 are explained in the text. B. Mass selected ion mobility waveforms correlating the identity and shape of the Cl^- and Br^- peak areas under the waveform in A.

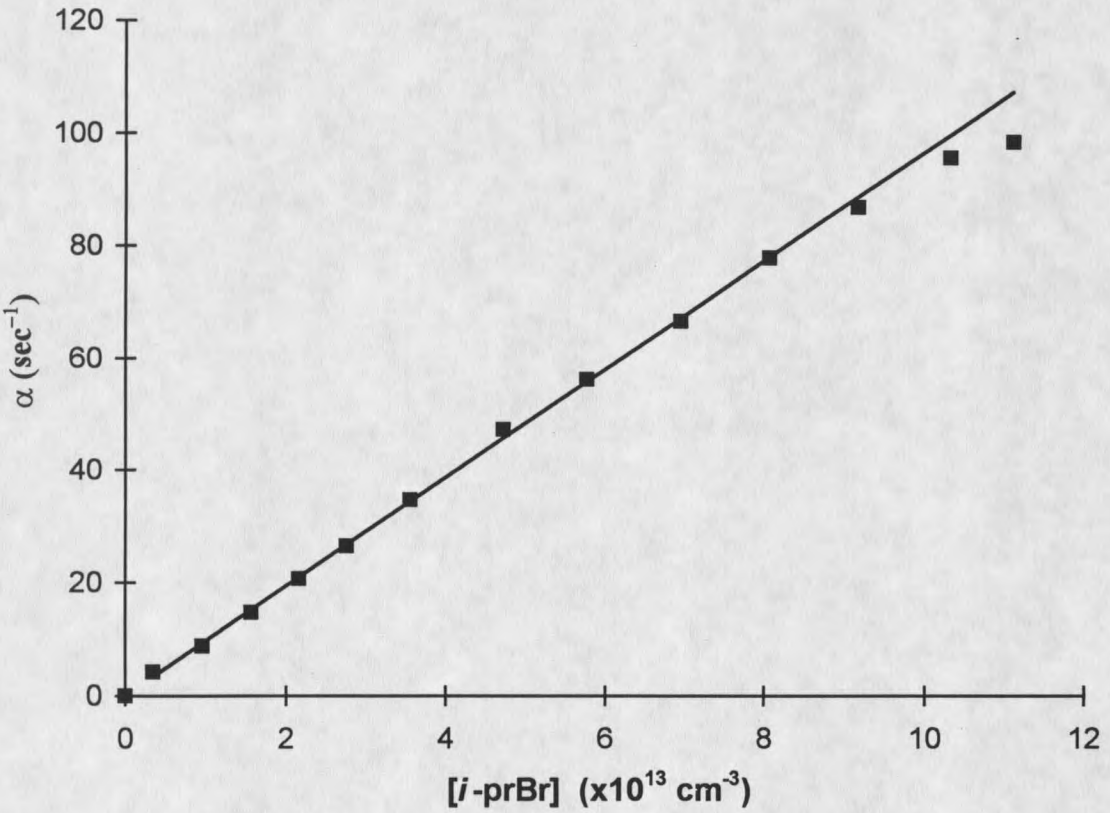

Figure 10. Plot of the pseudo-first order rate constant for reaction 6 versus concentration of *i*-PrBr in the drift tube and associated least squares line.

An alternative, and complementary, method for determining the rate constant of a bimolecular reaction involves the analysis of waveforms obtained as the reaction time is changed under conditions of constant neutral reagent (*i*-PrBr) concentration. This is accomplished by varying the electric field and thus changing the arrival time of the Cl^- reagent anions; higher field strengths resulting in a shorter t_d and lower field strengths resulting in a longer t_d (reaction time). This can be seen graphically in Figure 11, which shows five ion mobility spectra obtained under conditions of constant *i*-PrBr concentration (4.38×10^{13} molec. cm^{-3}) in the drift tube and varying electric field strength. It can be seen how the reactant ion peak area decreases and the product ion peak area increases as the reaction time increases from 30 to 62 milliseconds. A plot of ln $[(A_{Cl^-} + A_{Br^-})/A_{Cl^-}]$ vs t_d (equation 10 rearranged) for each of the waveforms of Figure 11 results in a straight line as shown in Figure 12 with slope equal to k_2[*i*-PrBr], the pseudo-first order rate constant for reaction 6. The second order rate constant is thus obtained by dividing this slope by the concentration of *i*-PrBr in the drift tube.

In addition to these methods, the attached mass spectrometer can be used to determine rate constants of bimolecular reactions. This does not rely on the interpretation of ion mobility spectrums; instead, product and reactant ion intensities are monitored by the MS as a function of [*i*-PrBr]. Applying pseudo first order kinetics, a plot of log Cl^- intensity vs [*i*-PrBr] results in a straight line with slope equal to $-k_2 t_d / 2.303$. An alternative method can be applied which

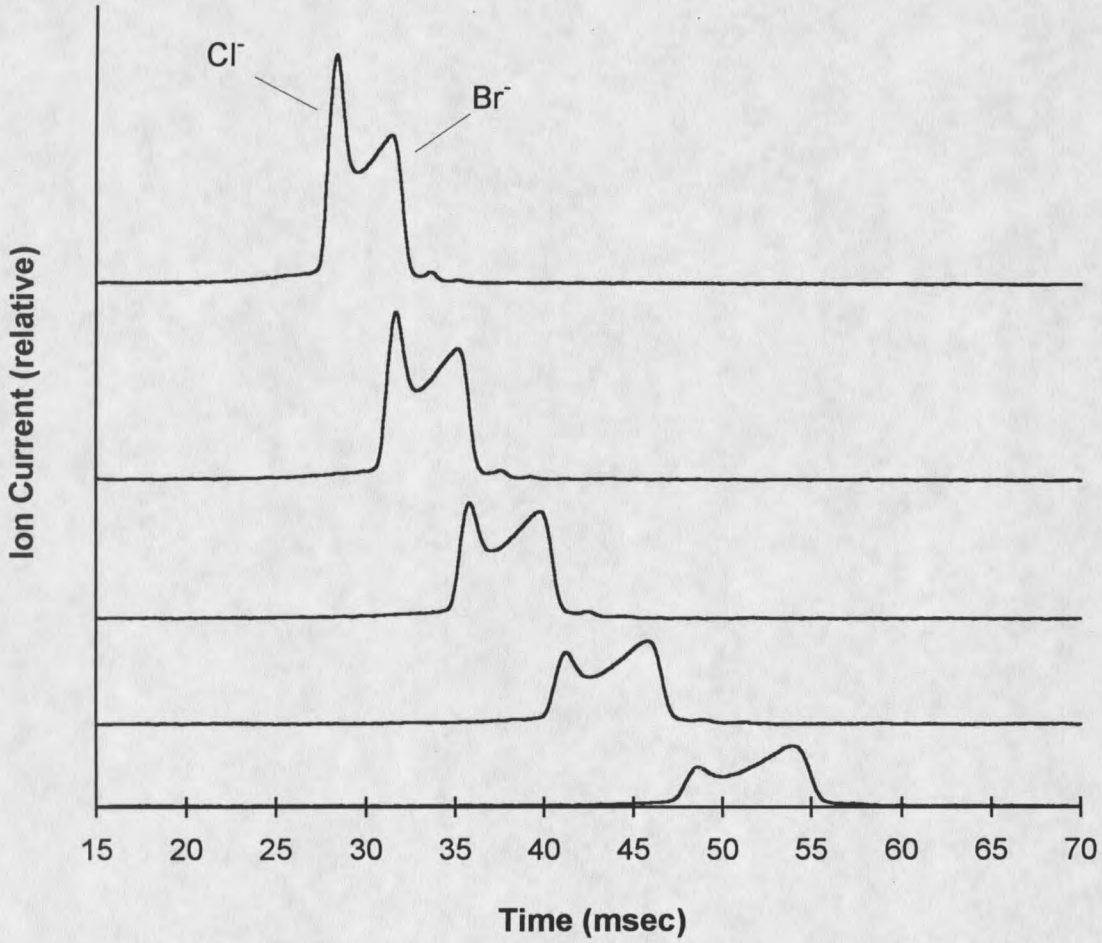

Figure 11. Reaction modified ion mobility waveforms as a function of electric field strength. Spectrum A = 160 , B =144, C = 128, D = 112 and E = 96 V cm^{-1}.

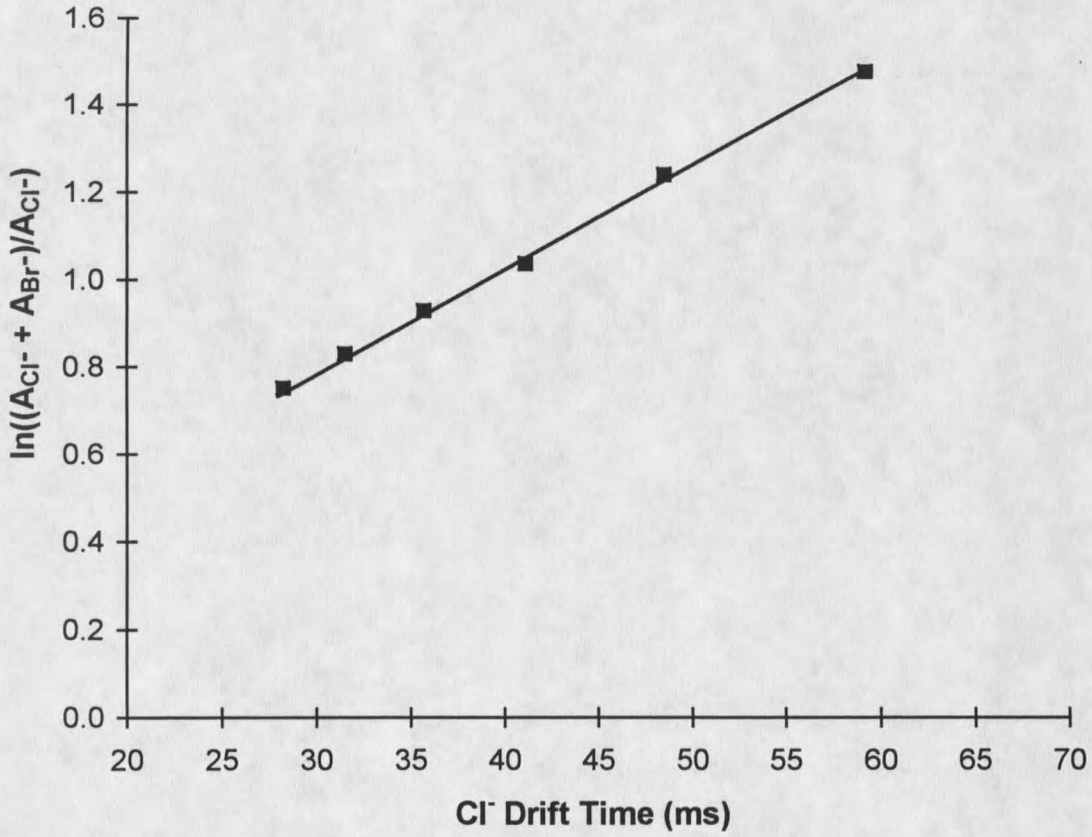

Figure 12. Plot of ln [(A_{Cl^-} + A_{Br^-})/A_{Cl^-}] vs t_d for each of the waveforms of Figure 11 with associated least squares line. Slope is equal to k_2[*i*-PrBr], the pseudo-first order rate constant for reaction 6.

does not require long-term stability of the mass spectrometer. This involves plotting log (Cl^- /(Cl^- + Br-)) vs [*i*-PrBr] and should result in a straight line with slope again equal to $-k_2 t_d/2.303$. While long term stability of the mass spectrometer is not a problem with this method, mass bias affects must be taken into consideration.

The final result of each of these methods, the second order rate constant, k_2, is obtained only after the measurement of numerous physical quantities, each of which has a certain amount of error associated with it. In order to estimate the uncertainty of these rate constants, and thus the accuracy of IM-MS as a method for their determination, it is necessary to analyze the cumulative effect of the uncertainties in each physical measurement.

Errors Analysis of Methods for Determining Rate Constants using IM-MS

Table 2 shows the physical measurements needed to determine IM reaction rate constants using IM-MS. In later discussions, other properties of IM reactions, such as clustering equilibrium constants and associated thermochemical properties (i.e. ΔH, ΔG, ΔS) as well as thermal electron detachment rate constants and activation energies will be determined. While each error analysis for these measurements will not be shown explicitly, they are performed for each property and are based on the same analytical methods and physical uncertainties described in this section and listed in Table 2. The standard methods of error analysis, taken from Bevington and Skoog and West (112, 113), will be applied here to the determination of a rate constant for Reaction 6 under the conditions specified in Table 1 as an example of the methods used in reporting other results.

Table 2.

Physical Measurements, Calculated Results and Associated Uncertainties in IM-MS

Physical Measurement	Uncertainty
IMS tube temperature	± 2 °C
GHP temperature	± 2 °C
Room Temperature	± 2 °C
GHP Pressure	± 20 Torr
Drift Tube Pressure	± 20 Torr
Drift Gas Flow Rate	± 3 %
Neutral Reagent Volume Injected into GHP	± 10 %
Room Pressure	± 5 Torr
Reactant or Product Peak Area	± 10 %
Capillary Flow Rate	± 15 %
Carrier Gas Flow Rate	± 3 %
Volume of GHP	± 40 ml
Calculated Result	**Uncertainty**
α, Pseudo First-Order Rate Constant	± 10 %
Concentration of Neutral Reagent	± 15 %
k_2, Second-Order Rate Constant	± 15 %

The determination of a second order rate constant for reaction 6 requires the use of all the physical parameters listed in Table 2. The associated uncertainties must be included in this determination and propagated throughout all requisite calculations. The fundamental equation used in the calculation of a second-order rate constant is shown in equation 10. The procedure for determining the overall error associated with this expression is to first determine the uncertainty in the pseudo-first order rate constant, α, and in the concentration of neutral

reagent, *i*-PrBr in this case, and then to calculate the cumulative effect of these errors on the second-order rate constant obtained through analysis of the slope of linear equation 10.

The uncertainty in α is based on the uncertainties in measuring the areas under the Cl^- and Br^- peaks and in the measurement of the reaction time, t_d, for reaction 6 according to equation 10. Repeated determinations of reactant or product ion peak areas have resulted in a "worse case" uncertainty (low intensity, low signal-to-noise) in peak areas of $\pm$ 10% (Table 2). The uncertainty in estimating the reaction time, t_d, is a function of the temporal resolution of the Nicolet 370 Digital Signal Averager and is, at worse, $\pm$ 100 μs, or, in the case of reaction 6, 0.35%. These errors are propagated through the subsequent calculations to determine α and leads to a relative uncertainty in α of $\pm$ 10%.

The determination of the concentration of neutral reagent in the drift tube is given by

$$[i-\mathrm{Pr\,Br}] = (\mathrm{DF_{ghp}})\,(\mathrm{DF_{drift}})\,(2.687\times10^{19})\,(\mathrm{P_{tube}}/760)\,(273/\mathrm{T_{tube}}) \qquad (11)$$

where DF_i are the dilution factors for the gas handling plant (ghp) and the drift gas (drift) and 2.687×10^{19} is the gas number density at STP. The relative uncertainty in the concentration of neutral reagent, $S_{[i\text{-PrBr}]}$, is determined by the relative uncertainties, S_i, associated with the parameters used in determining this quantity as shown in equation 12.

$$S_{[i-\mathrm{Pr\,Br}]} = \sqrt{(S_{\mathrm{DF,ghp}})^2 + (S_{\mathrm{DF,drift}})^2 + (S_{\mathrm{P,ghp}})^2 + (S_{\mathrm{T,ghp}})^2} \qquad (12)$$

These relative uncertainties are, in turn, determined in equations 13 through 19. Calculation of the gas handling plant dilution factor is given by

$$DF_{ghp} = \frac{n_{i-PrBr}}{n_{N_2}}. \quad (13)$$

Here, n is the number of moles of *i*-PrBr and N_2 where $n_{i\text{-}PrBr}$ is determined by

$$n_{i-PrBr} = (\mu l \text{ inj.})(\rho_{i-PrBr})(\text{M.W.}_{i-PrBr}) \quad (14)$$

and n_{N2} is determined by

$$n_{N_2} = (P_{ghp})(V_{ghp})\left(\frac{1}{R}\right)\left(\frac{1}{T_{ghp}}\right)\left(\frac{1}{760}\right) \quad (15)$$

where R is the universal gas constant, ρ is the density and M.W. is the molecular weight of *i*-PrBr. The relative uncertainties in equation 14 and 15 are obtained in the same manner as in equation 11 using the operating conditions listed in Table 1 and the uncertainties listed in Table 2. The total relative uncertainty in the gas handling plant dilution factor, DF_{ghp}, is thus

$$S_{DF,ghp} = \sqrt{(S_{n,[i-PrBr]})^2 + (S_{n,N_2})^2} = 10.5\%. \quad (16)$$

Calculation of the drift flow dilution factor is given by

$$DF_{drift} = \frac{F_{cap}}{F_{drift}}. \quad (17)$$

Here, F_{cap} is the capillary flow rate and F_{drift} is the drift gas flow rate given by equations 18 and 19, respectively,

$$F_{cap} = \left(\Delta P_{ghp}/\Delta t\right)\left(T_{room}/T_{ghp}\right)\left(V_{ghp}/P_{room}\right) \quad (18)$$

and F_{drift} is given in Table 1 as 350 sccm, ± 10 sccm. The total relative uncertainty in the drift gas dilution factor, DF_{drift}, is thus

$$S_{DF,drift} = \sqrt{(S_{F,cap})^2 + (S_{F,drift})^2} = 15.0\%. \quad (19)$$

These relative uncertainties in the dilution factors, combined with the uncertainties in the pressure and temperature of the gas handling plant (Table 2), allow the total uncertainty in the concentration of *i*-PrBr in the drift tube, [i-PrBr], to be estimated at ~ ± 15.0%.

The relative uncertainty in the second-order rate constant, k_2, can now be determined by analysis of the propagation of the errors in α and [*i*-PrBr] and by considering the error involved in calculating the average k_2 by analysis of the slope of equation 10. These calculations result in a relative uncertainty in the second-order rate constant, k_2, of just over 15% (the standard error in the linear regression is insignificant relative to the error in α and [i-PrBr]). The major uncertainties in these calculations are the amount of *i*-PrBr injected into the GHP and the flow rate of the capillary leading out of the GHP and into the drift gas line. Care was taken to ensure minimal loss of reagent during injection from the room pressure syringe (Hamilton, gas tight) into the pressurized GHP. The flow rate of the capillary was determined by measuring the pressure drop in the GHP over time; care was taken here to ensure that all possible leaks in the system were eliminated. The uncertainty in the capillary flow rate listed in

Table 2 was calculated from the quantities measured in determining the flow rate (equation 18). Throughout the following discussion of the applications of IM-MS to the investigation of various IM reactions, the associated uncertainties in the reported results determined in the same manner as discussed here, will be given.

The foregoing description of IM-MS; the instrumental layout, experimental methods and associated uncertainties, provide a good foundation from which to present the results of the three experimental investigations mentioned previously. The first investigation presented is the measurement of the rate of thermal electron detachment from the azulene molecular anion, Az^-, and the subsequent determination of the activation energy for this process over the pressure range 300 to 1100 Torr.

THERMAL ELECTRON DETACHMENT RATE CONSTANTS FOR AZULENE$^-$ AND THE ELECTRON AFFINITY OF AZULENE AT ELEVATED PRESSURES

The Electron Affinity (EA) of atoms and molecules and the related rate of electron attachment and detachment are fundamental and important properties in condensed phase and gas phase chemistry. Charge-transfer complexes and mechanisms, fundamental in organic, biochemical and catalytic reactions, and gas-phase analytical processes such as electron capture detection, negative ion MS, and gaseous electronics are three areas where knowledge of this information is essential. Measurements of atomic and molecular electron affinities and electron capture rate constants have been a very active area of research over the past three decades as is evident in numerous review articles (114 - 119). However, to date there have been only three direct measurements of thermal electron detachment (TED) from polyatomic molecules.

The first direct measurements of TED rate constants were made by Pack and Phelps (120) from the diatomic O_2^- anion using drift tube experiments. The first direct measurement of the electron detachment rate constant of a complex organic molecule was made by Grimsrud et al. (47). In this experiment, the PHPMS was used to measure the decay of Az^- as a function of temperature. In the PHPMS, the measured rate of decrease in Az^- ion intensity, measured with a mass spectrometer, depends not only to TED, but also on competing rates of ionic diffusion, electron re-attachment to azulene neutrals and electron transfer to C_7F_{14} (added to suppress re-attachment of thermal electrons to azulene). The possible complications associated with electron transfer to C_7F_{14} were avoided in subsequent measurements of Az^- TED rate constants by Mock and Grimsrud (46) using a Photodetachment Modulated Electron Capture

Detector (PDM-ECD). This method avoided many of the complications inherent in the PHPMS method, and resulted in TED rate constants approximately three times lower than that obtained with the PHPMS. This was attributed to possible uncertainties in the ion-ion recombination rate and in the photo-detachment cross section of Az^-. The high buffer gas pressure in the PDM-ECD (two atmospheres), relative to that in the PHPMS (4 Torr), was also considered to be directly related to the lower rate constants measured. These observations indicate that the high buffer gas pressures in the PDM-ECD might result in Az^-/buffer gas interactions which could stabilize the Az^- ion towards TED.

The need for reliable experimental methods to measure TED processes and the possibility to investigate the pressure dependence of Az^- TED led to the idea that IM-MS could be an ideal method for the study of Az^- TED. The TED of Az^- should be amenable to study using IM-MS because its EA ($\approx$ 10-20 kcal mol^{-1}) is such that a measurable change in the rate of TED should be observable within the temperature range available in IM-MS. Also, the formation of a relatively long-lived negative ion should be possible through resonance electron capture of thermal electrons by azulene introduced into the ^{63}Ni source (121). Thermal detachment of electrons from these Az^- ions in the drift region could be monitored since the electron and Az^- signals are expected to be distinguishable. The resulting ion mobility waveforms would then provide the information to determine first-order TED rate constants for Az^-. Measurements of these rate constants as a function of temperature were expected to provide an estimation of the activation energy (E_A) for the thermal detachment of electrons from Az^-, which could be related to the electron affinity (EA) of azulene. These values of

electron affinity and TED rate constants, obtained in buffer gas pressures from 300 to 1100 Torr, could then be compared with the values obtained using other experimental methods.

Experimental

The configuration of the IM-MS used in this investigation was as shown in Figure 4 with the exception that the gas handling plant and the heat exchanger were not needed. Also, a small (25 mm x 5 mm) glass vial was attached to a stainless-steel "Tee" in the source carrier gas line and heated with heater tape. Azulene crystals (Aldrich Chemical Co.) were placed in this cleaned and baked glass vial and heated to enhance the sublimation of azulene; the subsequent azulene vapor was carried with the N_2 carrier gas into the source region where resonant electron capture (reaction 20) occurs. The pressure of the drift tube was variable from a low pressure of 300 Torr to a high pressure of 1100 Torr by adjustable low and high pressure needle valves as illustrated in Figure 4. The response of the Faraday plate to the arrival of thermally detached electrons was monitored by the attached electrometer, analog to digital converter and digital signal averager. Periodic analysis of the gas composition in the drift tube and determinations of peak identities was accomplished with the attached mass spectrometer. Buffer gases of different composition (methane, helium and argon) were introduced to observe any possible effects on the appearance of the ion mobility waveforms and on the rates of reaction determined from their analysis.

Model of TED Waveforms and Waveform Analysis

The expected shape of the ion mobility waveforms obtained using IM-MS can be predicted by modeling the first-order decay of an initial number of anions undergoing thermal electron detachment. The results of this analysis, modeling TED from the packet of Az^- ions in the drift tube according to reaction 20, carried out over low, medium and high temperatures, are illustrated in Figure 13 .

$$Az^- \underset{k_a}{\overset{k_d}{\rightleftharpoons}} Az + e^- \qquad (20)$$

These waveforms were modeled after first-order kinetics with rate constants, k_d, of 600, 75 and 3 s^{-1}, characteristic of TED at relatively high, intermediate and low temperatures in waveforms A, B and C, respectively. The arrival time of the Az^- ion packet at the low and medium temperatures was estimated based on published values of the reduced mobility of azulene. It is important to note that the area under each of these waveforms is equivalent and reflects the fact that the same quantity of Az^- anions is released into the drift tube region in each case.

At high k_d, total depletion of the Az^- ion packet by TED occurs in the first several centimeters of the drift tube. The electron signal at the Faraday plate, i_{e^-}, under these conditions is expected to resemble waveform A in Figure 13 according to equation 21. This first order equation can be rearranged to linear equation 22, which when ln (i_{e^-}) is plotted versus time, t, leads to a straight line with slope equal to the first order rate constant for the thermal electron detachment, k_d, of Az^-.

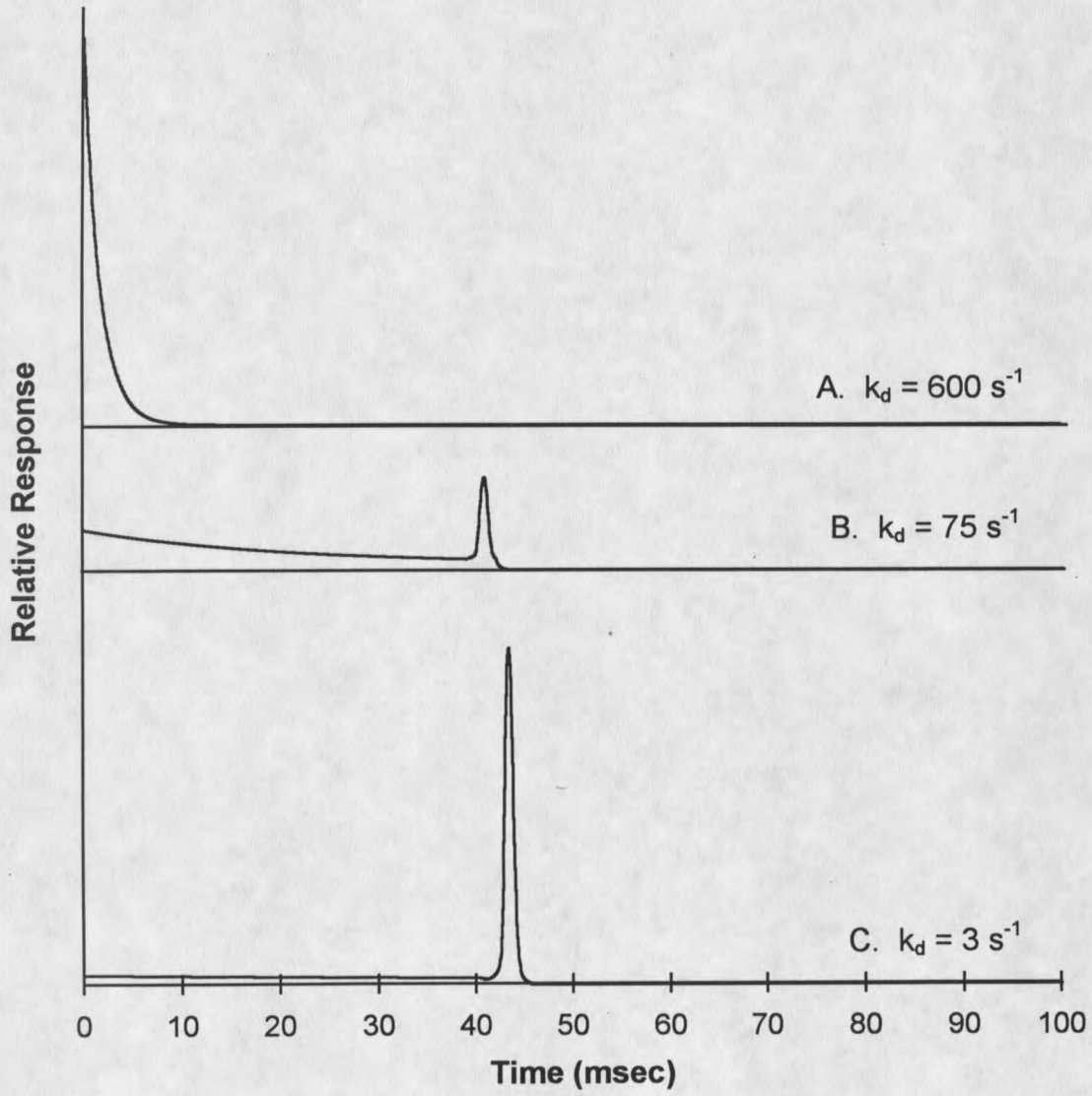

Figure 13. A series of ion mobility waveforms modeled after the first-order TED of Az^-. First order decay calculated with rate constants, k_d, of 600, 75 and 3 s^{-1} in spectra A, B and C, respectively. Total areas under each waveform are equivalent.

$$i_{e^-} = e^{-k_d t} \tag{21}$$

$$\ln (i_{e^-}) = - k_d t \tag{22}$$

An illustration of this procedure using waveform A in Figure 13 is given in Figure 14 and, in this example, results in the value of k_d chosen to model the initial waveform. This simple method for determining the rate constants of actual first order processes is expected to apply as long as the slope of equation 22 is determinable. However, at lower temperatures, represented by waveform C in Figure 13, the slope of the natural log plots will be too shallow to measure reliably; in these cases an alternative method of kinetic analysis must be used. At lower values of k_d, the Az^- ion packet is only partially depleted by TED occurring throughout the length of the drift tube, represented by waveforms B and C in Figure 13. The amount of Az^- ions present in the drift tube at time, t_d, is related to the original amount in the ion packet according to equation 23.

$$\left[Az^-\right]_t = \left[Az^-\right]_0 e^{-k_d t_d} \tag{23}$$

Rearranging this equation and assuming that the relative concentrations of Az^- ions, $[Az^-]_i$, are proportional to the relative areas under the waveforms results in equation 24 which can be used to determine the rate constant for thermal electron detachment at lower temperatures.

$$k_d = \frac{\ln\left[\left(A_{Az^-}\right)_0 / \left(A_{Az^-}\right)_t\right]}{t_d} \tag{24}$$

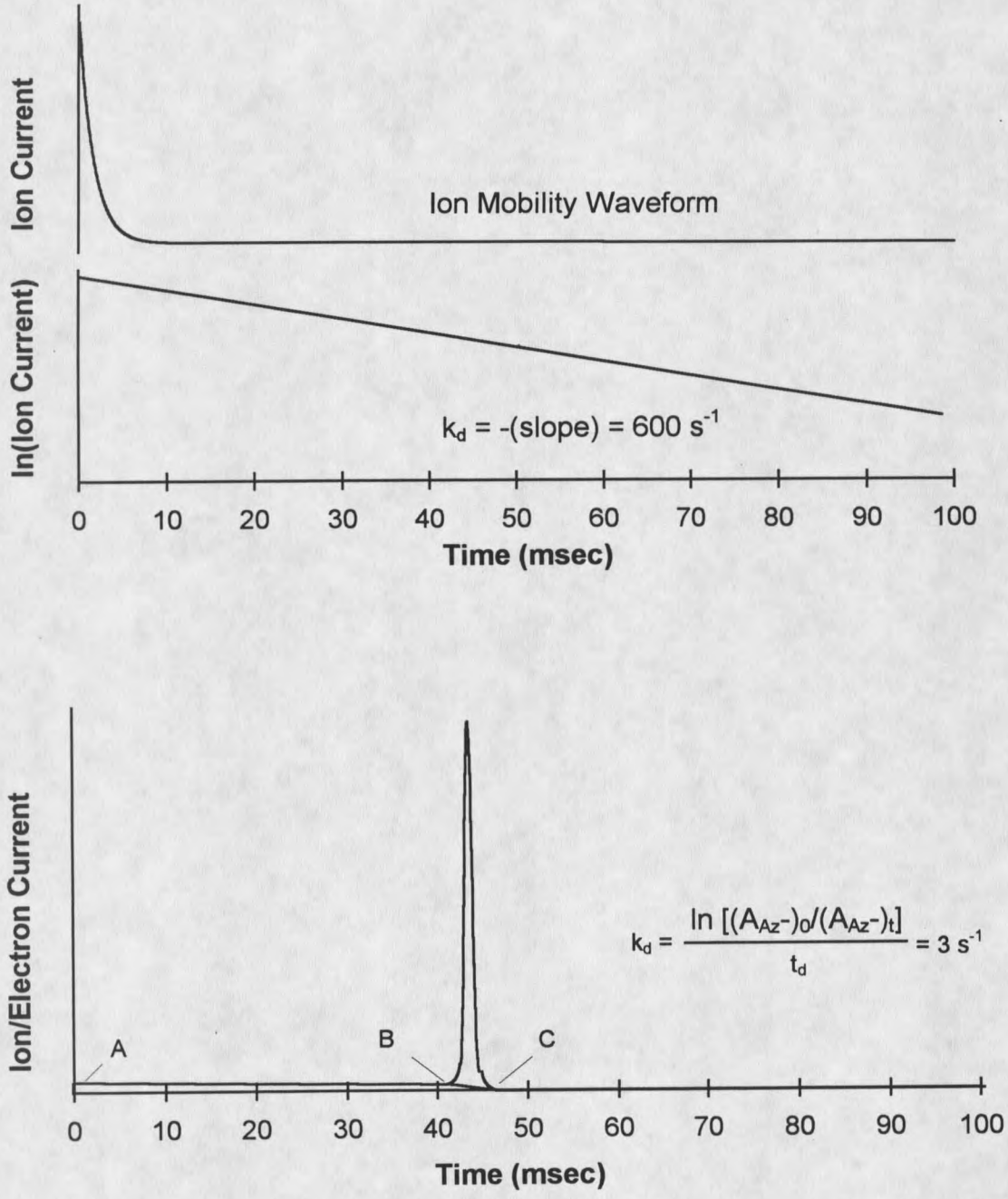

Figure 14. Modeled waveforms A and C from Figure 13 illustrating the methods used to determine rate constants, k_d, for first-order processes. Waveform A and resulting kinetic analysis applied at high temperatures and waveform B at lower temperatures.

Here, $(A_{Az^-})_0$ is the total area under the waveform from point A to point C in Figure 14, $(A_{Az^-})_t$ is the area under the azulene peak (area under the waveform between points B and C) and t_d is the arrival time of the packet of Az^- ions.

Thus, these methods of analysis, applied to ion mobility spectra obtained using the IM-MS, are expected to result in TED rate constants for Az^- over a range of temperatures. Also, determinations of k_d by either measuring the slope or the relative areas of an experimental ion mobility waveform should be possible at intermediate temperatures, such as waveform B in Figure 13. This could be a test for verifying the occurrence of first-order processes throughout the lifetime of Az^- in the drift tube and would show that these methods are self-consistent.

Three ion mobility waveforms obtained from the TED of azulene anions in the drift tube at 94, 124 and 154 °C are given in Figure 15. A comparison of these waveforms with the model waveforms in Figure 13 indicates good qualitative agreement with prediction but also reveals additional peaks not accounted for in the model. Additionally, kinetic analysis of higher temperature waveforms initially resulted in marked deviations from first-order behavior in contrast to the model illustrated in Figure 14. These additional peaks and deviations in kinetic behavior can be traced to modifications in the original waveforms due to chemical, physical and instrumental effects occurring in these IM-MS experiments. Understanding and accounting for these effects is essential to analysis of TED process at high and low temperatures.

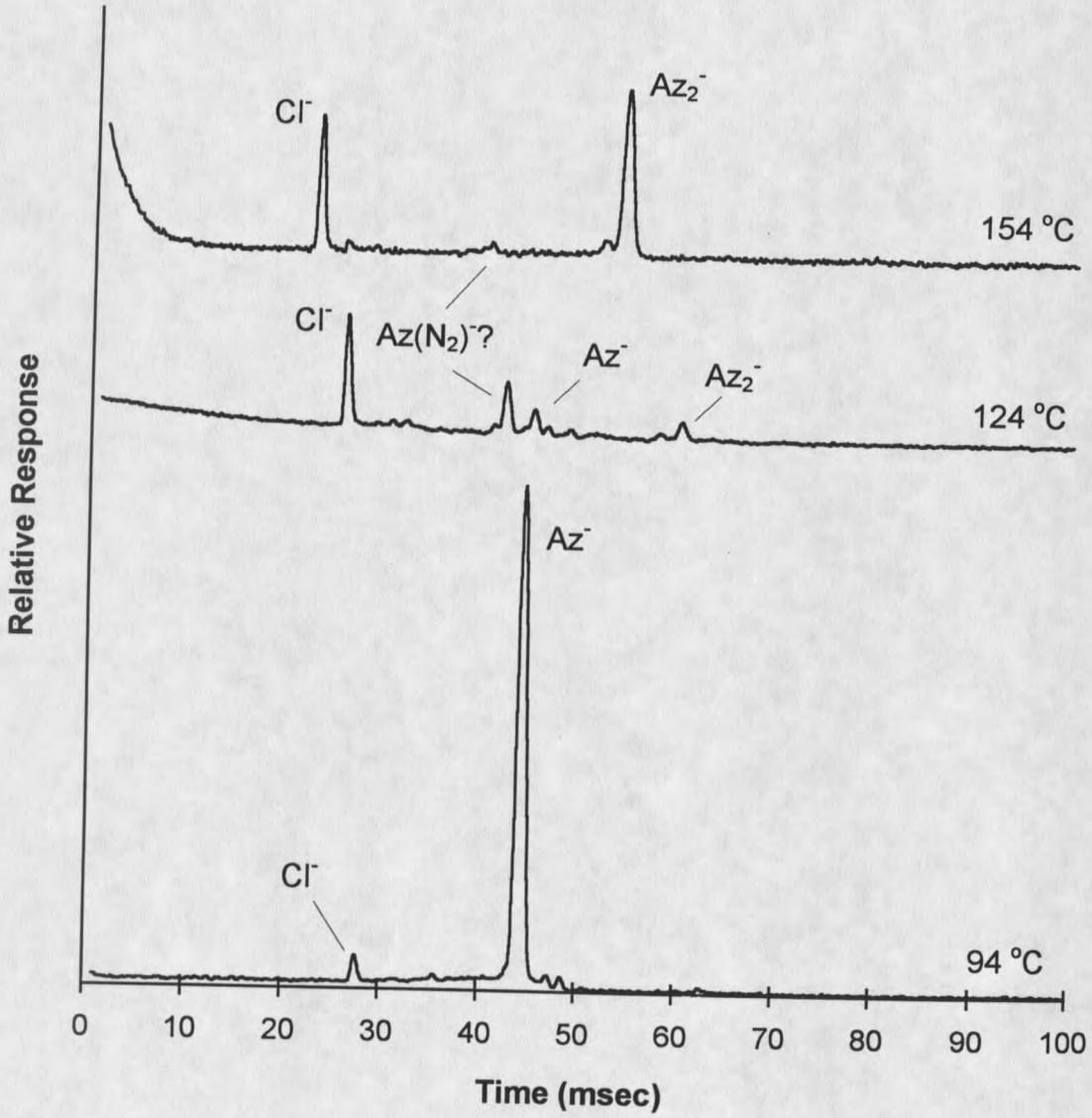

Figure 15. Three ion mobility waveforms obtained using the IM-MS at 94, 24 and 154 °C. Pressure = 740 Torr, electric field strength = 200 V cm^{-1}.

Instrumental Effects on TED Waveforms

The acquisition and analysis of waveforms using IM-MS was initially found to be complicated by a number of instrumental parameters. These consisted of reduced electron signal at high temperatures, waveform shapes dependent on drift and carrier gas flow rates, TED rate constants, k_d, measured at high temperatures remaining constant with increasing temperature and k_d being dependent on electric field strength. Determining the conditions under which reliable waveforms could be obtained and resolving these apparent non-first-order effects were essential before acquisition of meaningful data for kinetic analysis.

The rapid decrease of thermal electron signal at temperatures > 175 °C was assumed, and later verified by calculation, to be due to the high first-order decay of the packet of azulene anions at high temperatures. At these high TED decay rates, the packet of Az^- anions is virtually depleted of anions in the few milliseconds it takes to traverse the ~ 1 cm distance from the source to the BN gate. This observed loss of ion signal resulted in a practical upper temperature limit for this investigation of ~ 175 °C. While investigating this effect, it was noticed that the ion and electron signals measured at the Faraday plate were much lower in intensity than signal levels observed in previous studies (S_N2 investigations, for example) and that not all electrons in the ^{63}Ni ion source were captured to form Az^- anions. In previous applications of IM-MS, the reagent anions were usually Cl^-, which was obtained by dissociative electron capture of carbon tetrachloride (CCl_4) in the ^{63}Ni ion source. Prior to the introduction of any electron capturing species into the ion source, the free source electrons could be detected at the Faraday plate as an intense peak at very short drift times whenever the BN gate

was opened. This signal was normally observed to drop to zero whenever strongly electron capturing species, CCl_4, for example, were introduced into the source. However, the introduction of azulene vapor into the source caused only a very minor drop in this electron signal. This indicated that the ^{63}Ni source was not saturated with Az^- ions, leaving a substantial concentration of free source electrons. In order to obtain higher levels of Az^- in the source, the source carrier gas flow rate was increased, thereby bringing a greater amount of azulene vapor into the source. While this did result in an increase in Az^- signal, it also resulted in a distortion of the exponential peak shape at short drift times. This was attributed to the presence of a high concentration of azulene neutrals in the drift tube near the source caused by penetration of the carrier gas into the drift tube due to the increased carrier gas flow rate. The resulting peak distortion while the ion packet was in this region of high neutral Az concentration was attributed to an attenuation of the Az^- TED rate due to electron detachment and re-attachment processes. The extent of carrier gas penetration, and peak distortion, was found to be reduced by either increasing the counter-flowing drift gas flow rate or by decreasing the source carrier gas flow rate. The carrier gas and drift gas flow rates were adjusted to obtain the highest signal intensity without distortion of the ion mobility waveforms and were set to 25 and 700 sccm, respectively. The only other parameter that was anticipated to result in a higher concentration of azulene in the source was the temperature of the vial containing the azulene crystals; this was optimized at 80 °C. Rate constants were measured and observed to remain constant over the range of these variable changes. A condition in which the ^{63}Ni source was unsaturated (not all source electrons converted to ions) was thus unavoidable in these experiments. While

optimizing these parameters was important, it was also important to resolve the apparent non-first-order behavior at high temperatures (k_d remaining constant) and with changing electric field strength (k_d did not remain constant) if IM-MS was to be useful in this investigation.

The cause of the unchanging rate constant with changes in temperature at higher temperatures was discovered while considering the possible effects that an unsaturated source might have on experimental results. Due to this condition of unsaturation, the exponential decay observed at very short drift times is due not only to thermally detached electrons from the Az^- packet, but also to excess source electrons released from the source while the BN gate was open. The signal from these two sources of electrons, however, should appear different due to their origin. It was expected that the arrival time distribution of the highly mobile, source-generated electrons would closely reflect the opening and closing of the BN gate while the arrival of the electrons generated by TED would be delayed due to the finite rate of thermal detachment from the Az^- ions. In attempting to differentiate these signals at very short drift times, it was noticed that the signal due to source electrons persisted a few milliseconds after the BN gate had closed. This signal would thus overwhelm any signal due to TED from Az^- at high temperatures. This effect can be seen in Figure 16 which shows the response of the Faraday plate to source electrons and also to electrons originating from TED reactions. The slow response of the Faraday plate to source electrons was found to be due to the electrometer response rate (rise time). Once the rise time was set to 10 μsec (fastest available), the signal due to TED could be detected and rate constants at higher temperatures, up to the temperature limit discussed previously, could be determined. It can be seen in Figure 16 that the decay of

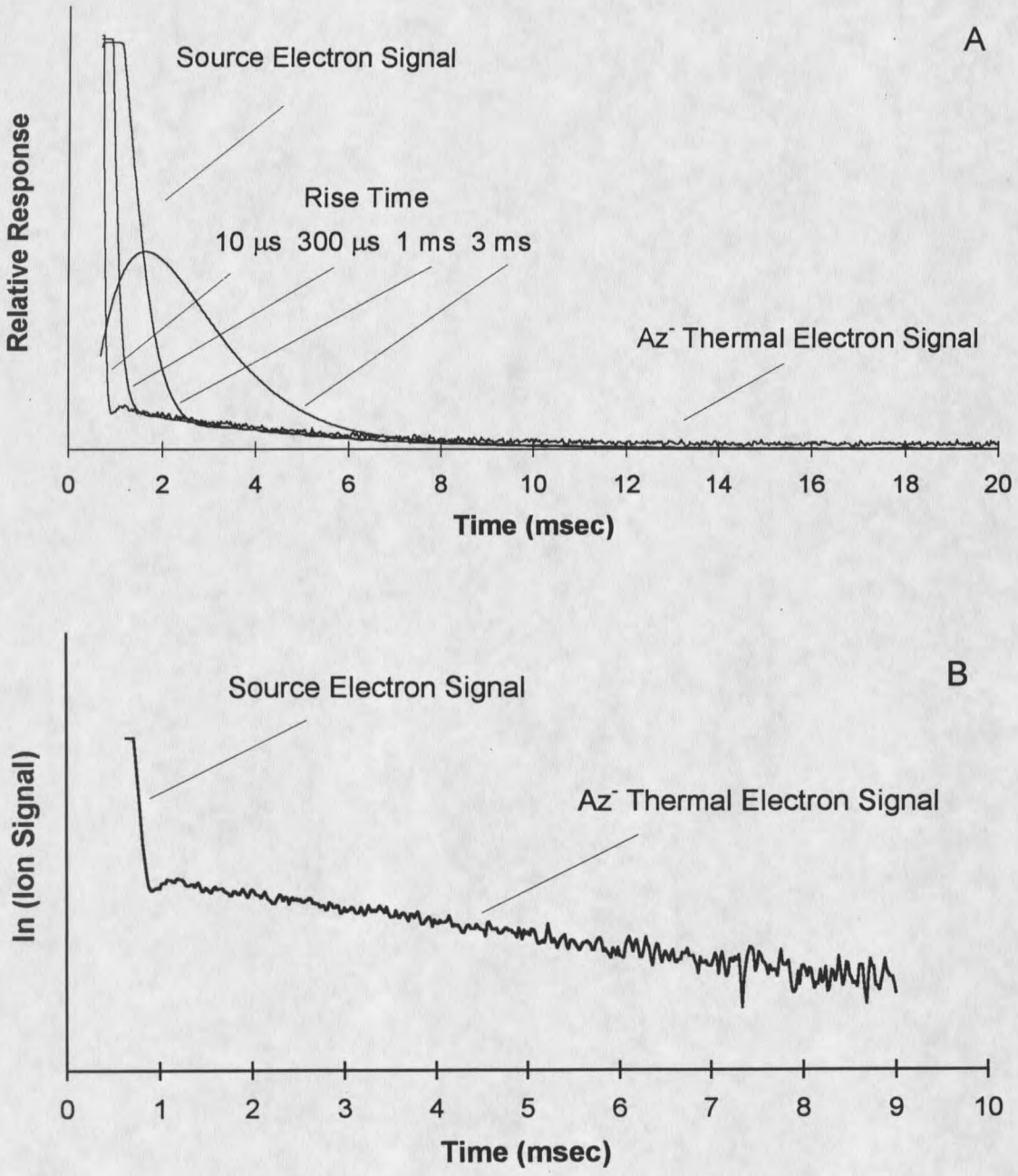

Figure 16. A: IMS waveforms corresponding to TED of Az^- at 144 °C under various settings of electrometer rise time. B: ln (IMS waveform) corresponding to TED of Az^- at 165 °C, slope of these plots give first order decay of source and thermally detached electrons. Signals due to source generated and thermally detached electrons are indicated. Drift tube pressure = 640 Torr, electric field strength = 144 V cm^{-1}.

source electrons as a function of electrometer rise time is exponential. Determining the first-order rate constant for the fastest rise time (10 μsec) in the same manner described previously resulted in a k_r (rise time rate constant) of ~ 10,000 s^{-1}. This effectively defines the upper limit for the study of fast unimolecular processes using IM-MS in its present configuration.

In first-order processes, the reaction time should have no effect on the measured rate constant of the reaction. The reaction time in IM-MS is determined by the residence time of the reagent ions in the drift tube which, in turn, is established by the strength of the applied electric field. If a true thermal, first-order process is occurring, there should be no change in the measured rate constant as a function of electric field. Initially it was found, however, that rate constants changed substantially with electric field strength. This effect is evident in Figure 17 where the measured TED rate constant is plotted (open squares) as a function of electric field at 158 °C. It can be seen that deviations from the true k_d are most evident at low electric field strengths where the signal is usually very weak. This led to the realization that as the exponentially decreasing signal reached the same level as the constant background noise, deviations in linearity in the natural log plot (Figure 14) could be expected. Thus, all ion mobility waveforms were "noise reduced," before kinetic analysis, by subtracting the average background noise from the original signal. The results of this process are indicated by the filled black squares in Figure 17. Also given in Figure 17 are two natural log plots taken from the same waveform; one noise reduced and one not noise reduced.

In this, as in all experiments using IM-MS, it has been assumed that the electric field is not affecting the measured kinetics, even at the highest fields obtainable, due to the very high

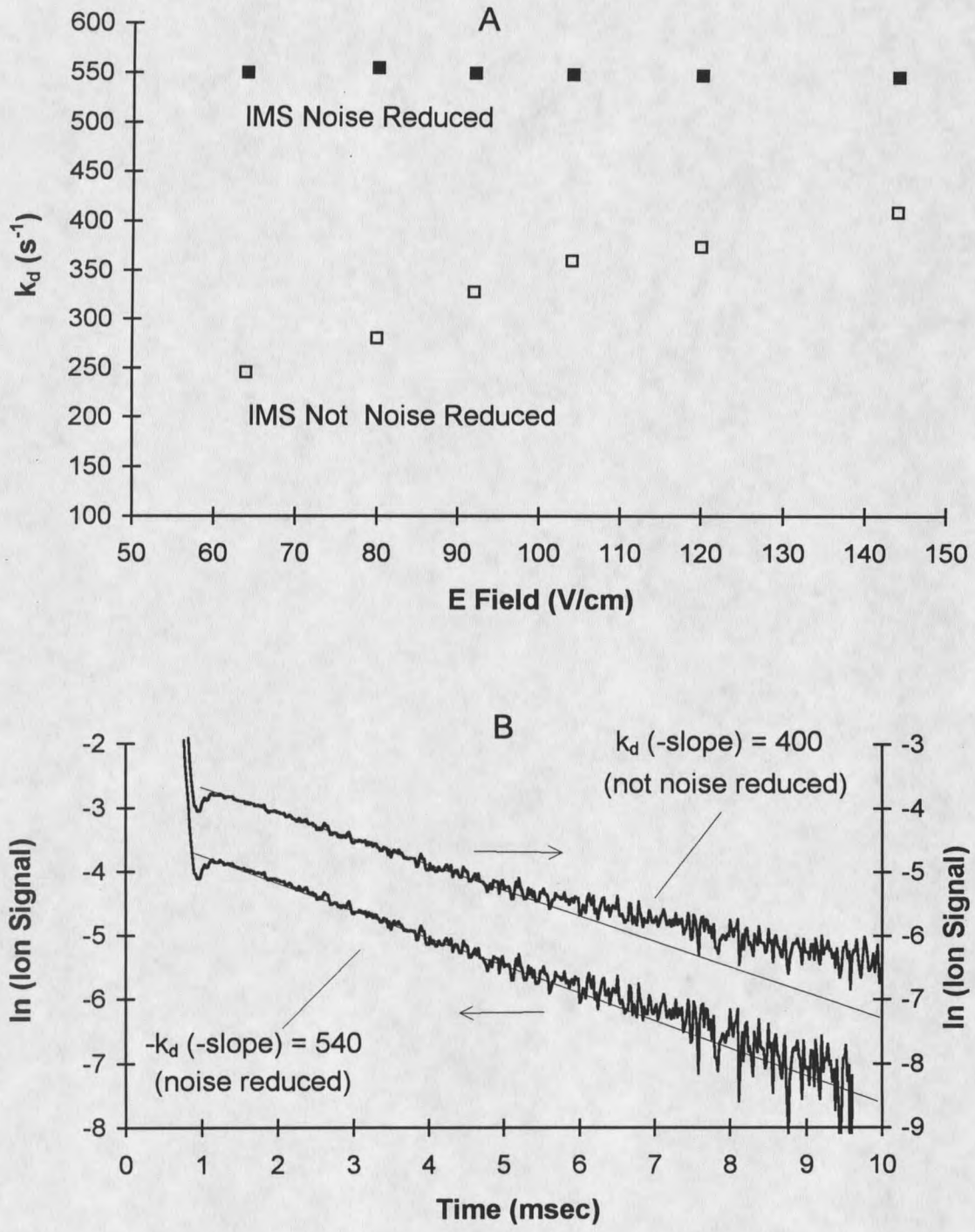

Figure 17. A: Plot of TED first-order rate constants as a function of applied electric field. Open squares not noise reduced, filled squares noise reduced. B: Ion mobility spectra of TED of Az^- at 158 °C. Primary Y axis noise reduced, secondary Y axis not noise reduced. Pressure = 640 Torr, electric field strength in bottom mobility spectra = 144 V cm^{-1}.

buffer gas pressures involved. In their discussion on the mobility of ions in gases, Revercomb and Mason (111) derived a criterion for low-field behavior of ions in an electric field. This was obtained by determining those values of the drift velocity for which the effective temperature of the ions was essentially equal to the temperature of the gas. The necessary criterion thus established for low field behavior at room temperature was an E/N ratio of < 1-3 Td (1 Td = 1 Townsend = 1.0×10^{-17} V cm^2). In Figure 17, the electric field is varied from 64 to 144 V cm^{-1}; at the temperature and pressure used, this corresponds to a variation in E/N of 0.13 - 0.29 Td, well below the established criterion for low field behavior. In the experiments discussed here, both the electric field strength and the gas number density (N, in E/N, above) were varied. Even at the lowest pressure and highest electric field strengths used, 300 Torr and 200 V cm^{-1}, respectively, the E/N ratio, at 0.86, is still well below the low field criterion. It must be mentioned that the derivation of this low field criterion was obtained in the analysis of the mobility of monatomic ions in a buffer gas. It is recognized that partitioning of the electric field energy into internal vibrational and rotational modes in complex molecules, such as azulene, was not addressed. The assumption is made herein that the process responsible for thermalization of the initially excited Az^-* species (due to the electron affinity of azulene) also holds for any excitation processes occurring due to the external electric field. The test of this assumption lies in measurements of the rate constant (for TED in this case) as a function of applied electric field. As noted in Figure 17, the first order rate constant, k_d, for TED is invariant over the electric field strength shown. These studies of instrumental effects helped

establish experimental conditions which resulted in optimum signal intensity and in true first-order behavior at high and low temperatures.

Chemical Effects on TED Waveforms

Inspection of the waveforms in Figure 15 reveals a number of differences from the predicted waveforms in Figure 14. In the low temperature (94 °C) spectrum, the major Az^- peak is evident at ~ 44 msec, but minor peaks at ~ 27 and 62 msec and small shoulder peaks at ~ 48 and 49 msec are also noted. At 124 and 154 °C, the Az^- peaks are diminished while the minor peaks are increased in intensity. The loss of Az^- ion signal at higher temperatures is expected due to faster TED in the drift tube. The identity of the other ions observed in Figure 15 can be determined by inspection of Figures 18 and 19. Figure 18 gives the mobility spectrum and the mass spectrum obtained at 87 °C and Figure 19 gives the same information, as well as the mass selected ion mobility spectra, at 160 °C.

The longer drift times of Az^- (~ 62 msec) and of the minor peak (~ 39 msec) observed in these spectra as compared to those in Figure 15 are due to the lower electric field strength applied in these experiments. It is evident from the mass spectrum in Figure 18 that the minor peak is due to the chloride ion and the major peak is due to the azulene ion. These assignments were based on the isotopic abundance of the $^{35}Cl^-$ and $^{37}Cl^-$ ions and on the known molecular weight of azulene (molecular weight of azulene = 128 amu). Inspection of the ion mobility waveform in Figure 19 at 160 °C reveals three peaks at drift times of ~ 31, 53 and 71 msec. This spectrum also shows the exponentially decreasing slope at short drift times characteristic of high temperature TED processes. The mass spectrum indicates three major ions at 35, 158

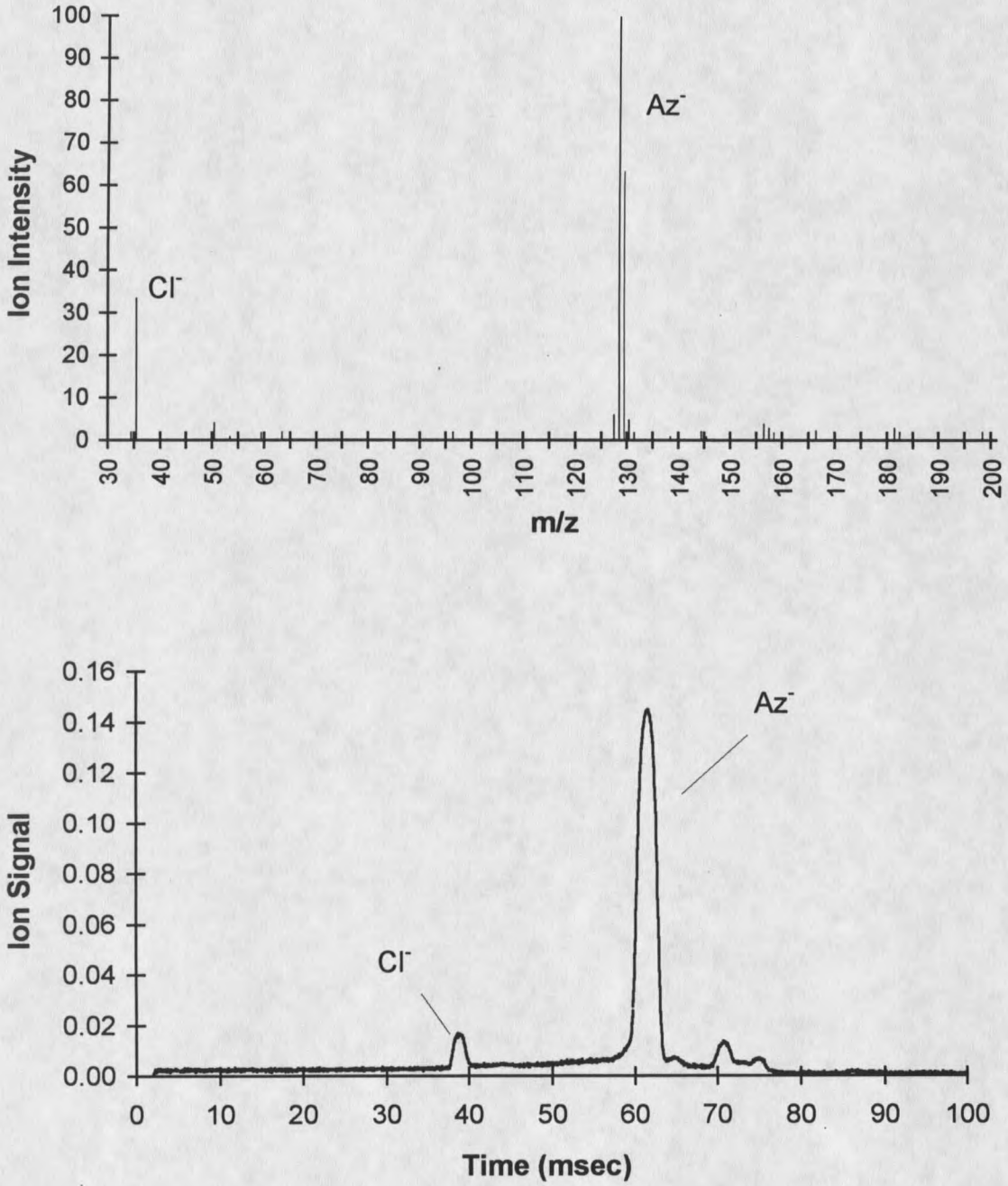

Figure 18. Mass Spectrum and Ion Mobility Spectrum of Az^- TED at 87 °C. Pressure = 640 Torr, electric field strength = 144 V cm^{-1}.

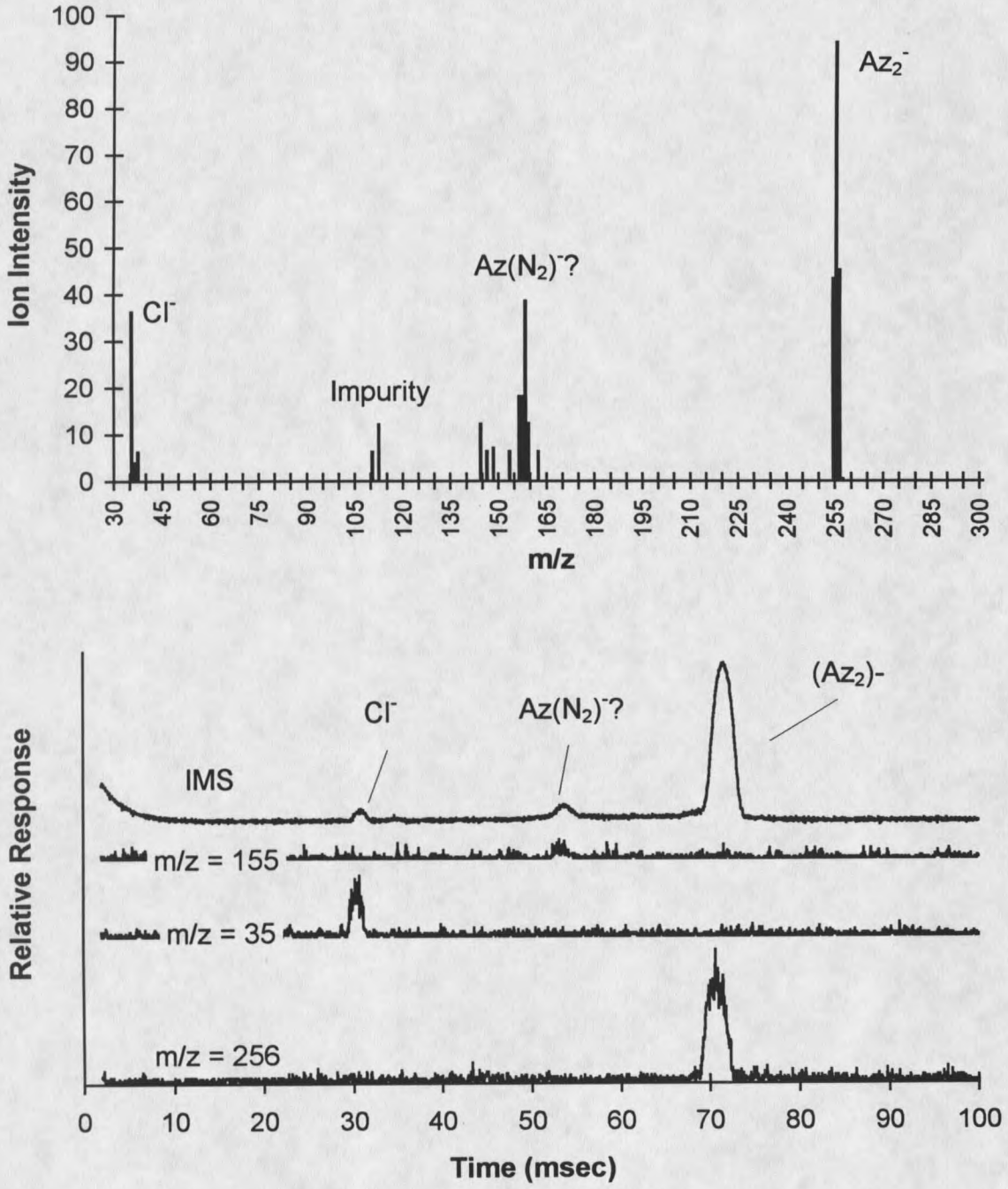

Figure 19. Mass Spectrum and Ion Mobility Spectrum with associated Mass Selected Ion Mobility Spectra of Az^- TED at 160 °C. Pressure = 640 Torr, electric field strength = 144 V cm^{-1}.

and 256 amu and a minor ion at 114 amu. The location of these ions in the ion mobility spectrum was determined using the mass spectrometer in the single ion monitoring mode. It is evident from the mass selected ion mobilty spectra (MSIMS) that the ions of mass 35, 156 and 256 are responsible for the peaks in the ion mobility spectrum at 31, 53 and 71 msec, respectively. The peak at 31 msec is due to chloride ions and the peak at 53 msec was attributed to an impurity or to the possible formation of the $Az^-(N_2)$ adduct species. The fact that this peak is evident at 160 °C and is less intense at 87 °C indicates that it is most likely not due to formation of the $Az^-(N_2)$ adduct and is probably due to an impurity. The peak at 71 msec is either an azulene adduct, $Az^-(Az)$, or an azulene dimer, Az_2^-, in the case of the ion at 256, by coincidence of the molecular weight with these likely species. The lack of any ion of mass 128 amu is apparent in the mass spectrum and indicates the loss of Az^- due to TED processes at this high temperature.

Physical and Chemical Effects of the Buffer Gas on TED Waveforms

The effect of buffer gas pressure on the appearance of ion mobility waveforms can be seen in Figure 20 and the effect of buffer gas composition (CH_4 versus N_2) can be seen in Figure 21; both at high and low temperatures. The waveforms in Figure 20 show the same differences at high and low temperatures observed previously (Figure 14), regardless of buffer gas pressure. The increased drift time of all ions due to higher buffer gas pressures is observed and is in accordance with the expression for ion mobility (equation 8). While the applied electric field was the same at 740 and 1100 Torr (200 V cm^{-1}), the occurrence of electrical breakdown ("arcing") limited the field potential at 300 Torr to 160 V cm^{-1}. This means that

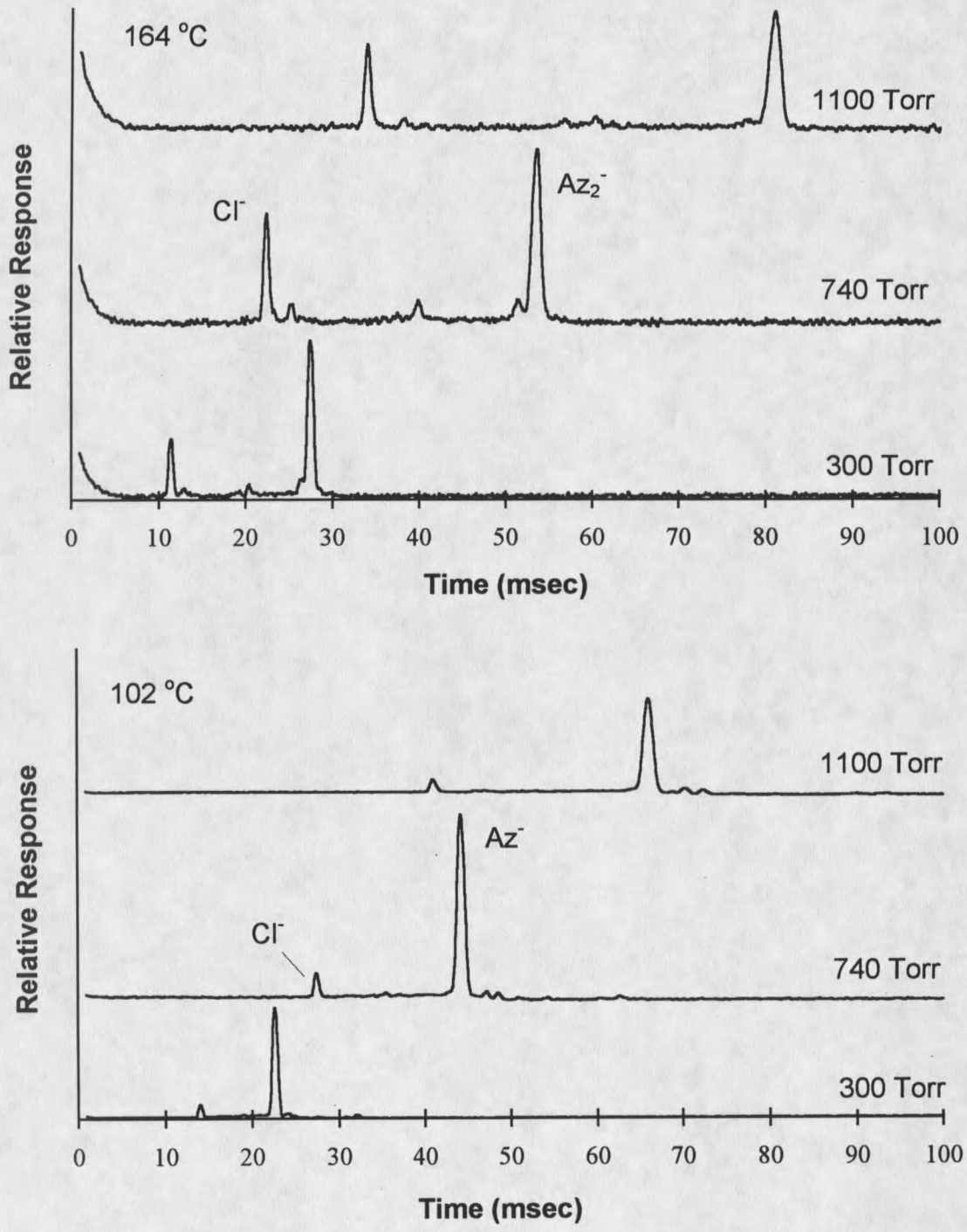

Figure 20. Series of IMS waveforms at 164 and 102 °C at 300, 640 and 1100 Torr drift tube pressure (N_2). Electric field strength = 200 V cm^{-1} at 740 and 1100 Torr and 160 V cm^{-1} at 300 Torr.

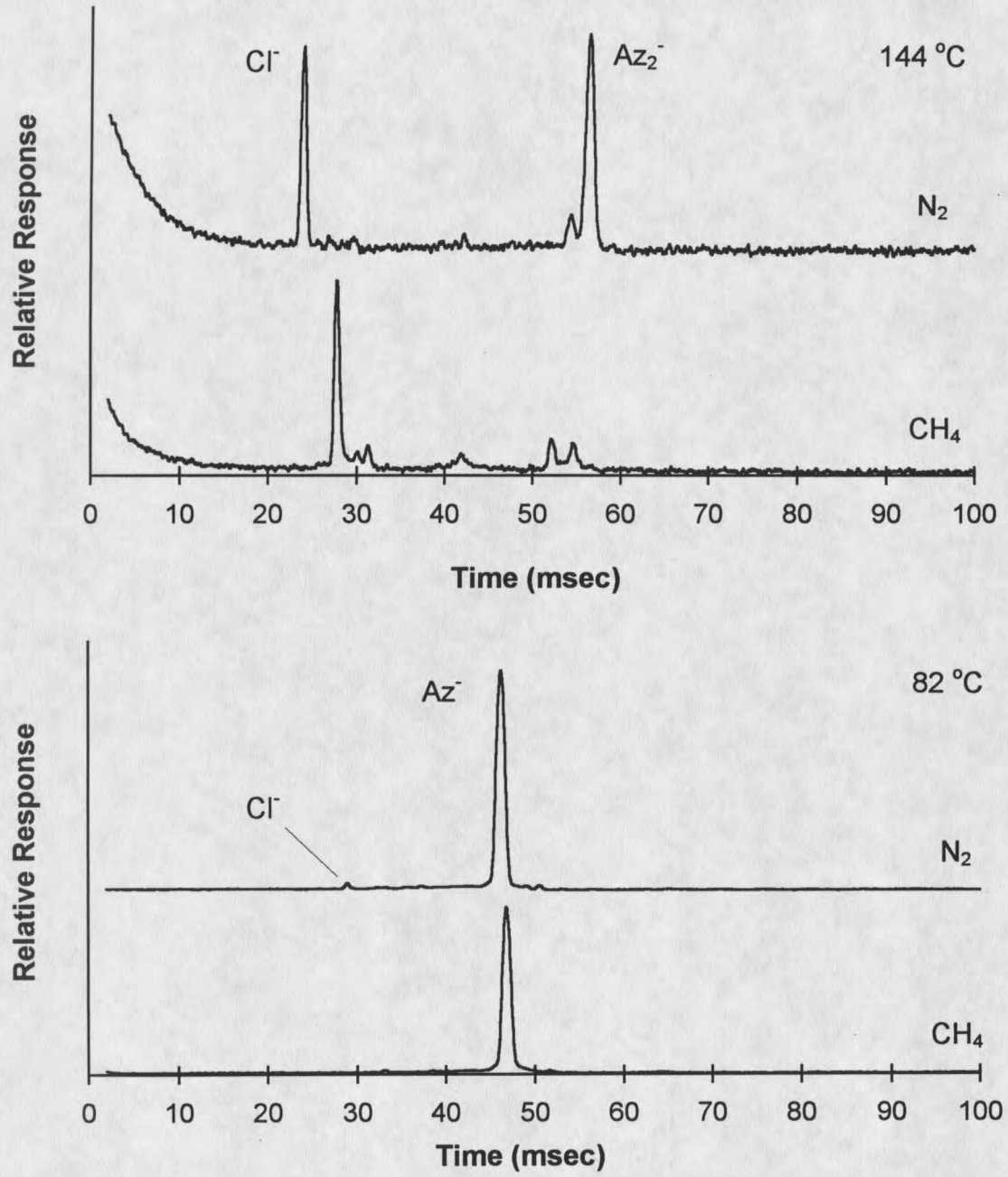

Figure 21. Ion mobility spectra of Az^- TED in CH_4 and N_2 buffer gases at 82 and 144 °C. All spectra obtained at 740 Torr pressure and 200 V cm^{-1} applied electric field.

the difference in drift times at 740 and 1100 Torr is due only to changes in ionic mobility while the change at 300 Torr is due to the change in mobility and electric field strength. Also, increases in buffer gas pressures were observed to result in improved signal intensity due to increased concentration of Az^- in the source region.

The possibility that chemical, as well as physical, interactions between the buffer gas and Az^- ions could be influencing the kinetics of TED was investigated by carrying out TED rate constant measurements using CH_4, instead of N_2, as a buffer gas. Inspection of Figure 21 shows no observable difference in spectra between these two buffer gases at low temperature while the loss of the major ion at ~ 58 msec in CH_4, as opposed to N_2, is very evident at higher temperature. Also, the total waveform in CH_4 at both high and low temperatures appears to be more compressed than those obtained in N_2. Unfortunately, it was not possible to analyze the contents of the drift tube using the mass spectrometer with CH_4 as the buffer gas due to instability of the electron multiplier and quadrupole analyzer at these relatively high CH_4 buffer gas pressures. In both the high and low temperature experiments, CH_4 was used both as the drift gas and as the source carrier gas.

Helium and argon were also investigated with the assumption that the interactions of these gases with Az^- could be much different than with CH_4 or N_2, which might be imagined to behave similarly. However, these gases proved to be unsuitable for use with IM-MS in its present configuration due to severe problems with electrical discharge in the source region or to a complete loss of electrons, in the case of helium, assumed to be due to elastic scattering.

Results and Discussion

The preceding investigations have revealed the limitations for investigating the TED of Az^- and have resulted in conditions within which reliable ion mobility waveforms can be acquired. The experimental parameters under which rate constants for the TED of Az^- over the temperature range 82 to 174 °C and over the pressure range 300 to 1100 Torr were obtained are summarized in Table 3.

A series of ion mobility waveforms representing high and low temperature TED processes under the conditions listed in Table 3 are given in Figure 22. Subsequent kinetic analysis according to the methods outlined in Figure 14 allowed the determination of k_d values for the TED of Az^-. The areas under the low temperature waveforms due to the Cl^- and

Table 3.

Experimental Conditions for the Measurements of the Thermal Electron Detachment Rate Constant of Azulene$^-$.

Parameter	Setting
IMS Tube Temperature	82 - 174 °C
Az Vial Temperature	80 °C
Source Temperature	80 °C
Drift Tube Pressure	300 - 1100 Torr
Drift Gas Flow Rate	700 sccm
Carrier Gas Flow Rate	25 sccm
Electrometer Rise Time	10 μsec
Electrometer Gain	10^9 - 10^{10} V/A
Time per Channel (2000 Channels)	2 - 50 μsec
Electric Field Strength	40 - 200 V/cm

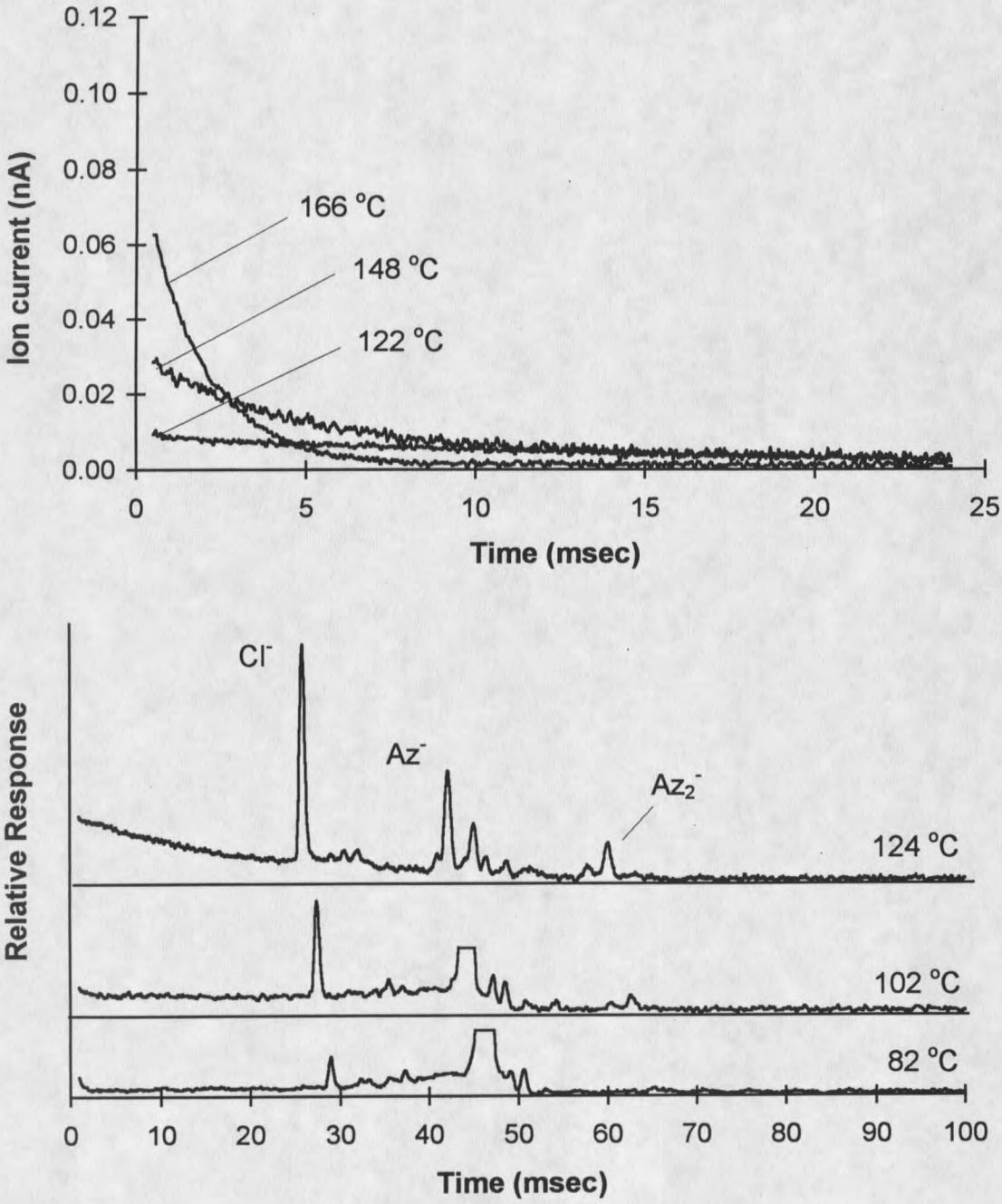

Figure 22. A series of IMS waveforms corresponding to TED of Az^- at high (166, 148 and 122 °C) and low (82, 102 and 113 °C) temperatures used in determining the rate constants for the TED of Az^-. The areas in the low temperature waveforms due to Cl^- and impurity peaks were subtracted from the areas due to $(Az^-)_0$ and $(Az^-)_t$ in determining rate constants. The high Az^- peak was truncated at equal levels to reveal low level details at 82 and 102 °C.

impurity species were subtracted from the areas of interest, if necessary, in all measurements. At the lowest temperatures, these "noise" areas were significant fractions of the Az^- peak and of the baseline area. Table 4 shows the results of TED rate constant measurements over the high, ambient and low pressure ranges at all temperatures used as well as those measurements determined by Grimsrud et al. using a PHPMS (47) and by Mock et al. using a PDM-ECD (46). These results are also presented graphically in Figure 23. The data given by Kebarle et al. was published in terms of the activation energy and pre-exponential factor; the analytical expression in Figure 23 is obtained when these parameters are expressed in standard Arrhenius form over the temperature range indicated.

Table 4.

Thermal Electron Detachment Rate Constants of $Azulene^-$ Using IM-MS, PDM-ECD and PHPMS[a].

Temp.	IM-MS Pressure: (N_2)			IM-MS Pressure: (CH_4)			PDM-ECD	PHPMS
(°C)	300	740	1100	300	740	1100	2 atm.	4 Torr
82	3.12	3.30	3.14	5.98	6.11	5.05	-	25
94	8.39	7.94	7.83	8.25	9.68	7.52	-	51
102	13.4	13.6	13.3	18.8	20.8	20.8	-	81
113	28.2	25.9	25.3	-	-	-	-	147
124	62.1	58.5	57.5	66.8	59.0	58.1	-	259
135	126	109	89	-	-	-	105	446
143	230	216	159	269	251	167	200	643
154	406	348	292	-	-	-	310	1048
164	803	693	614	-	-	-	460	1601
174	1247	1082	1013	-	-	-	710	2400

[a]Estimated uncertainty at high temperature (>124 °C) = ± 10%

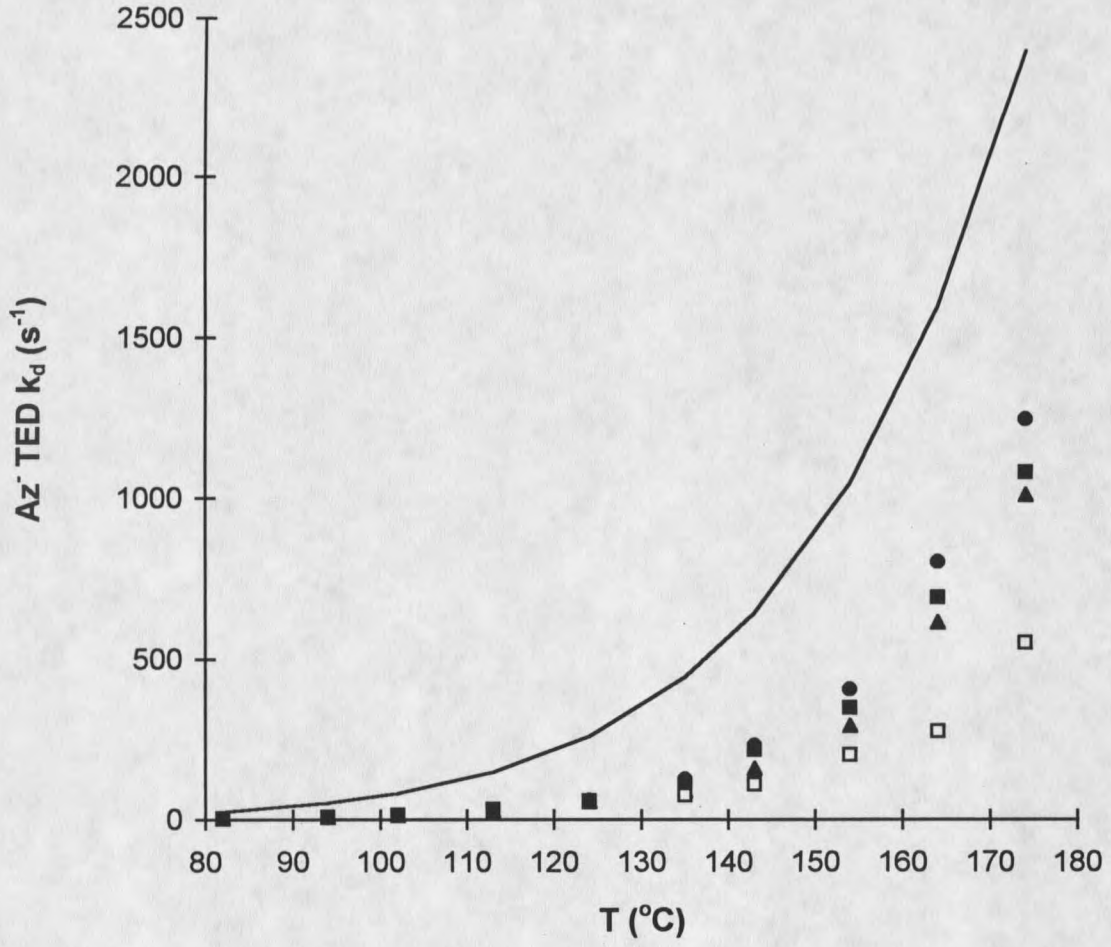

Figure 23. Az^- TED rate constants as a function of temperature, pressure and experimental method. Analytical expression for PHPMS is derived from Arrhenius data and given as a solid line. Open squares are PDM-ECD, filled triangles, squares and circles are IM-MS at 1100, 740 and 300 Torr, respectively.

The IM-MS data in Table 4 taken at 740 Torr are plotted in Figure 24 in the form of Arrhenius plots according to equations 25 and 26.

$$\ln(k_d) = \ln A - E_A/RT \tag{25}$$

and

$$\ln\left(k_d T^{-3/2}\right) = \ln A - E_A/RT \tag{26}$$

Equation 26 is derived from the expression for the thermal electron detachment-attachment equilibrium constant expression given in equation 27.

$$K_{eq} = \frac{k_a}{k_d} = 2\left(\frac{2\pi m_e kT}{h^2}\right)^{-3/2} \exp\left(\Delta S^o/R + E_A/RT\right) \tag{27}$$

Equation 27 is obtained from transition state theory (equation 5) where the first term on the right hand side is the partition function for an electron and the ratio of the partition functions for Az^- and Az is given by $Q_{az^-}/Q_{az} = \exp.(\Delta S^o/R)$ (49, 120). The change in entropy, ΔS^o, for the TED of Az^- has been experimentally determined (115) as has the rate of thermal electron attachment, k_a, (120) and both are assumed to be independent of temperature. Thus, a more accurate determination of the activation energy for electron detachment of azulene should be obtained with the use of equation 26 (temperature dependence of the pre-exponential A term accounted for). The activation energy and the pre-exponential A terms determined from the slopes of the Arrhenius plots in Figure 24, and also from Kebarle et al., are compiled in Table 5. Due to the large uncertainty in measuring the areas under the waveforms at low

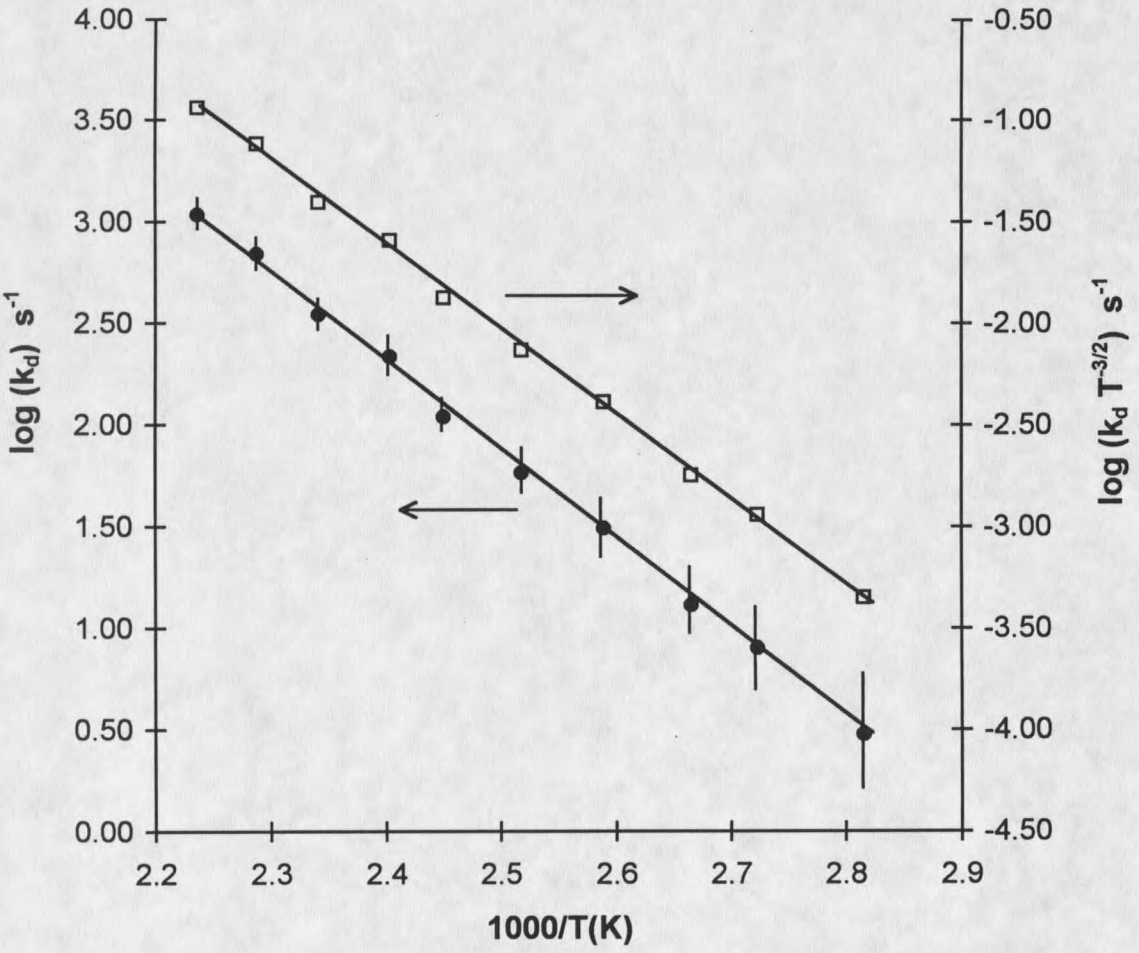

Figure 24. Arrhenius plots of the IM-MS data taken at 740 Torr in Table 4. An explanation of the two methods of analysis is given in the text. Estimated error bars included for log plot.

temperature, it was decided not to include the rate constants determined at the five lowest temperatures in the calculation of the activation energy from the Arrhenius plots. These data points are included on the Arrhenius plots for completeness; estimated error bars indicate the relative uncertainty. The uncertainty at low temperatures ranged from ~ 100% at 82 °C to ~ 15% at 124 °C. The estimated uncertainty of the rate constants measured at high temperatures was less than ± 10%.

Table 5.

Activation Energy (E_A) and A Terms for the Thermal Electron Detachment of Azulene$^-$.

IM-MS	log ($k_d T^{-3/2}$)		log (k_d)	
Pressure (Torr)	E_A (kcal mol^{-1})[a]	log A	E_A (kcal mol^{-1})[a]	log A
300	20.1	8.94	21.3	13.54
640	19.7	8.73	21.0	13.32
1100	21.4	9.52	22.7	14.12
PHPMS	14.5	6.39	16	11.05

[a]Estimated uncertainty = ± 2.0 kcal mol^{-1}

Inspection of the data in Table 5 reveals that the activation energies obtained for the TED reactions measured using IM-MS are substantially greater than those (assumed to be equal to electron affinities, EA) obtained with the PHPMS and PDM-ECD. A slight increase in activation energy is noted from low to high pressures in the IM-MS data, as expected, but is within experimental error. Also, there does not seem to be a significant difference in kinetic parameters obtained with or without consideration of a pre-exponential temperature dependence. Inspection of Figure 23 and Table 4 reveals that the rate constants of TED

obtained using IM-MS are intermediate between those obtained using PDM-ECD and PHPMS and that a small pressure dependence is evident within the 300 to 1100 Torr pressure range. Because these differences in rate constants and Arrhenius parameters may depend on chemical, rather than physical, effects, it is important to consider the origination of the chemical species observed in IM-MS spectra in more detail..

If the TED rate constants for Az^- are dependent on pressure through increased interactions with some chemical species, x, then these species, $Az^-(x)$ should be detected either by the Faraday plate or by the attached mass spectrometer. It is recognized, however, that absolute determinations of the presence of chemical species in the drift tube using only the mass spectrum is not unambiguous. Adiabatic cooling and collisionally induced dissociation (CID) in the jet of the mass spectrometer can give rise to the formation of new chemical species or dissociate species that were stable in the drift tube. These limitations will be considered where species created in the jet may be likely. The mass spectrum and mass selected ion mobility spectrum obtained previously at 160 °C (Figure 19) indicated the presence of three ions of mass 35, 156 and 256 amu; these ions will be considered here in more detail.

The ion at nominal mass 35 has been identified previously as Cl^- and results from chlorinated impurities present in the IM-MS. A number of mass selected ion mobility spectra (not given) have revealed that the ion at mass 156 appears at two slightly different drift times in ion mobility spectra. The arrival time of one of these ions was identical to that observed for Az^- while the other was shifted to longer drift times by ~ 2 msec. Due to the limitations in mass spectrometry mentioned previously, it was not possible to unambiguously attribute the

equal ion arrival times of Az^- and $Az^-(N_2)$ to the formation of $Az^-(N_2)$ in the drift tube. Ions of this mass are most likely formed in the jet region of the mass spectrometer, although it is recognized that their existence in the drift tube under high N_2 buffer gas pressures is very likely. The second ion of mass 156 arriving at slightly longer drift times is an impurity of unknown origin. The ion of high intensity at a drift time of ~ 71 msec has a mass of 256 which corresponds to a species consisting of two azulene molecules; which could be either an adduct species, $Az^-(Az)$, or a dimer, Az_2^-, of azulene. The increased intensity of this ion with temperature indicates that the major ion contributing to this signal is not an adduct. Further support of the formation of an azulene dimer is given by Scott (122) in his proposed radical-based mechanism for the thermal rearrangement of azulene to naphthalene. The mechanism he proposed involved the formation of radical dimers of azulene in the steps initiating rearrangement and the production of the neutral azulene dimer as the step terminating the reaction. The observed loss of the dimer in CH_4 (Figure 21) can also be explained by loss of the radical intermediates involved in dimer formation by interaction with the CH_4 buffer gas. It is uncertain whether or not the dimer is formed in the source or in heated vial. The lack of the dimer in the CH_4 experiment may indicate that the species is formed in the source where radicals from the CH_4 buffer gas could interfere with the production of the dimer. While the dimer is thus considered to be the predominant species, a slight connectivity observed in some spectra between the Az_2^- species and the Az^- peak implies that some adduct forming reactions with Az^- might be occurring in the tube to a very small extent. While a large concentration of adduct would influence the kinetics of TED, the very small concentration observed is assumed

to have no significant effect. In addition, the sharp form of the Az_2^- peak indicates its origination in the source and relative stability in the drift tube.

It is suggested that the dependence of the TED rate constants on buffer gas pressure is due to the equilibrium formation of adduct species according to reaction 28.

$$Az^- + M \rightleftharpoons Az^-(M) \qquad (28)$$

Here, M is a buffer gas species such as N_2 or CH_4, both of which were used in the IM-MS; N_2 was used in the PDM-ECD and CH_4 was used in the PHPMS. Higher buffer gas pressures would result in a higher concentration of adduct, $Az^-(M)$, species due to the higher concentration of buffer gas molecules, M. It is envisioned that the Az^- ion is stabilized towards TED by the association energy of the adduct species and by the average fraction of its occurrence (lifetime) as the $Az^-(M)$ species. No literature values have been found for the $Az^-(N_2)$ or $Az^-(CH_4)$ species although the interaction is assumed to be weak and, if present, their relative intensities would be altered in the sampling aperture of the mass spectrometer.

While these chemical interactions might be responsible for the observed differences in TED, it is important to also consider the physical processes involving the TED of Az^-. The processes considered here are thermalization of the initially excited azulene species, Az^-*, and the maintenance of a continuous gausian (thermal) distribution of Az^-. Both of these processes are described in reaction 29

$$Az^- \underset{k_q[M]}{\overset{k_b[M]}{\rightleftharpoons}} Az^-* \xrightarrow{k_{auto}} Az + e^- \qquad (29)$$

where $k_b[M]$ is the rate of replenishment of the Az^{-}* species, $k_q[M]$ is the quenching rate of Az^{-}* and k_{auto} is the autodetachment rate constant. Due to the high and very high pressure buffer gases involved, it has been assumed in IM-MS, PDM-ECD and in PHPMS that thermalization is complete and maintenance of a gausian distribution of Az^{-} ions is continuous. Kebarle et al. (47) assumed that the activation energy (E_A) for the detachment of thermal electrons was equivalent to the electron affinity (EA) of azulene based on complete thermalization of the Az^{-}* species. These assumptions are supported by the fact that any inefficiencies in these processes of thermalization and gausian maintenance would result in an increase of the rate constant for TED, rather than the observed decrease in rate constant with pressure. Thus, it is apparent that the observed decrease in TED rate constants for Az^{-} in very high pressure buffer gases is most likely due to the formation of stable $Az^{-}(M)$ adduct species.

Conclusion

It has been demonstrated that the rate constants for the thermal electron detachment of Az^{-} show a negative dependence on buffer gas pressure in the IM-MS. The decrease in rate constants with increasing pressure is not only indicated by comparisons between other instrumental methods, but also by the change noted over the pressure range used in the IM-MS experiments (300 - 1100 Torr). While these differences over the pressure range used in IM-MS are not large, they are significant in their relative persistence over the temperature range used. The cause of this pressure effect is thought to be the formation of the adducts $Az^{-}(N_2)$ or $Az^{-}(CH_4)$ which would be more stable towards thermal electron detachment.

RATE CONSTANTS FOR THE GAS PHASE REACTION OF CHLORIDE ION WITH METHYLBROMIDE OVER THE PRESSURE RANGE, 300 TO 1100 TORR

As discussed previously, the gas-phase S_N2 reaction of chloride ion with methylbromide has been extensively studied by a variety of experimental and theoretical methods (10, 12, 24, 31, 36-38, 44, 123 - 130) and has become the prototype example of an ion-molecule reaction that is strongly affected by non-statistical energy distributions within its rate determining reaction intermediates (31, 36, 38, 44, 130). This reaction is thought to proceed along a double-well potential energy surface (Figure 1) with a central barrier that separates the entrance and exit channel complexes. Both of the entrance and exit channel ion-dipole complexes have been shown to behave in distinctly non-statistical manners and, therefore, are not well-described by conventional statistical theories of reaction rates, such as RRKM theory (31, 44, 130). As a result, the rate constants observed for this S_N2 reaction have been difficult to interpret in terms of the potential energy surface (for this reaction).

In order to study this reaction under physical conditions in which the complexities described above would be removed, the use of unusually high buffer gas pressure has been envisioned (10, 12, 69). If the buffer gas pressure could be made sufficiently high, a point should eventually be reached where all (rate-determining) reaction intermediates would be maintained in a state of thermal equilibrium with the medium during their lifetimes on the reaction coordinates. This would constitute the high pressure limit (HPL) of kinetic behavior, discussed previously. Under this condition, the reaction complexes could be assumed to have

Boltzman energy distributions and interpretation of the observed rate constants would be greatly facilitated.

Recently, Giles and Grimsrud (12) investigated the reaction of Cl^- ion with CH_3Br by IM-MS and reported rate constants observed under the relatively high pressure conditions of 640 Torr (nitrogen buffer gas) over a temperature range from 35 to 150 °C. A significant enhancement, (roughly, a doubling) of the observed rate constants was noted at 640 Torr at all temperatures relative to the corresponding rate constants determined by a PHPMS using buffer gas pressures of 3 Torr. At 640 Torr, the efficiency (observed rate constant relative to the calculated ADO collision rate constants) of this reaction increased continuously with a decrease in temperature, from about 1.5% at 150 °C to about 3.5% at 35 °C. In interpreting the significance of these rate constants at near-atmospheric pressure, an unresolved question was whether or not these measurements reflected the HPL of kinetic behavior for the Cl^-/CH_3Br reaction system.

Recent theoretical studies of the $Cl^-(CH_3Br)$ and $Br^-(CH_3Cl)$ reaction complexes by Wang et al. (31) have provided additional insight concerning the question raised above. They predicted distinctly non-statistical behaviors and exceedingly short lifetimes for both the entrance and exit-channel ion-complexes. From inspection of the set of mode-specific lifetimes they provided, the average lifetimes of the collision-formed complexes, $Cl^-(CH_3Br)$, might be expected to be even less than the calculated RRKM lifetime of 3 picoseconds. Since the time between collisions of this ion complex with buffer gas molecules at near-atmospheric pressure will be about 50 ps, the theoretical considerations of Wang et al. suggest that the HPL of

kinetic behavior for this reaction could not have been reached in a buffer gas of 640 Torr pressure.

Recent experimental studies of the Cl^-/CH_3Br reaction by Seeley et al. (131) also provide new insight into this reaction. They found that when the entrance-channel reaction complex, $Cl^-(CH_3Br)$, was made by the endothermic ligand exchange reaction, $Cl^-(H_2O) + CH_3Br \rightarrow Cl^-(CH_3Br) + H_2O$, in He buffer gas at a pressure of 0.5 Torr, the complex (thermally) dissociated primarily in the forward direction to form the Br^- ion and CH_3Cl. Since the reaction efficiencies observed by Grimsrud et al. in 640 Torr buffer gas did not exceed 3.5%, the result of Seeley et al. suggests that the entrance channel complexes in this investigation were not efficiently thermalized by collisions and that the HPL had not been reached.

The modifications to the IM-MS (Figure 1) have made it possible to determine rate constants for the reaction of Cl^- with CH_3Br over the pressure range, 300 to 1100 Torr at 125 °C. Additional insight into the dynamics of this reaction has thereby been obtained.

Experimental

The IM-MS instrument and the methods used here are almost identical to those described previously for a typical S_N2 reaction. In the present study, the only experimental change that has been made is that the buffer gas pressure within the IMS was varied from 300 to 1100 Torr. For successful operation at pressures below the ambient level, much greater care was required to eliminate all microscopic leaks in all external connections of the IMS. The major difficulty caused by such leaks was the introduction of trace levels of water, which tends

to cluster to the chloride ion. In order to ensure that this undesirable effect of trace water was not of importance, a relatively high temperature, 125 °C, was always used in the present study. At this temperature, the ratio of the intensity of the $Cl^-(H_2O)$ ion to that of the Cl^- ion (as determined by the associated mass spectrometer) was always less than 0.005.

Results and Discussion

Rate constant determinations made here for the reaction of chloride ion with methylbromide and with n-butylbromide are shown in Figure 25. Each point shown has been determined by the standard IMS method illustrated earlier and was the result of four or more independent IMS measurements using a range of alkylbromide concentrations. The uncertainty of each of these measurements is estimated to be less than +/- 15%.

The rate constants determined for the reaction of chloride ion with n-butylbromide are shown within data set B in Figure 25 and bear no detectable dependence on buffer gas pressure over the pressure range, 300 to 1100 Torr. Also, these rate constants were not significantly affected by a change from nitrogen to methane buffer gas. This result was expected based on prior observations that a change in nitrogen buffer gas pressure from 3 Torr (PHPMS) to 640 Torr (IMS) caused no observable change in the rate constant of this reaction (see Figure 4 of reference (12)). This lack of buffer gas pressure dependence for the Cl^-/n-butylbromide reaction system is consistent with either of two potential explanations. One is that this reaction system is operating within its HPL of kinetic behavior at all pressures of 3 Torr or greater. The other is that the rate constants for this reaction system happen to be the same in the high pressure and low pressure limits. Since the present investigation will focus on the Cl^-/CH_3Br

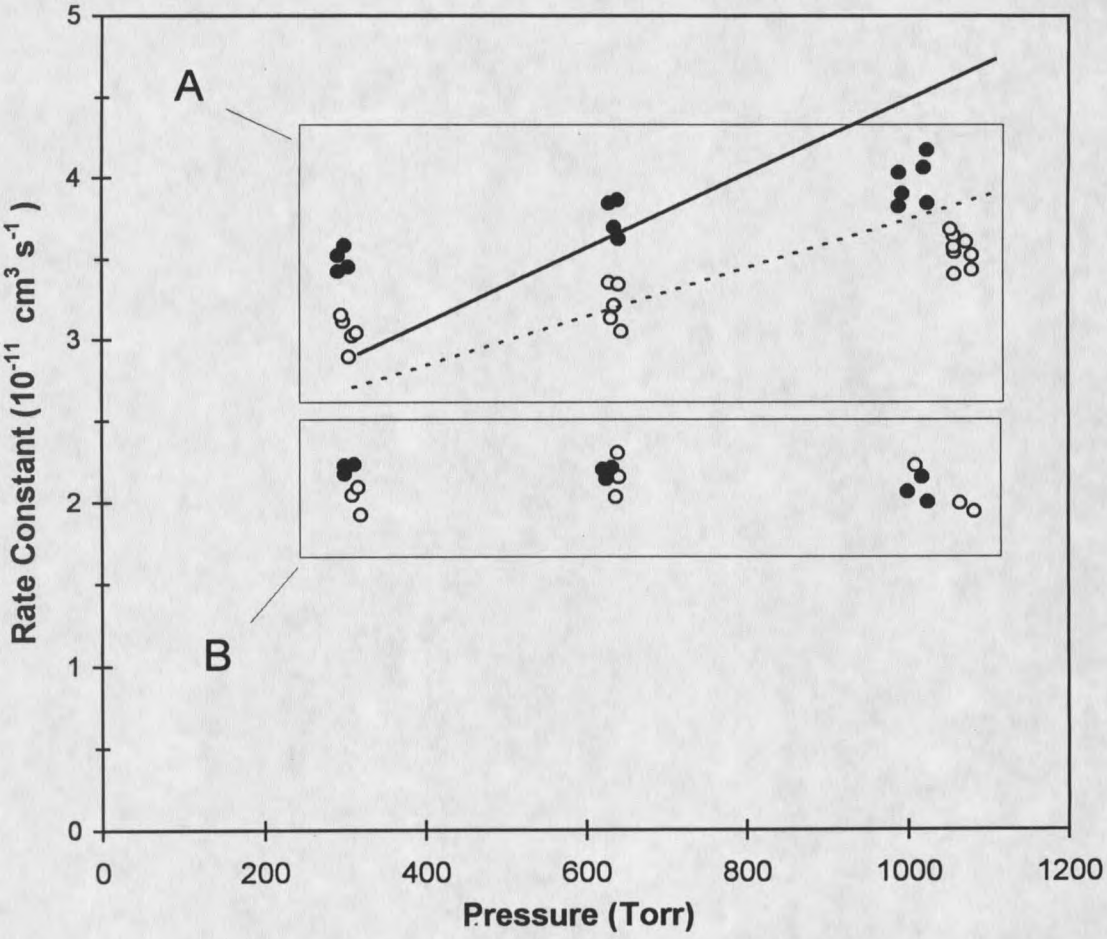

Figure 25. Rate constants observed for the reaction of chloride ion with methyl bromide (rectangle A) and with n-butylbromide (rectangle B) by ion mobility spectrometry at 125 °C as a function of buffer gas pressure. Measurements were made using both nitrogen (open circles) and methane (solid dots) as the buffer gas.

reaction, the set of n-butylchloride measurements provided in Figure 25 serve primarily to validate the experimental method developed here. By this method, no significant pressure dependence was noted for a reaction system that was expected to have none.

The rate constants for the reactions of chloride ion with methylbromide are shown within data set A in Figure 25 and indicates a small, but significant positive pressure dependence. An increase in the pressure of a given buffer gas from about 300 to 1100 Torr causes an increase of about 15% in the rate constant. Both of these observations suggest that the HPL of kinetic behavior has not been reached for the Cl^-/CH_3Br reaction system in the pressure range near one atmosphere.

It is instructive to consider whether the measurements shown in Figure 25 for the Cl^-/CH_3Br reaction system are consistent with the new information concerning this reaction recently reported by Wang et al. (31) and by Seeley et al. (131). A slightly modified version of the Cl^-/CH_3Br reaction shown earlier (reaction 1) is presented here for purposes of discussion.

$$Cl^- + CH_3Br \underset{k_r}{\overset{k_c}{\rightleftharpoons}} (Cl^- \circ CH_3Br)^* \begin{cases} \xrightarrow{k_p} Br^- + CH_3Cl \\ \xrightarrow{k_q[B]} Cl^-(CH_3Br) \longrightarrow Br^- + CH_3Cl \end{cases} \qquad (30)$$

By this sequence, reaction products are envisioned to be formed by two simultaneously operative mechanisms. In both mechanisms, a set of excited entrance channel complexes is first formed at a rate determined by the collisional rate constant, k_c. Since the efficiency of this reaction under the present reaction conditions has been observed to be low, it can be assumed that most of the complexes will backdissociate to reform the reactants, (k_r). A small fraction of

the excited complexes will move forward to form products (k_p). Another small fraction of the excited complexes will undergo collisions with buffer gas molecules and will become thermalized with a pseudo-first order rate constant for quenching, $k_q[M]$, where [M] is the number density of the buffer gas. In accordance with the recent report of Seeley et al., the principal fate of the thermalized complex shown in reaction sequence 30 will be assumed to be dissociation to the reaction products, Br^- and CH_3Cl. Since the ion complex is not detected under our experimental conditions, it can be assumed that this latter step occurs very quickly on the time scale of the IM-MS-based experiment and does not affect the overall rate of this pathway.

For the sake of this discussion, several oversimplifications of the detailed reaction dynamics represented by reaction sequence 30 will be made and the possible implications of these assumptions should be pointed out. One of these is that the rate at which the initially-formed set of entrance channel ion complexes undergo back-dissociation will be described here by a single rate constant, k_r. It is acknowledged, however, that a more rigorous treatment of the backdissociation process would involve a sum of several exponential decay constants representing all of the important mode-specific species initially formed in the ion-molecule collision. In the present study, it is possible that only a subset of the entrance channel complexes that have relatively long lifetimes (smaller k_r's) are being affected by increased buffer gas pressure. Therefore, the simplified model developed here can be expected to provide only a semiquantitative description of the actual events and has validity only to the

extent that the relatively long-lived fraction of the collision-formed complexes constitutes a significantly large portion of the total population.

Another point of oversimplification in reaction sequence 30 is that the passage of $Cl^-(CH_3Br)^*$ over the transition state barrier is shown to lead directly to products. Wang et al. (31) have shown, however, that the exit channel complex, $Br^-(CH_3Cl)^*$, that is first formed upon passage over the transition state is likely to recross the transition state barrier to reform $Cl^-(CH_3Br)^*$. In addition, Wang et al. predict that several such recrossings of the central barrier will then occur prior to the dissociation of one of the two complexes to either reactants or to products. Therefore, the rate constant, k_p, shown in reaction sequence 30 should be viewed to represent the passage over the central barrier only of those entrance-channel complexes that do not re-cross the barrier. In addition, it is recognized that our use here of a single value for k_p is also an oversimplification of a much more complex reality in which a set of mode-specific rate constants would actually be required in a rigorous treatment of the forward motion of the excited entrance-channel complexes along the reaction coordinate.

Within the oversimplified view described above of reaction sequence 30, and with the reasonable assumption that $k_r >> (k_p + k_q[M])$ under our experimental conditions, the observed rate constant, k_{obs}, would be given by:

$$k_{obs} = k_c k_p / k_r + k_c k_q [M] / k_r \qquad (31)$$

Since the rate constant observed for this reaction under buffer gas conditions of relatively low pressure will be given by $k_{LP} = k_c k_p / k_r$, equation 32 can be written.

$$k_{obs} = k_{LP} + k_c k_q [M] / k_r \qquad (32)$$

Also shown in Figure 25 are predictions of k_{obs} based on Equation 32 where the following values of k_{LP}, k_c, k_q, and k_r were selected. From prior measurement (12) of this reaction by PHPMS in 3 Torr buffer gas at 125 °C, k_{LP}, was determined to be equal to 2.2×10^{-11} cm^3 s^{-1}. by ADO theory (1), k_c is predicted to be equal to 1.42×10^{-9} cm^3 s^{-1} at 125 °C. Accurate predictions of k_q are more difficult to obtain because the efficiency of collisional quenching of the excited complexes by nitrogen and methane buffer gases are not known. If it is first assumed that k_q will be equal to the rate constant for collisions between the ion complex and the buffer gas molecules, Langevin theory (1) predicts $k_q = 1.00 \times 10^{-9}$ cm^3 s^{-1} for methane buffer gas and $k_q = 6.5 \times 10^{-10}$ cm^3 s^{-1} for nitrogen buffer gas. The best fit to the experimental data shown in Figure 25 was then obtained if the lifetime of the entrance-channel complex was assumed to be about 0.7 ps (i.e., $k_r = 1.5 \times 10^{12}$ s^{-1}). These predictions are shown as the solid (methane) line and dashed (nitrogen) lines in Figure 25.

If the efficiency for collisional quenching of the entrance-channel ion complex is less than unity, the value of $k_r = 1.5 \times 10^{12}$ s^{-1} would have been overestimated in the above treatment. For example, if the quenching efficiency of one of the buffer gases is only 10%, then the best fit of k_r to the data in Figure 25 would be about $k_r = 1.5 \times 10^{11}$ s^{-1} (corresponding to a complex lifetime of 7 psec). For this reaction system, it seems reasonable to speculate that the efficiency of quenching by methane buffer gas would be at least 10% (132). Therefore, it seems reasonable to conclude that the $1/k_r$ lifetime suggested by the present set of

measurements and the above simple model for the reaction dynamics operative in the atmospheric-pressure range is somewhere in the low picosecond range.

If all of the rate constants for the Cl/CH_3Br reaction system measured over the entire pressure range between 300 and 1100 Torr (Figure 25) are considered, significant differences between the values measured in both buffer gases and the predictions of the simple model are apparent. Both sets of experimental values form lines of lower slopes than those of the predictions and extrapolate to low-pressure limits that lie significantly above the experimentally determined value of $k_{LP} = 2.2 \times 10^{-11}$ cm^3 s^{-1}. While the cause of this discrepancy is not presently known, it could result from limitations of the simplified model described above. For example, if the simplified model was altered only slightly in a manner that allowed just one percent of the initially-formed complexes in reaction sequence 30 to have distinctly longer lifetimes (i.e. $1/k_r > 50$ ps) against backdissociation, an initial increase of about 1×10^{-11} cm^3 s^{-1} in the rate constant would then be expected over the pressure range below 300 Torr. This change would account for the observed extrapolations to higher-than-expected low-pressure limits for the rate constants. Within this modified view, the slopes of the measurements shown in Figure 25 over the pressure range from 300 to 1100 Torr would then lead to deductions for k_r that are about five times greater than those derived above from the simplified model (these modified k_r values would apply only to the set of collision complexes that are being affected by the pressure change from 300 to 1100 Torr and not to the set that are affected by lower pressures). In order to more completely characterize the dynamics of this and other reaction systems, experimental methods that are operative over all the pressure ranges of interest are

clearly needed. For this purpose, an IMS-based apparatus that will operate over the pressure range from about 10 to 300 Torr is presently being constructed in our laboratory.

Conclusions

The experiments performed here indicate that the reaction of chloride ion with methylbromide is not moved onto its high pressure limit of kinetic behavior by use of buffer gas pressures near one atmosphere. The pressure dependence of the rate constants observed in this pressure range is consistent with predictions by Wang et al. (31) of very short lifetimes for the reaction complexes of this reaction and with the prediction by Seeley et al. (131) that this reaction should proceed with high efficiency in its high pressure limit.

THE REACTION OF CHLORIDE ION WITH ISOPROPYL BROMIDE AT ATMOSPHERIC PRESSURE

The principle motivation for the previous investigation of the Cl^-/CH_3Br system was to gain some insight into the pressure conditions under which IM reactions can be observed where all species along their reaction coordinate, including short-lived intermediates as well as reactants, are maintained in a state of thermal equilibrium with the medium. Kinetic behavior under such conditions is of fundamental interest to the field of gas phase ion chemistry and can greatly facilitate the interpretation of kinetic data in terms of the potential energy surfaces (reaction coordinate) of the reactions (39, 69 - 71, 133).

As mentioned previously and illustrated in the two previous applications, IM-MS has been used for the study of several relatively simple IM processes occurring in a buffer gas of one atmosphere pressure (69, 10 - 12). Rate constants for various bimolecular reactions, in addition to the $Cl^-\backslash CH_3Br$ system, have been reliably determined in an atmospheric pressure buffer gas. It has also been shown (11) that equilibrium constants for clustering reactions, such as that shown in reaction 33,

$$Cl^-(CHCl_3)_{n-1} + CHCl_3 \overset{K_{eq}}{\rightleftharpoons} Cl^-(CHCl_3)_n \qquad (33)$$

where $n = 1$ and 2, can be reliably measured at atmospheric pressure by IM-MS. The average rate constant for the bimolecular reactions of various sets of equilibrated cluster ions, as shown by reaction 34,

$$Cl^-(CHCl_3)_n + CH_3Br \rightarrow Br^-(CHCl_3)_m + CH_3Cl \qquad (34)$$

where *n* and *m* vary from 0 to 2, have also been measured by IMS (11).

In the present investigation, IMS was used to investigate the nucleophilic displacement reaction of chloride ion with isopropylbromide (*i*-PrBr). As compared to bimolecular reaction 30, the reaction of Cl^- with *i*-PrBr is complicated by two factors. One is that the nucleophilic attack of the chloride ion on this secondary alkylbromide proceeds much more slowly due to increased steric hindrance expected in its S_N2 transition state. The other is that the enthalpy of association between chloride and isopropylbromide will be significantly greater so that a significant fraction of the total chloride ion population can be present in the single-clustered form, Cl^- (*i*-PrBr), and even the double-clustered form, $Cl^-(i\text{-PrBr})_2$, under conditions of low-to-moderate temperatures and relatively high *i*-PrBr concentrations. For these reasons, the reaction of Cl^- with *i*-PrBr is more appropriately represented by reaction sequence 35,

$$\begin{array}{ccccc} Cl^- & \underset{K_1}{\overset{\text{i-PrBr}}{\rightleftharpoons}} & Cl^-(i-PrBr) & \underset{K_2}{\overset{\text{i-PrBr}}{\rightleftharpoons}} & Cl^-(i-PrBr)_2 \\ \downarrow k_2,\ i\text{-PrBr} & & \downarrow k_1 & & \\ Br^- + RCl & & Br^- + RCl & & \end{array} \qquad (35)$$

where the clustering reactions are indicated on the top line with equilibrium constants K_1 and K_2, along with two likely S_N2 reaction pathways. One pathway involves the direct bimolecular reaction of Cl^- ion with *i*-PrBr with second-order rate constant, k_2, and another involves the unimolecular dissociation of the thermalized single-cluster ion, Cl^-(*i*-PrBr), with first order rate

constant, k_1, to form the displacement products, Br^- and *i*-PrCl. It is recognized that an S_N2 displacement reaction could also occur within the second-order cluster ion, $Cl^-(i\text{-PrBr})_2$, shown in reaction sequence 35. However, it will be assumed here that this third reaction pathway will not be of importance under any conditions used here in which the bare Cl^- ion or the single-clustered ions, $Cl^-(i\text{-PrBr})$, have significant relative abundance. This assumption is supported by the fact that the attachment of neutral molecules to atomic anions such as Cl^- has been shown to greatly reduce the nucleophilic reactivity of the core anion (11, 43, 134 - 136).

A characterization of the reaction of Cl^- with *i*-PrBr in 4 Torr methane buffer gas has been previously described by Caldwell, Magnera, and Kebarle (124) using a pulsed electron-beam high pressure mass spectrometer (PHPMS). In that study, rate constants were reported only under relatively high temperature conditions, where the fraction of Cl^- ions held in the *i*-PrBr clustered forms was very small. In this way, their PHPMS measurements could be treated as if the reaction always occurred by a simple bimolecular process, even though Caldwell et al. recognized that the actual mechanism might have involved the prior formation of a thermalized ion complex, as shown in reaction sequence 35.

Under the conditions of the present study, it will be shown that equilibrium constants for the clustering reactions and rate constants for the substitution reactions can be simultaneously determined from IMS measurements over a range of temperatures in a near atmospheric pressure buffer gas. By comparison of the present results obtained in 640 Torr nitrogen buffer gas (ambient pressure in Bozeman, Montana) with those obtained by Caldwell, et al. (124) in 4 Torr of methane buffer gas, the relative importance of the bimolecular S_N2

mechanism (k_2) and the unimolecular S_N2 mechanism (k_1) shown in reaction 4 under atmospheric pressure conditions will be assessed.

Experimental

The instrumental configuration of the IM-MS used in this study is as shown in Figure 1 with the exhaust port of the IMS tube set to ambient pressure and with the heat exchanger installed and utilized as necessary for sub-ambient temperature conditions. Chloride or bromide ions and neutral reagents were produced in the source and drift tube as described previously. The reagent grade *i*-PrBr (Aldrich) that was injected into the GHP was first treated in order to remove any traces of HBr that would have complicated the present measurements by its fast reaction with Cl^-. This was accomplished by shaking equal volumes of *i*-PrBr and an aqueous solution of saturated $NaHCO_3$ in a separation funnel. After repeating this separation six times, the final volume of *i*-PrBr was dried with $MgSO_4$.

Results and Discussion

Reaction Modified IMS Spectra

The interaction of Cl^- reagent ions and *i*-PrBr neutrals in the drift tube results in a series of waveforms as shown in Figure 26 for a range of *i*-PrBr concentrations at relatively high drift tube temperatures. Under these conditions, the IMS spectrum is relatively simple and a determination of a second-order rate constant for the apparent bimolecular reaction between Cl^- and *i*-PrBr could be obtained, if desired, by analysis of the relative areas underlying the Cl^-

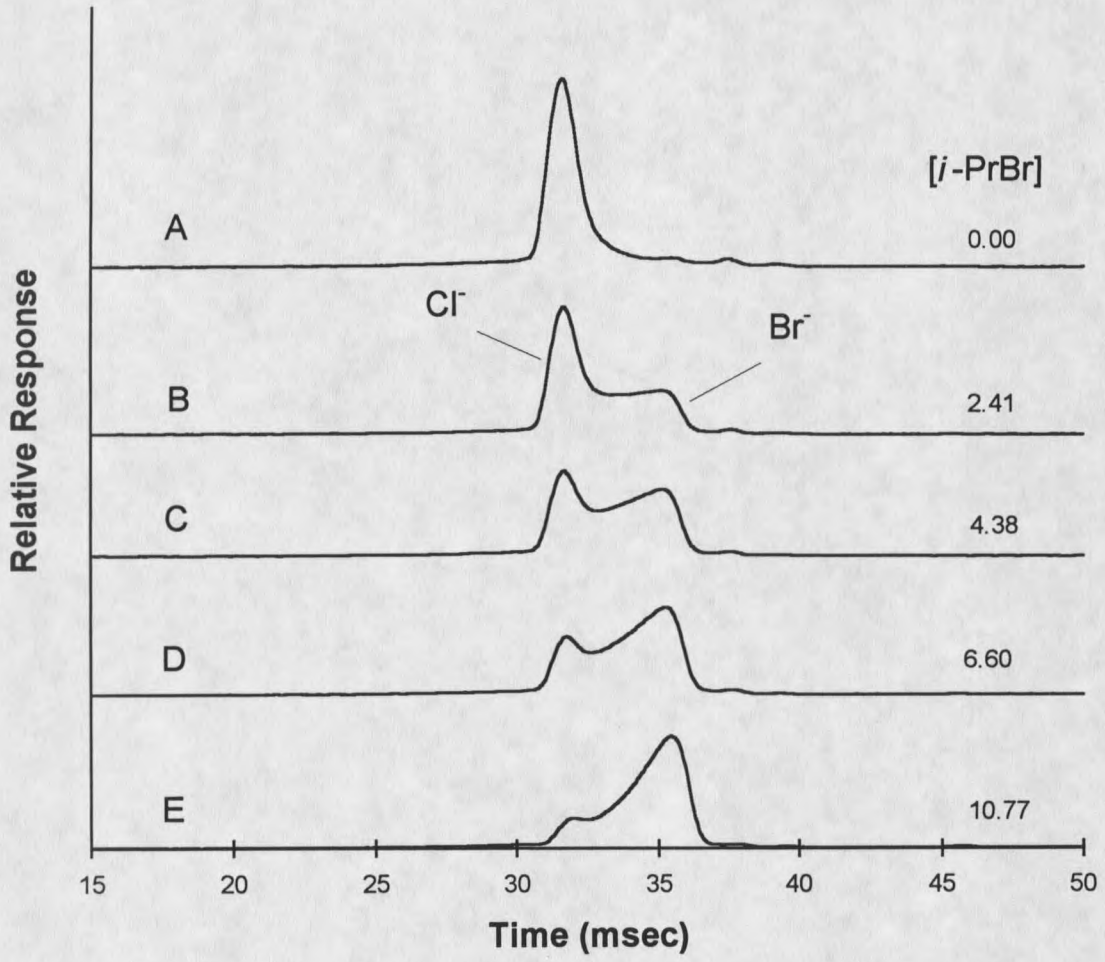

Figure 26. Reaction-modified ion mobility spectra observed at relatively high temperature, 150 °C. The reactant ion, Cl^-, is made in the ion source by electron capture to CCl_4. The product ion, Br^-, is produced at all points along the drift tube by the reaction of Cl^- with *i*-PrBr. The concentration of *i*-PrBr added to the drift tube is indicated (in units of 10^{13} molecules/cm^3). The electric field within the drift tube is set to 144 V cm^{-1}. Note that the drift times of the ions are not significantly increased by the successive addition of *i*-PrBr to the drift gas at this temperature.

and Br^- portions of the reaction-modified total-ion spectrum as described previously. A more comprehensive discussion of how rate constants were determined in this study will be deferred until later, however, while attention is now drawn to the observed drift times of the ions. It is noted in Figure 26 that the drift times of the Cl^- and Br^- ions are almost constant and are increased only slightly by the successive additions of *i*-PrBr to the drift gas at 150 ° C. This indicates that almost all of the chloride and bromide ions are in the unclustered form at 150 ° C under all of the conditions shown in Figure 26. In addition, no clustered ions of the types, Cl^-(*i*-PrBr) or Br^-(*i*-PrBr), were detected by the mass spectrometer under these conditions.

When analogous experiments were performed at relatively low temperatures, IMS spectra such as that shown in Figure 27 at 35 ° C were obtained. These IMS spectra are clearly much more complex than those in Figure 26 and require additional explanation. Again, the magnitude of the peak containing the Cl^- ion decreases continuously as greater amounts of *i*-PrBr are added to the drift gas. In addition, a large shift of the Cl^--containing peak to longer drift times is caused by an increase in the concentration of *i*-PrBr. The Br^--containing ions that are generated that are generated in the drift tube are also shifted to longer drift times with increasing amounts of *i*-PrBr, but to a lesser extent than those containing Cl^-. These shifts in drift time cause the Cl^--containing peak to move through and then to the right of the position of the Br^--containing ions within the reaction-modified IMS waveform as successively greater amounts of *i*-PrBr are added to the drift gas.

The identities of the ions that contribute to the total IMS spectra observed at 35 °C are indicated in Figure 28 where numerous mass-selected single-ion IMS measurements are shown

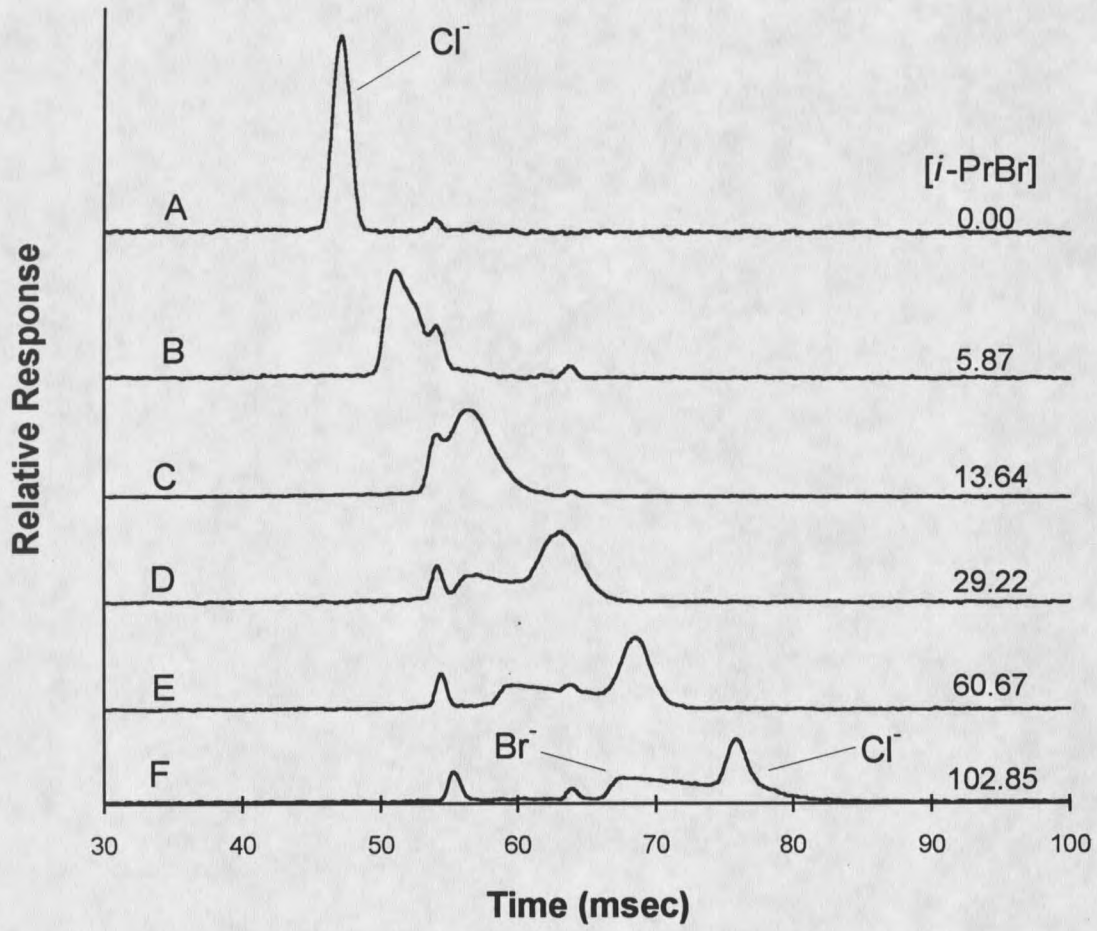

Figure 27. Reaction-modified ion mobility spectra observed at relatively low temperature, 35 °C, as a function of the *i*-PrBr concentration (in units of 10^{13} molecules/cm^3) added to the drift gas. The electric field is 144 V cm^{-1}. At this temperature, the drift times of the Cl^- reactant and Br^- product ions are significantly increased with increased [*i*-PrBr] due to the clustering of both halide ions with *i*-PrBr. At this temperature, additional ions are also noted at drift times of about 55 and 64 msec. These two ions are formed unintentionally in the ion source and are transported through the drift region without change. The identities of the primary ions that contribute to these IMS spectra are provided by associated mass spectrometry measurements, as shown in Figure 28.

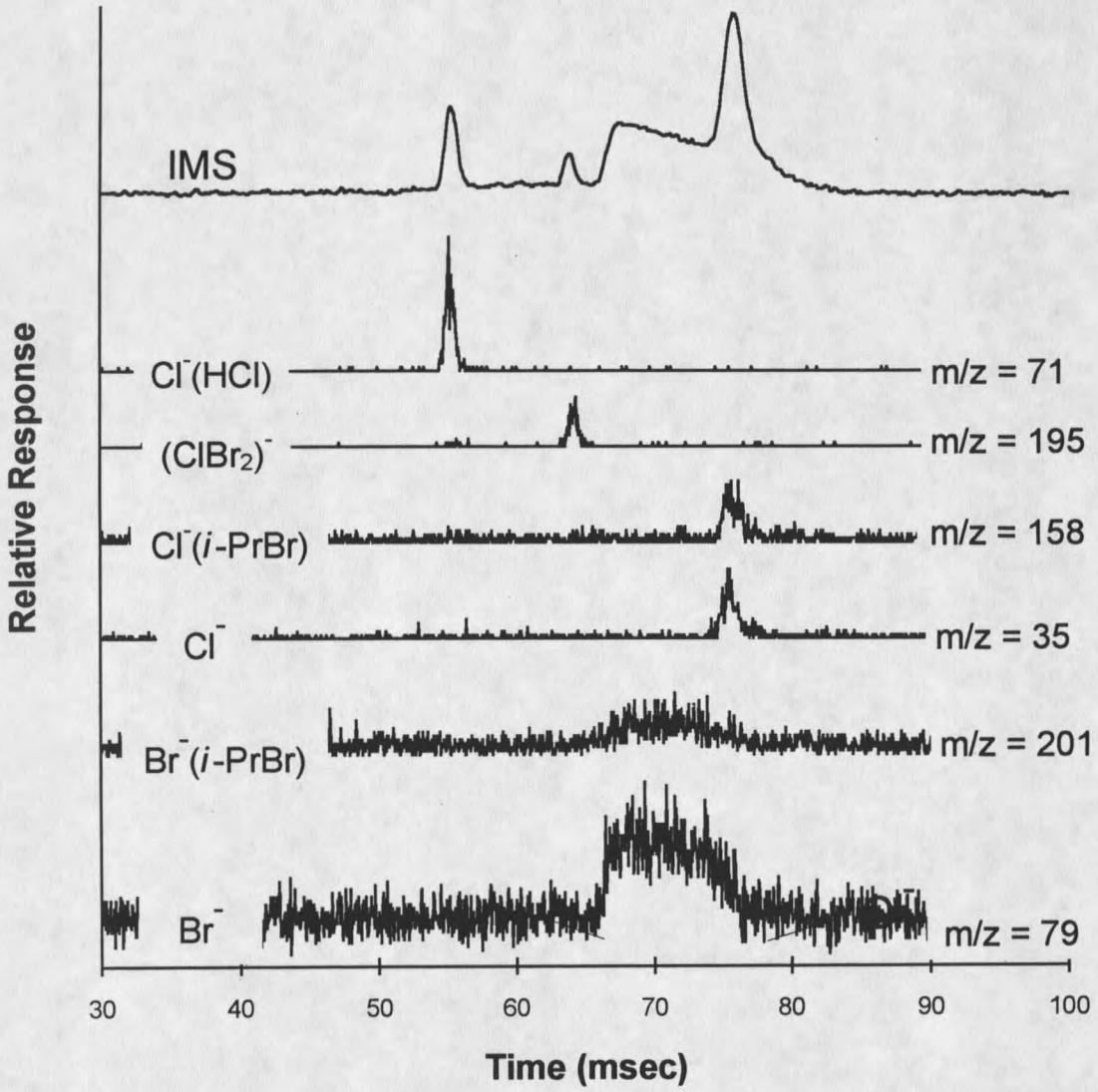

Figure 28. Several single-ion mass spectra for principal ions that contribute to the total ion IMS spectrum observed for condition F in Figure 27. The ion identities indicated in this figure were confirmed by parallel measurements in which the intensity of other expected ions within the $^{35}Cl/^{37}Cl$ and/or $^{79}Br/^{81}Br$ isotopic cluster groups of each ion type were measured. The origins of all ions indicated here are explained in the text.

under condition F of Figure 27. The identities of the ions that are thought to cause the signals at each m/z value are also indicated. These identity assignments were verified by parallel measurements (not shown) in which the expected ions of the other abundant isotopes of chlorine and bromine were monitored. The last four IMS spectra in Figure 28 indicate that the shifts in the drift times of the Cl^- and Br^- ions noted in Figure 27 are due to the clustering of these ions with *i*-PrBr. The fact that the bare and clustered halide ions have the same IMS peak shapes and drift times indicates that the clustering of *i*-PrBr to Cl^- and Br^- ions are very fast processes under these conditions relative to the rates at which these ions are transported through the drift tube.

Additional ions not seen in the IMS spectra at high temperatures are also noted in the IMS experiments performed at low temperatures in Figures 27 and 28. At ~ 55 ms, an ion which has been identified as $Cl^-(HCl)$ is consistently observed in all IMS spectra at low temperature. This ion appears to be formed only in the ion source by the association of some of the Cl^- ions with a trace quantity of HCl formed by radiation chemistry within the ^{63}Ni ion source. With CCl_4 continuously present in the ion source, the production of trace quantities of HCl appears to be unavoidable. (The source of hydrogen atoms is thought to be water which, in spite of considerable efforts for its removal, is always present at trace levels.) However, as evidenced by the constancy of the intensities and drift times of the $Cl^-(HCl)$ peaks in the IMS spectra in Figure 27, the ion, $Cl^-(HCl)$, appears to undergo no reactions in the drift region. Therefore, this ion is thought to have no effect on the IMS reaction waveform of interest, and its presence was ignored. With use of higher ion source and drift tube temperatures

(Figure 26), the $Cl^-(HCl)$ ion is not observed in either IMS or MS spectra. This is either because less HCl is produced in the ion source at the higher temperatures or because the $Cl^-(HCl)$ ion thermally decomposes at higher temperatures prior to its passage into the drift region.

Another unexpected ion, $ClBr_2^-$, of drift time 64 ms is also noted in Figure 28 whenever *i*-PrBr has been added to the drift gas. This ion is thought to be produced by a reaction of some of the Cl^- ions with trace quantities of Br_2 in the ion source. Apparently, a trace amount of Br_2 is also produced by radiation chemistry within the ion source whenever small amounts of *i*-PrBr diffuse into the source region. The presence of this ion in subsequent IMS spectra can also be ignored, however, because this ion is stable and unreactive (as evidenced by its persistence in Figure 27F where a relatively large amount of *i*-PrBr has been added to the drift gas).

It would be very difficult to determine accurate rate constants for the S_N2 displacement reaction of interest from measurements of the type shown in Figure 27, and therefore, a different approach to such measurements will be described later. However, measurements of the type shown in Figure 27 do provide an excellent means of determining clustering equilibrium constants, K_1 and K_2, at any temperature of interest, as will be described in the following section.

Equilibrium Constants for Clustering

Numerous measurements, of the type shown in Figure 27, were made over the temperature range 20-85 °C, where a significant shift in the observed drift time, t_{obs}, of the ion

packet containing the Cl^- and $Cl^-(i\text{-PrBr})$ ions was caused by the successive addition of *i*-PrBr to the drift gas. The t_{obs} values were then recorded as a function of the *i*-PrBr concentration added to the drift gas at each temperature as illustrated in Figure 29 for a set of measurements made at 35 °C. Since the bare and clustered ions of Cl^- identified in Figure 28 were shown to have the same drift times and peak shapes, it can be assumed that the equilibration time for cluster ion formation is very short compared with ionic drift times. Therefore, the observed drift time, t_{obs}, and ionic mobility, K_{obs}, can be expected to be related to the equilibrium constants for the clustering reactions and the individual mobilities of the bare and clustered Cl^- ions by the following set of relationships (49):

$$K_{obs} = \frac{L}{t_{obs} E} \tag{36}$$

$$K_{obs} = K_0\alpha_0 + K_1\alpha_1 + K_2\alpha_2 \tag{37}$$

$$\alpha_{obs} = 1/\left(1 + K_{eq,1}[i - PrBr] + K_{eq,1}K_{eq,2}[i - PrBr]^2\right) \tag{38}$$

$$\alpha_1 = K_{eq,1}[i - PrBr]/D \tag{39}$$

$$\alpha_2 = K_{eq,1}K_{eq,2}[i - PrBr]^2/D \tag{40}$$

where L is the length (23.7 cm) from the BN gate to the Faraday plate, E is the electric field strength (140 V cm^{-1}), K_i is the mobility expected for an individual Cl^- cluster ion containing *i* *i*-PrBr molecules, α_i, is the fraction of ions under a mobility peak containing *i* *i*-PrBr molecules,

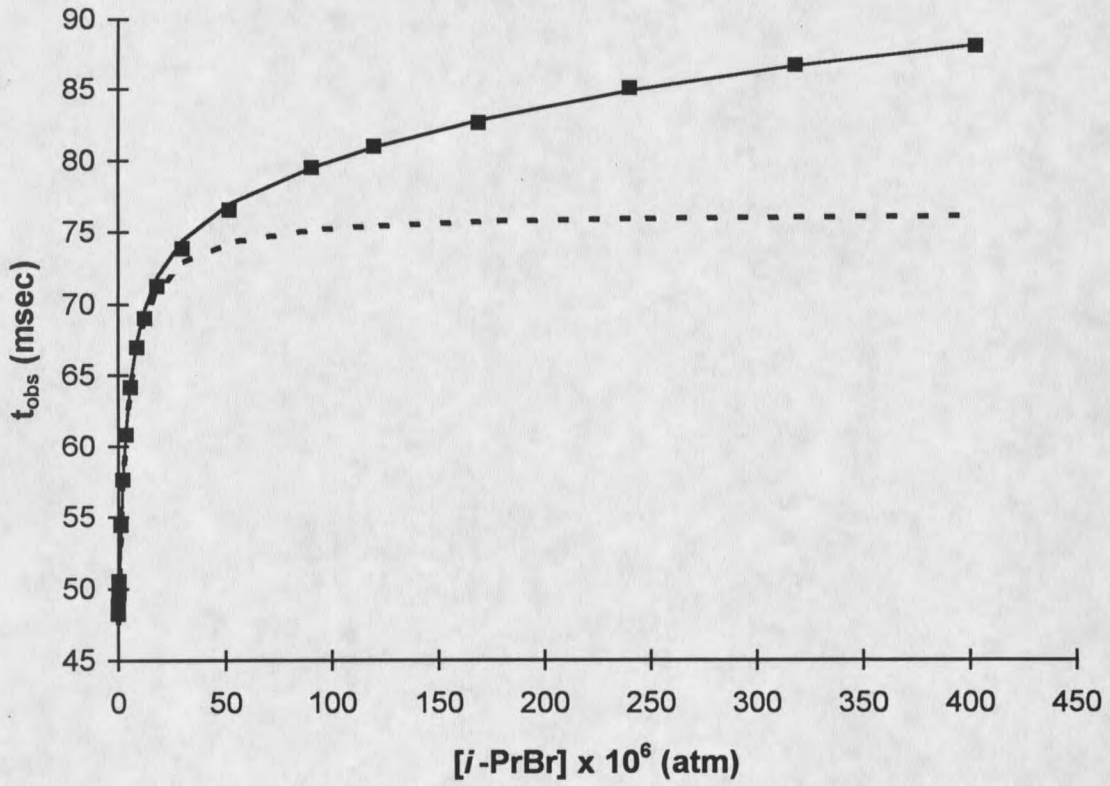

Figure 29. A typical measurement for the observed drift time, t_{obs}, for the Cl^--containing ion packet versus the concentration of *i*-PrBr added to the drift gas at a relatively low temperature, 35 °C. The dashed line indicates the t_{obs} values expected if only first-order clustering with $K_{eq,1} = 3.7 \times 10^5$ atm^{-1} were important, with $K_{eq,2}$ assumed to be zero. The point at which the t_{obs} values begin to diverge from this dashed line indicates the onset of significant second-order clustering. The solid line indicates the t_{obs} values expected if both first- and second-order clustering are assumed to be important, with $K_{eq,1} = 3.7 \times 10^5$ atm^{-1} and $K_{eq,2} = 3.0 \times 10^3$ atm^{-1}. Excellent fit to all drift time measurements is then obtained

$K_{eq,i}$ is the clustering equilibrium constant leading to the cluster ion $Cl^-(i\text{-PrBr})_i$, [*i*-PrBr] is the concentration of isopropyl bromide in the drift gas, and D is the denominator written in equation 38. Over the range of *i*-PrBr concentrations used in the present study, it will be shown that only cluster ions for which $i = 0$, 1, or 2 have significant relative abundance so that contributions of higher-order terms can be ignored. Under conditions of relatively small [*i*-PrBr] and with the reasonable assumption that $K_{eq,1}$ will be greater than $K_{eq,i}$ for all $i > 2$, equations 37-40 can be combined to form equation 41.

$$(K_{obs} - K_o)^{-1} = (K_{eq,1}(K_1 - K_o)[i - PrBr])^{-1} + (K_1 - K_o)^{-1} \qquad (41)$$

In Figure 30, the mobility data for the Cl^-/*i*-PrBr system at temperatures of 20, 40, and 60 °C have been plotted in the form $(K_{obs} - K_0)^{-1}$ vs $[i\text{-PrBr}]^{-1}$. In accordance with Equation 41, a straight line is obtained over the range of measurements where [*i*-PrBr] is relatively small ($[i\text{-PrBr}]^{-1}$ is large). From the intercept of this line and from measurements of K_0 for Cl^- (in the absence of added *i*-PrBr), the single ion mobility, K_1, was obtained for the cluster ion, $Cl^-(i\text{-PrBr})_1$, at each temperature. Since the slopes of the lines shown in Figure 30 are expected (Equation 41) to be equal to $K_{eq,1}(K_1 - K_0)^{-1}$, and the mobilities, K_0 and K_1, have been determined, $K_{eq,1}$ is obtained at each temperature. The uncertainty of the $K_{eq,1}$ values thereby obtained is estimated to be no greater than ± 20%. By the treatment of 15 data sets at 15 different temperatures, 15 $K_{eq,1}$ values for the Cl^-/*i*-PrBr system were thereby determined and have been plotted in Figure 31 in the form of a van't Hoff plot. This log $K_{eq,1}$ vs 1/T plot produces a straight line, as expected. By standard treatment (137) of the slopes and intercepts

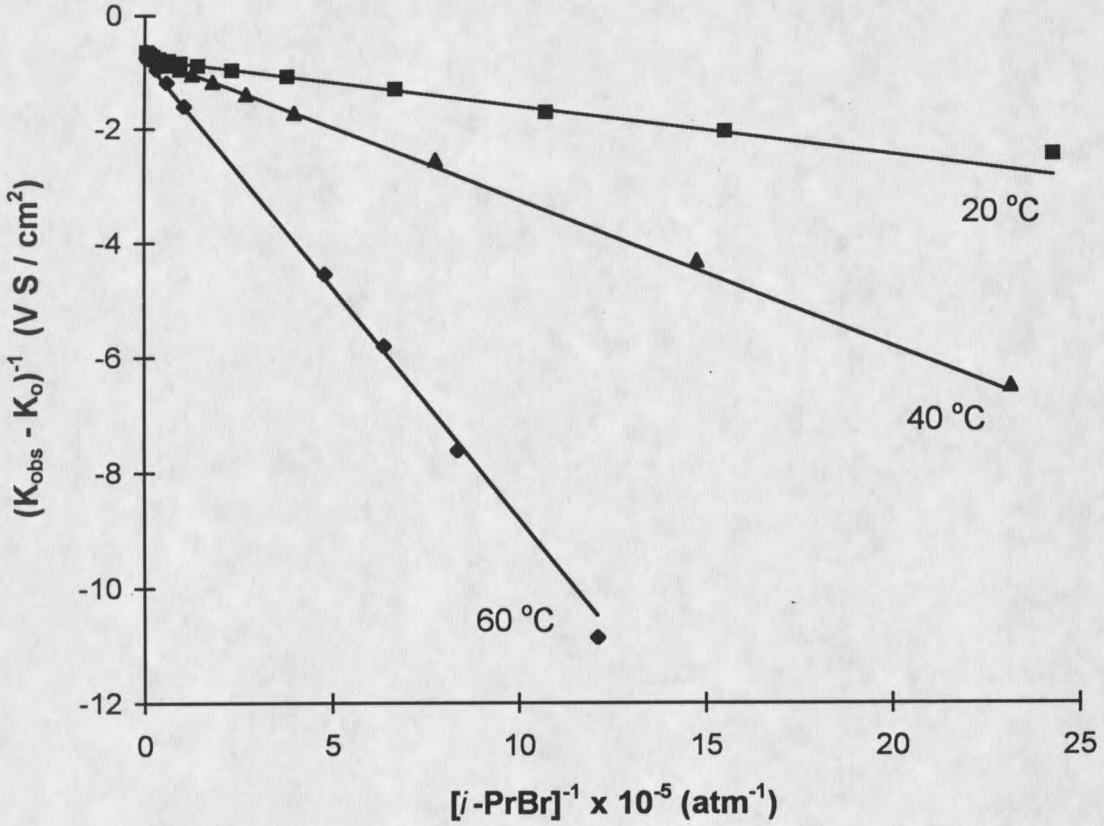

Figure 30. Changes in the mobility of the Cl^-/Cl^-(*i*-PrBr) ion packet as a function of *i*-PrBr concentration in the drift region, plotted in the form of Equation 41. Equilibrium constants for the association of Cl^- with *i*-PrBr are determined from the intercepts and the slopes of the least-squares lines thereby formed, as explained in the text.

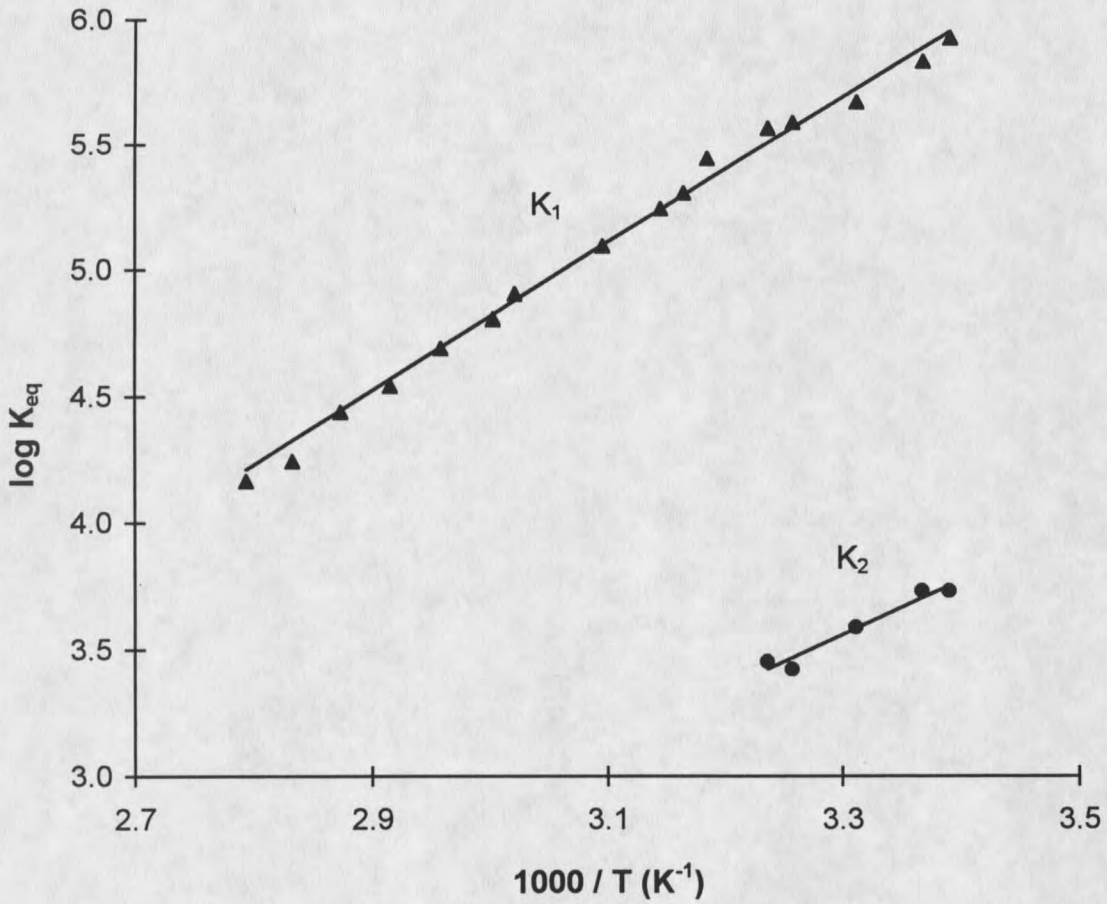

Figure 31. Van't Hoff plots of the equilibrium constants, $K_{eq,1}$, for the association of Cl^- with *i*-PrBr over the temperature range 20 - 85 °C, and for the equilibrium constants, $K_{eq,2}$, for the second-order clustering reaction, $Cl^-(i\text{-PrBr}) + i\text{-PrBr} \leftrightarrow Cl^-(i\text{-PrBr})_2$, over the temperature range 20 - 36 °C as determined by reaction-modified IMS measurements.

of these lines ($\ln K_{eq} = -\Delta H/RT + \Delta S/R$), the standard enthalpy, ΔH^0_1, and standard entropy, ΔS^0_1, associated with the addition of one *i*-PrBr molecule to Cl^- is found to be $\Delta H^0_1 = -13.4 \pm 1.0$ kcal mol^{-1} and $\Delta S^0_1 = -18 \pm 3$ cal deg^{-1} mol^{-1}. These values, along with the corresponding value of $\Delta G^0_1 = -8.0 \pm 0.1$ at 25 °C, are listed in Table 6. The only previous measurement of this equilibrium reaction is that of Caldwell et al. (124) by high-pressure mass spectrometry, who reported $K_{eq,1} = 3.9 \times 10^5$ atm^{-1} at a temperature of 304 K. From the ΔH^0_1 and ΔS^0_1 values determined here by IM-MS, $K_{eq,1}$ is predicted to be 4.7×10^5 atm^{-1} at 304 K, in good agreement with the single measurement by Caldwell et al.

Table 6.

Thermodynamic Properties Determined by IM-MS for the Association of Chloride and Bromide Ions with Isopropyl Chloride and Isopropyl Bromide

Reaction	$-\Delta H^o$ [a]	$-\Delta S^o$ [b]	$-\Delta G^o_{298}$ [c]
Cl^- + *i*-PrBr	13.4	18	8.0
Cl^- + *i*-PrCl	13.0	19	7.4
Br^- + *i*-PrBr[d]	13.0	20	6.9
Br^- + *i*-PrCl	11.7	18	6.3

[a] Units are kcal mol^{-1}. Estimated uncertainty is ± 1.0 kcal mol^{-1}.
[b] Units are cal mol^{-1} K^{-1}. Estimated uncertainty is ± 3.0 cal mol^{-1} K^{-1}.
[c] Units are kcal mol^{-1}. Estimated uncertainty is ± 0.1 kcal mol^{-1}.
[d] Dougherty (146) previously reported $-\Delta H^o$ = 12.2 kcal mol^{-1}, $-\Delta S^o$ = 20 cal mol^{-1} K^{-1}, and $-\Delta G^o_{298}$ = 6.3 kcal mol^{-1} for this system.

The dashed curve shown in Figure 29 is a prediction of t_{obs} obtained by Equations 36-40 using the values of K_0, K_1 and $K_{eq,1}$ determined here and with the assumption that $K_{eq,2} = 0$. It is clear that, with this assumption of no clustering beyond the single cluster ion, a good

fit is observed only over a specific range of relatively low *i*-PrBr concentrations. With use of higher *i*-PrBr concentrations, both the t_{obs} values in Figure 29 and accompanying mass spectrometric measurements indicated that higher-order clustering, leading to the $Cl^-(i\text{-PrBr})_2$ ion, is also important. In order to determine the equilibrium constant, $K_{eq,2}$, from these t_{obs} measurements, Equation 42 can be used.

$$W = -K_{eq,2}K_{obs} + K_{eq,2}K_2 \qquad (42)$$

where $W = (K_{obs} + K_{obs}K_{eq,1}[i\text{-PrBr}] - K_0 - K_1K_{eq,1}[i\text{-PrBr}]) / K_{eq,1}[i\text{-PrBr}]_2$. Equation 42 has also been derived from Equations 36 - 40 under conditions of relatively high [*i*-PrBr] where second-order clustering is significant and with the assumption that $K_{eq,i} = 0$ for all $i \geq 3$. (Note that all terms contributing to W are known). In Figure 32, the portion of the K_{obs} measurements at 35 °C (Figure 29) corresponding to t_{obs} exceeding 70 ms has been plotted in the form W vs K_{obs}. In accordance with equation 42, a linear relationship is observed for the set of K_{obs} measurements for t_{obs} in excess of about 80 ms where second-order clustering has become dominant. Analysis of the slope of this line leads to $K_{eq,2} = (3.0 \pm 0.4) \times 10^3$ atm^{-1} at 35 °C. The curve formed by the solid line in Figure 29 has been calculated from equations 36 - 40 using values for K_0, K_1, K_2, $K_{eq,1}$ and $K_{eq,2}$ determined as described above from the graphical methods illustrated in Figures 30 and 32 (with the assumption that $K_{eq,i} = 0$ for all $i \geq 3$). It is seen that this curve is in excellent agreement with all of the drift time measurements.

Measurements of $K_{eq,2}$ were made over a narrow range of temperatures (20-36 °C), and these results are also shown in Figure 31 in the form of a van't Hoff plot. From the slope

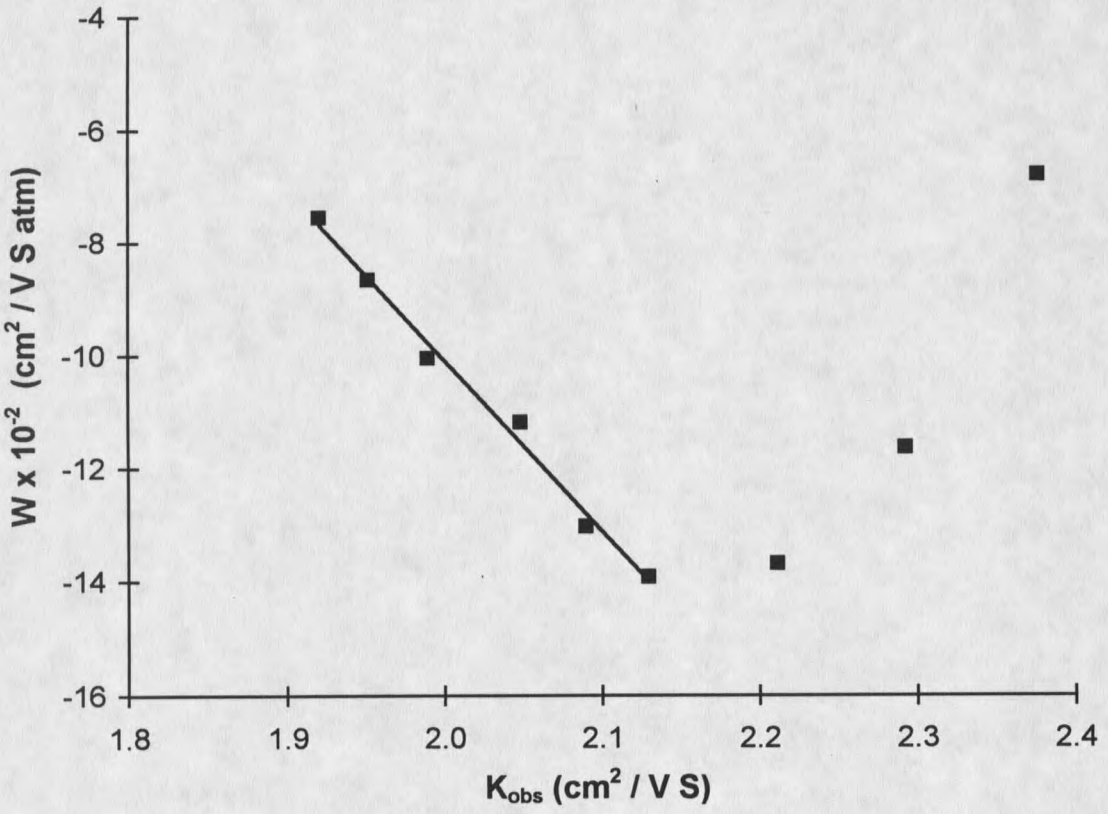

Figure 32. Mobility measurements for Cl^--containing ions observed in reaction-modified IMS spectra under conditions of relatively high *i*-PrBr concentration at 35 °C, plotted in the form of equation 42 where $W = (K_{obs} + K_{obs}K_{eq,1}[i\text{-PrBr}] - K_0 - K_1K_{eq,1}[i\text{-PrBr}])/K_{eq,1}[i\text{-PrBr}]_2$. The slope of the straight line formed by K_{obs} measurements in excess of 80 msec provides a means of determining the equilibrium constant for second-order clustering, $K_{eq,2}$.

and intercept of this plot, ΔH^0_2 = -9.9 ± 2.2 kcal mol^{-1} and ΔS^0_2 = -16 ± 6 cal mol^{-1} K^{-1} are deduced for the addition of a second *i*-PrBr molecule to Cl^-(*i*-PrBr). A free energy change of ΔG^0_2 = -5.0 ± 0.1 kcal mol^{-1} at 25 °C is also obtained. Also listed in Table 6 are IMS equilibrium measurements made in the present study for the first-order clustering reactions, Cl^- + *i*-PrCl ⟷ Cl^-(*i*-PrCl)1, Br^- + *i*-PrBr ⟷ Br^-(*i*-PrBr), and Br^- + *i*-PrCl ⟷ Br^-(*i*-PrCl). For those cases where Br^- is the core ion, Br^- was made in the source by electron capture to CF_3Br, and the drift time of the Br^--containing ion packet was then monitored as a function of the concentration of either *i*-PrCl or *i*-PrBr added to the drift gas. The determination of these equilibrium constants from IMS spectra was relatively straightforward because a simultaneous change in the core halide ion does not occur for these reaction systems either because an S_N2 displacement does not occur or because the S_N2 reaction system is symmetrical. The results summarized in Table 6 provide additional support for the accuracy of the $K_{eq,1}$ determinations made here for the Cl^-/*i*-PrBr system from reaction-modified IMS spectra. While the four equilibrium systems have similar thermochemical parameters, a small but significant increase is noted in the magnitude of the free energy change upon a change of the core anion from Br^- to Cl^-. A small increase is expected due to the smaller size of the Cl^- ion. Also, a small increase in the free energy change is noted upon changing the clustering agent from *i*-PrCl to *i*-PrBr. This result is consistent with the view that the greater polarizability expected for *i*-PrBr has a greater effect on the clustering interaction than the slightly greater acidity expected for the secondary hydrogen atom in *i*-PrCl.

Determination of Rate Constants

Rate constants for the S_N2 displacement reaction between Cl^- and *i*-PrBr were determined by varying the electric field strength as described previously and as illustrated in Figure 33. By this procedure, the reaction time (defined to be equal to the drift time of the $Cl^-/Cl^-(i\text{-PrBr})_i$ ion packet) is progressively increased by decreasing the electric field in the drift region. As is noted in Figure 33, the fraction of the IMS wave form that is due to the $Cl^-/Cl^-(i\text{-PrBr})_i$ ion packet is decreased and the fraction of the IMS waveform that is due to the $Br^-/Br^-(i\text{-PrBr})_i$ ion packet is increased as the reaction time is increased. The relative contribution of the reactant ion packet, containing Cl^- and $Cl^-(i\text{-PrBr})_i$ ions, to the total area of the reaction-modified IMS waveform was determined by graphical analysis of each waveform as described previously and the magnitude of this quantity, called A_{Cl^-}/A_{total}, was determined as a function of the reaction time.

In the analysis of these measurements, the following mathematical description of reaction sequence 35 has been applied. It is assumed that the sum of all Br^--containing product ions are formed by one or both of the two pathways shown in reaction 35. Therefore, the general rate law for the formation of product ions is given by

$$d(\text{prod})/dt = k_2[i-\text{PrBr}][Cl^-] + k_1[Cl^-(i-\text{PrBr})] \qquad (43)$$

Since the concentrations of the Cl^-, $Cl^-(i\text{-PrBr})$, and $Cl^-(i\text{-PrBr})_2$ ions are coupled by very fast equilibrium reactions, the following three relationships will also apply at all times:

$$K_{eq,1} = [Cl^-(i-\text{PrBr})]/[i-\text{PrBr}][Cl^-] \qquad (44)$$

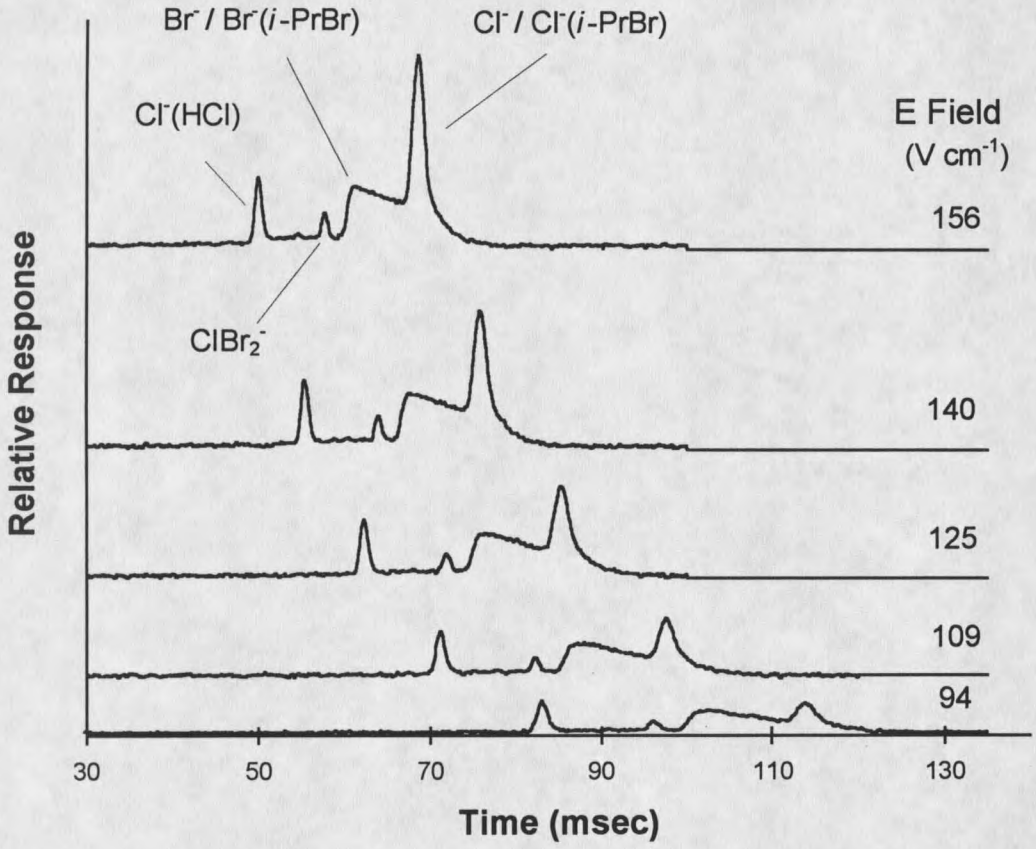

Figure 33. Typical reaction-modified IMS spectra from which rate constants were determined at relatively low temperature. By this procedure, the drift times of all ions are progressively increased by decreasing the electric field of the drift tube. The reaction time is defined to be equal to the drift time of the Cl^--containing ion packet. The relative contribution of the Cl^--containing ions to the IMS reaction-modified waveform is progressively increased as the reaction time is increased. Temperature is 35 °C.

$$K_{eq,2} = [Cl^-(i-PrBr)_2]/[Cl^-(i-PrBr)][i-PrBr] \quad (45)$$

$$-\frac{d(prod)}{dt} = \frac{d(Cl-)}{dt} + \frac{d[Cl^-(i-PrBr)]}{dt} + \frac{d[Cl^-(i-PrBr)_2]}{dt} \quad (46)$$

The combination of these three equations leads to equation 47.

$$-\frac{d(prod)}{dt} = \frac{d(Cl^-)}{dt} + K_{eq,1}[i-PrBr]\frac{d[Cl^-]}{dt} + K_{eq,1}K_{eq,2}[i-PrBr]^2\frac{d[Cl^-]}{dt} \quad (47)$$

Finally, the combination of Equations 43 and 47 then provides the defining differential equation which, after integration over the reaction time, takes the following form:

$$([i-PrBr]^{-1} + K_{eq,1} + K_{eq,1}K_{eq,2}[i-PrBr])\ln([Cl^-]_0/[Cl^-]_t) = (k_2 + k_1K_{eq,1})t \quad (48)$$

where $[Cl^-]_0$ is the initial Cl^- ion concentration and $[Cl^-]_t$ is the Cl^- ion concentration remaining after reaction time, t. Since the ratio $[Cl^-]_t/[Cl^-]_0$, will be equal to the measured quantity A_{cl^-}/A_{total} described above, equation 49 can be written:

$$Y = k_2't \quad (49)$$

where $Y = ([i\text{-}PrBr]^{-1} + K_{eq,1} + K_{eq,1}K_{eq,2}[i\text{-}PrBr])\ln(A_{total}/A_{cl^-})$ and $k_2' = k_2 + k_1K_{eq,1}$. (Note that the equilibrium constants $K_{eq,1}$ and $K_{eq,2}$ must be converted to units of cm^3 $molecule^{-1}$ prior to use in equation 49). By equation 49, a plot of the known quantities, Y, versus time is

known from the equilibrium measurements described above. The sum of k_2 and $k_1K_{eq,1}$ will be referred to here as the phenomenological second-order rate constant, k_2'. In Figure 34, plots of Y versus t for a range of reaction temperatures are shown. As expected, straight lines are observed in each case from which values of k_2' were determined from the slopes.

In Figure 35, the k_2' values obtained at all temperatures are shown (dots) in the form of an Arrhenius plot ($\log k_2'$ vs 1/T). If viewed in the standard Arrhenius form $k = A \exp(-E_A/RT)$, the least-squares line formed by these k_2' measurements indicate a pre-exponential factor of $A = 1.6 \times 10^{-11}$ cm^3 s^{-1} and an activation energy of $E_A = 2.4$ +/- 0.3 kcal mol^{-1}. Also shown in Figure 35 (squares) are the determinations of k_2' for this reaction previously reported by Caldwell et al. (124) in 4 Torr of methane buffer gas and over a somewhat higher temperature range. While these two data sets indicate a moderate level of agreement at the common temperatures used, the line formed by the Caldwell measurements leads to significantly different Arrhenius parameters, $A = 1.2 \times 10^{-10}$ cm^3 s^{-1} and $E_A = 5.6$ +/- 0.5 kcal mol^{-1}, than those determined by the present IM-MS method. These differences in Arrhenius parameters suggest that different reaction mechanisms might be operative at the two buffer gas pressures, 4 and 640 Torr, used in these studies.

The possibility of a change to an E2 elimination mechanism, as shown by reaction 50 under one of the two conditions of buffer gas pressures has been considered.

$$Cl^- + i\text{-}PrBr \rightarrow HCl + CH_3CH=CH_2 + Br^- \qquad (50)$$

The E2 mechanism does not seem likely for a direct bimolecular interaction between Cl^- and

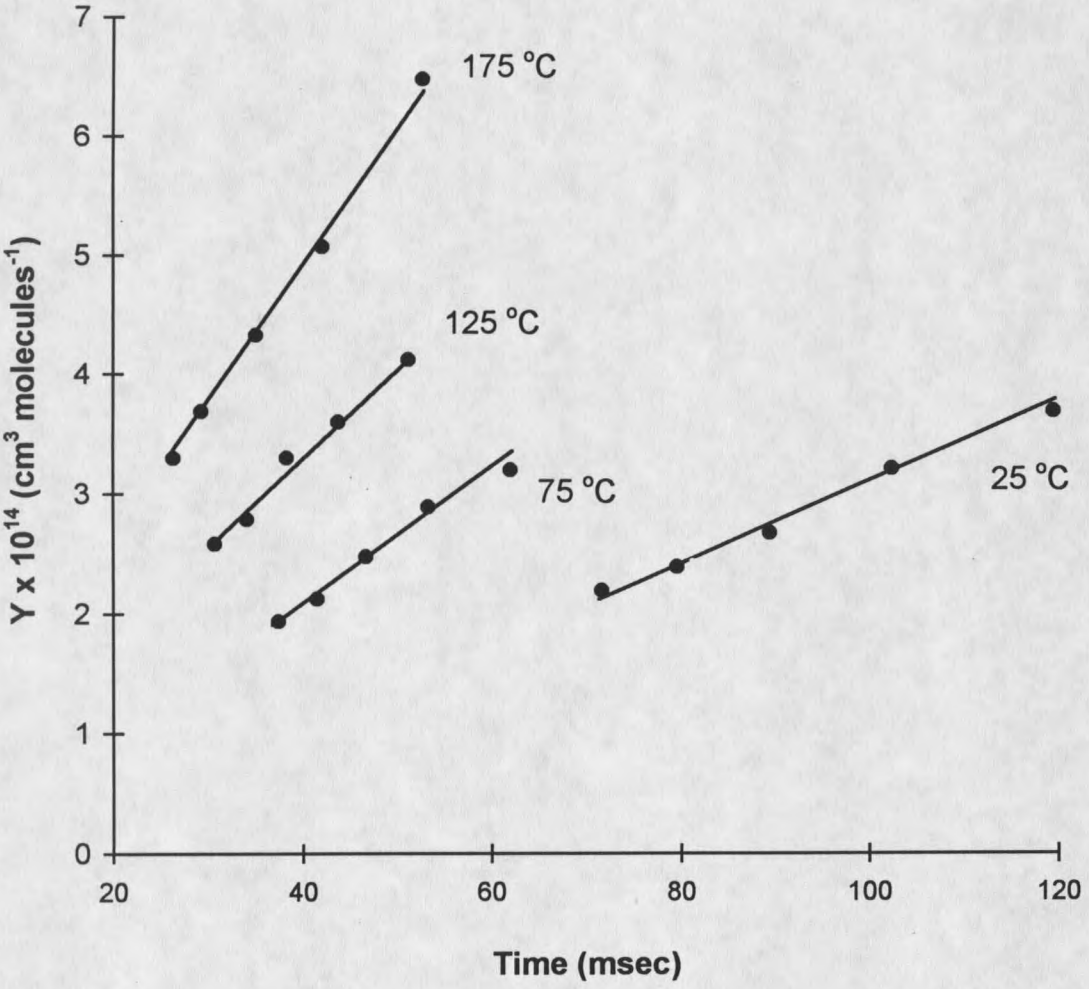

Figure 34. Extent of Cl^--containing reactant ion loss determined by IMS measurements versus reaction time for several temperatures, plotted in the form of Equation 49. The slopes of the lines thereby formed provide a phenomenological second-order rate constant, $k_2' = k_2 + k_1K_{eq,1}$, at each temperature. The concentrations of *i*-PrBr used at each temperature in order of increasing temperature are 7.3×10^{14}, 4.14×10^{14}, 5.89×10^{13}, and 2.43×10^{13} molecules cm^{-3}.

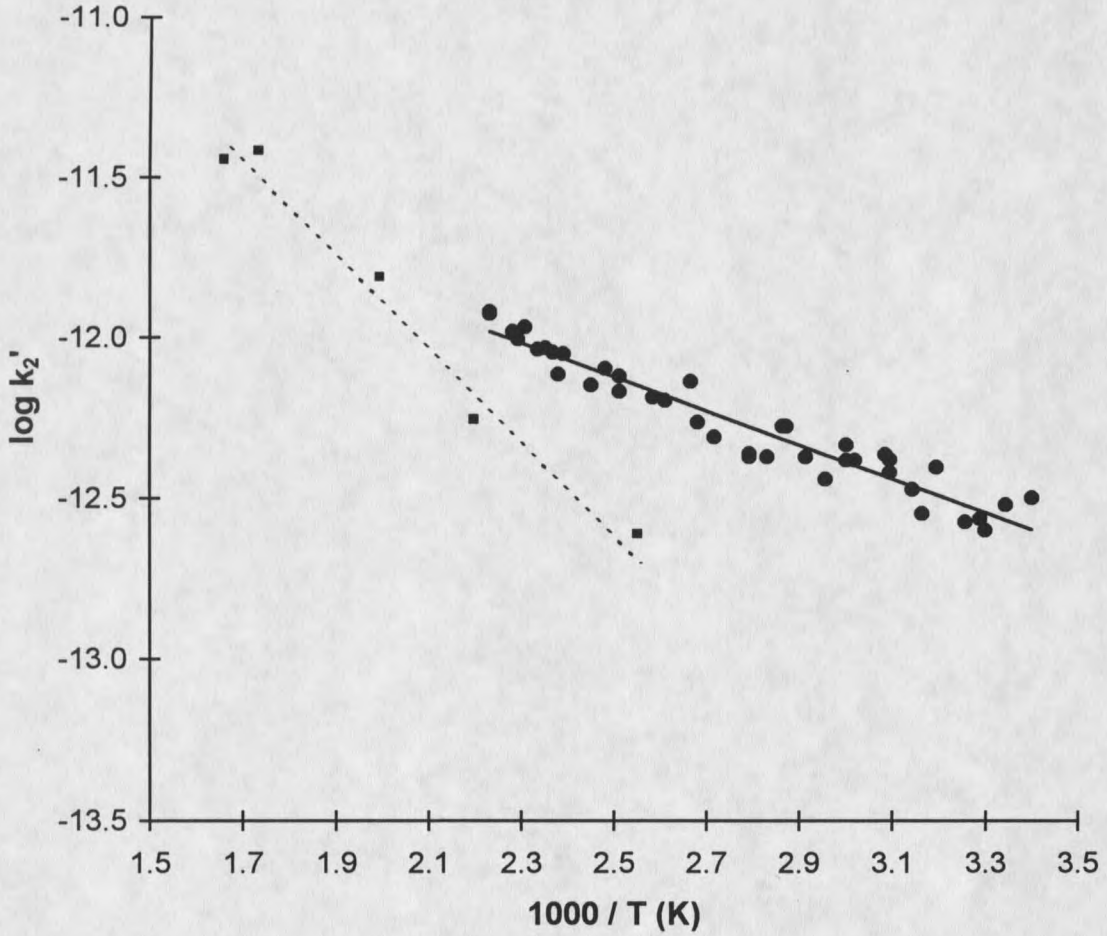

Figure 35. Phenomenological second-order rate constants, $k_2' = k_2 + k_1K_{eq,1}$, for the reaction of chloride ion with isopropyl bromide determined here (dots) by IMS in atmospheric pressure nitrogen buffer gas and those reported by Caldwell et al. (squares) by PHPMS in 4 Torr of methane buffer gas, plotted in Arrhenius form log k = log A - (E_A/2.3RT). The estimated uncertainty of individual k_2' measurements in both studies is about ± 20%.

i-PrBr due to the fact that reaction 50 would be endothermic by about 10 kcal mol^{-1} (deduced from known (138) heats of formation. If, on the other hand, reaction 50 proceeded through a thermalized ion complex, Cl^-(*i*-PrBr), the reaction enthalpy of the first-order decomposition of this ion by the E2 elimination pathway would be even greater, about 23 kcal mol^{-1} (given by the reaction enthalpy for reaction 41 less that of the Cl^-/*i*-PrBr association reaction, listed in Table 6). Since the activation barrier for the observed decomposition of the Cl^-(*i*-PrBr) ion will be shown later to be significantly less than 23 kcal mol^{-1}, an E2 reaction within a thermalized ion complex also does not appear to be possible.

It could be argued that the E2 reaction leads to the strongly hydrogen-bonded species, Br^-(HCl), instead of Br^- and HCl as shown in reaction 50. This would make the overall reaction about 15 kcal mol^{-1} more favorable and exothermic (141). However, if the ion Br^-(HCl) was a product of an E2 reaction, it would be stable and observable under the relatively low- temperature conditions of the IMS used here. This ion was not observed here under low-temperature conditions (see Figure 28).

Having ruled out the possibility of a change to a distinctly different E2 mechanism, consideration will now be given to the feasibility of more subtle expected effects of pressure that could alter the detailed means by which an S_N2 displacement reaction proceeds at the two pressures represented in Figure 35.

Associated Rate Measurements at Lower Pressures

In assessing the relative importance of the direct S_N2 reaction (k_2) and the indirect mechanism ($k_1K_{eq,1}$) in determining the displacement mechanism, it is useful to consider more closely the present results and those of Caldwell et al. (124) shown in Figure 35. In both studies, a second-order rate constant is obtained that is expected to be equal to the phenomenological second-order rate constant, $k_2' = k_2 + k_1K_{eq,1}$, under each of the two reaction conditions. The fact that the Arrhenius parameters that define the two sets of rate constants in Figure 35 are significantly different implies that the mechanisms are not exactly the same under the two conditions of buffer gas pressure. Therefore, it might be suggested that the direct displacement reaction (k_2) was more important and that the indirect mechanism ($k_1K_{eq,1}$) was less important in the study of Caldwell et al. performed at relatively low pressures than in the present study.

In considering the relative importance of the direct and indirect displacement mechanisms, it is necessary to view these processes in somewhat greater detail, as in reaction 51.

$$Cl^- + i\text{-}PrBr \underset{k_b}{\overset{k_c}{\rightleftharpoons}} (Cl^- \circ i\text{-}PrBr)^* \overset{k_B[M]}{\rightleftharpoons} Cl^-(i\text{-}PrBr) \qquad (51)$$

$$(Cl^- \circ i\text{-}PrBr)^* \xrightarrow{k_p} \text{products}$$

The production of Br^--containing products by the direct displacement mechanism will proceed through a short-lived excited intermediate, $(Cl^- \circ i\text{-}PrBr)^*$, whose rate of formation is

determined by the collisional rate constant, k_c, and whose rate of destruction is determined by the sum of three rate constants: k_p for formation of the displacement product, k_b for back-dissociation of the excited ion complex, and $k_b[M]$ for the collisional stabilization of the intermediate by the buffer gas, B. The overall rate constant, k_2, for the direct S_N2 displacement reaction will be given by

$$k_2 = k_c k_p (k_p + k_b + k_B[M])^{-1} \tag{52}$$

Since the reaction under consideration is very much slower than the collision rate under all reaction conditions, it can be assumed that $k_p << k_b + k_B[M]$ under all conditions. Therefore, equation 52 can be rewritten in the form

$$k_2 = (k_c k_p / k_b) / (1 + k_B[M] / k_b) \tag{53}$$

where the effect of buffer gas pressure change on k_2 will be provided by the unitless collective term, $k_B[M]/k_b$.

With a pulsed high-pressure mass spectrometer (140, 141), we have been able to measure the collective term, $k_B[M]/k_b$, for the closely related reaction system involving Cl^- ion and isopropyl chloride (*i*-PrCl) in methane buffer gas at a pressure of 0.5 Torr at room temperature. The mechanism for the foreword association reaction of Cl^- and *i*-PrCl is analogous to that shown in reaction 51. However, since any displacement reaction that might occur causes no net change in the identity of the halide ion, this reaction system can be expressed as follows:

$$Cl^- + i-PrCl \underset{k_b}{\overset{k_c}{\rightleftharpoons}} (Cl^- \circ i-PrCl)^* \overset{k_B[M]}{\rightleftharpoons} Cl^-(i-PrCl) \qquad (54)$$

The rate constant, k_{assoc}, for this reaction will be given by

$$k_{assoc} = k_c k_b [B] / (k_b + k_B[M]) \qquad (55)$$

Which can be rearranged to form

$$k_{assoc} / k_c = (k_b[B] / k_b) / (1 + k_B[M] / k_b) \qquad (56)$$

Our PHPMS measurements of this reaction system (with 1.0 mTorr of *i*-PrCl in 0.50 Torr of methane buffer gas at 25 °C) indicate that a state of clustering equilibrium is reached after about 500 μs. Analysis of the rate at which this equilibrium condition is reached, using the standard equations for relaxation processes (142), indicated that $k_{assoc} = (1.5 +/- 0.5) \times 10^{-11}$ $cm^3\ s^{-1}$ under these conditions. A collision rate constant of $k_c = 1.8 \times 10^{-9}$ $cm^3\ s^{-1}$ is deduced from ADO theory (1). By equation 56, $k_B[M]/k_b = 0.008$ is thereby deduced for this reaction system at a pressure of 0.5 Torr. Therefore, in a buffer gas of 4 Torr of methane, as was used in the study of Caldwell et al. (124) for study of the reaction of Cl^- with *i*-PrBr, $k_B[M]/k_b$ might be expected to be equal to = 0.06, from which $k_2 = 0.95(k_c k_p/k_b)$ is predicted by equation 53. In a nitrogen buffer gas of 640 Torr, as is used in the present IM-MS studies of the reaction of Cl^- with *i*-PrBr, $k_B[M]/k_b = 10$ would be expected (assuming the efficiency of collisional quenching is the same for methane and nitrogen), from which $k_2 = 0.10(k_c k_p/k_b)$ is predicted by equation 53. From these considerations, one might expect that k_2 would decrease by about 1

order of magnitude, with a pressure change from 4 to 640 Torr. This, of course, would greatly increase the importance of the direct S_N2 mechanism under the lower pressure conditions used by Caldwell et al. and would greatly decrease its importance in the present study.

In addition, the discussion of reaction 54 indicates that the use of lower buffer gas pressures would decrease the rate of the forward clustering reaction that has been shown here to lead to a condition of clustering equilibrium within the IM-MS at atmospheric pressure. Therefore, under the lower pressure conditions of Caldwell et al. (124), it is much more likely than in the present study that the rates of the forward clustering reactions are not sufficiently fast so as to maintain a condition of true equilibrium. In that case a steady-state condition of clustering that is short of the true equilibrium position would be achieved. This would cause the rate constant for the indirect mechanism to be less than the product term, $k_1K_{eq,1}$, and would additionally increase the relative importance of the direct mechanism at lower pressures.

In view of the above considerations, it is reasonable to suggest that the dominant mechanism for the S_N2 displacement reaction studied here under conditions of atmospheric pressure is the indirect mechanism for which the observed rate constant, k_2', is equal to the product of k_1 and $K_{eq,1}$.

Enthalpy of Activation for S_N2 Displacement within the Ion Complex

In Figure 36, rate constants, k_1, determined here from the relationship $k_1 = k_2'/K_{eq,1}$ have been plotted in the form, $\ln(k_1/T)$ vs $1/T$ (K). A plot of this form is expected to provide a straight line for gas phase unimolecular processes in which the reactant is maintained in a

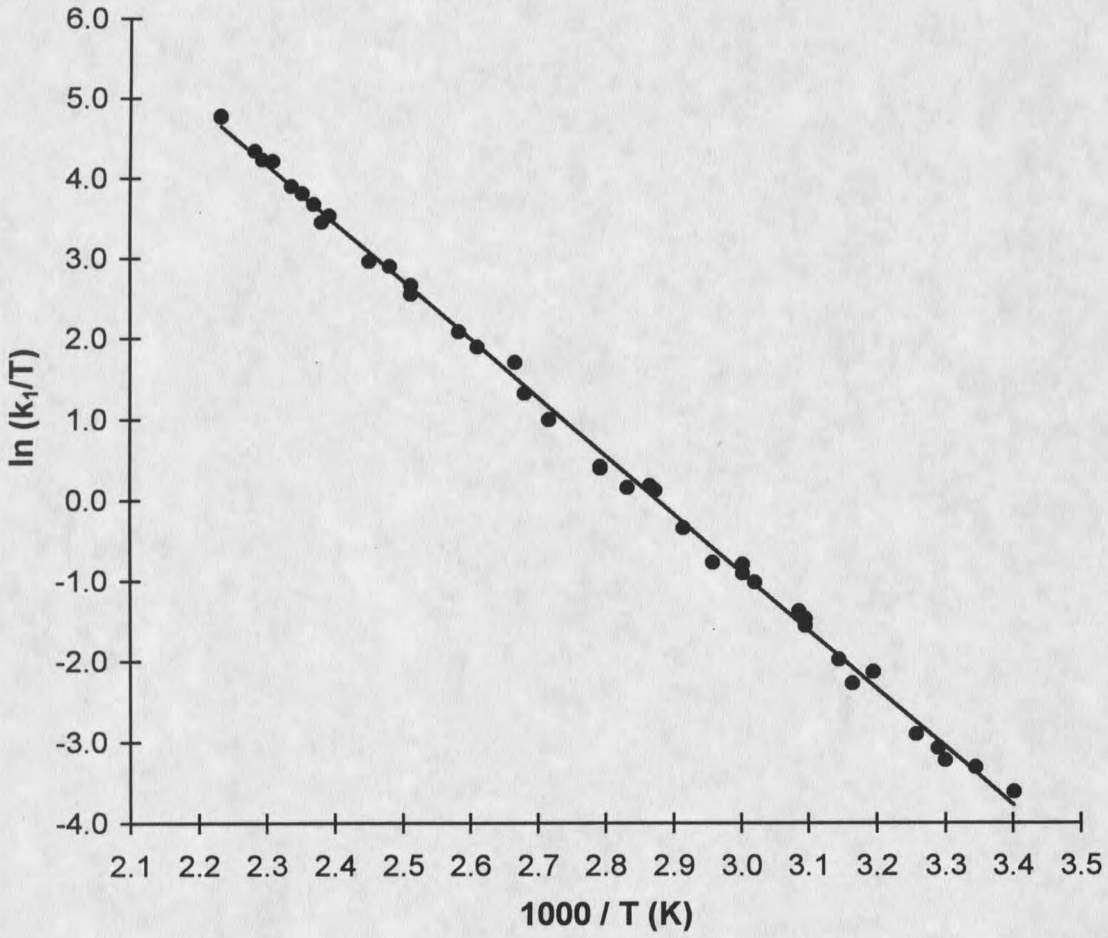

Figure 36. First-order rate constant, k_1', for conversion of the thermal energy ion complex, Cl^-(*i*-PrBr), to Br^--containing products determined from the present IM-MS measurements at atmospheric pressure over the temperature range 20 - 175 °C.

continuous state of thermal equilibrium with the medium ($k_1/T = (k/h) \exp(\Delta S^{\ddagger}/R) \exp(-\Delta H^{\ddagger}/RT)$, where $\Delta S^{\ddagger}$ and $\Delta H^{\ddagger}$ are the entropy and enthalpy of activation (143). From the slope of this line, $\Delta H^{\ddagger} = 14.3$ kcal mol^{-1} and $\Delta S^{\ddagger} = -5.8$ cal mol^{-1} K^{-1} are deduced for the unimolecular decomposition of the thermal energy ion complex to form Br^--containing product ions. The combination of this $\Delta H^{\ddagger}$ measurement with the measurements of the enthalpy of clustering equilibria reported in Table 6 allows the potential energy surface shown in Figure 37 to be constructed. The energy of the products indicated in this figure have been calculated from the known electron affinities of the chlorine (83.4 kcal mol^{-1} (144)) and bromine (77.6 kcal mol^{-1} (144)) atoms and the known C-Cl and C-Br bond energies of *i*-PrCl (81 kcal mol^{-1} (145)) and *i*-PrBr (68 kcal mol^{-1} (145)) while assuming that all C-H and C-C bonds within *i*-PrCl and *i*-PrBr are the same. From the present IMS measurements, it is therefore concluded that the energy of the S_N2 transition state for the reaction of chloride with isopropylbromide lies about 2.4 kcal mol^{-1} above that of the reactants. Corresponding IM-MS measurements made previously in our laboratory for the reactions of chloride ion with methyl bromide, ethyl bromide, and n-butyl bromide placed the S_N2 transition states for those reactions at 2.2, 0.0, and 1.3 kcal mol^{-1}, respectively, below the energies of the reactants. The higher transition state energy observed here for the reaction of chloride ion with isopropyl bromide can be attributed to increased steric hindrance to backside attack for this secondary alkyl bromide.

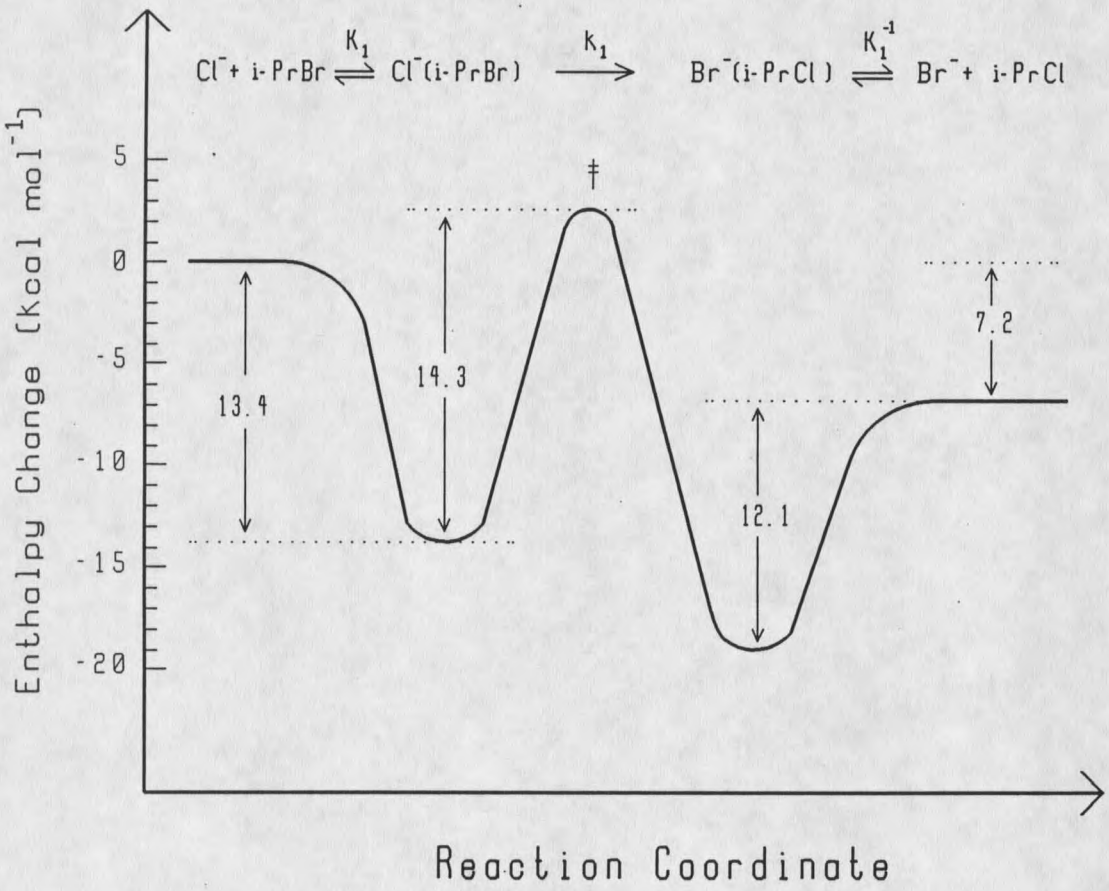

Figure 37. Principle energy changes along the Cl^-/*i*-PrBr reaction coordinate. The first three magnitudes indicated in the figure have been determined here by IM-MS measurements of rate constants, k_1, and equilibrium constants, $K_{eq,1}$. These measurements place the S_N2 transition state for this reaction at 2.4 kcal mol^{-1} above the energy of the reactants. The enthalpy of the final products has been calculated from known thermochemical data.

Conclusions

In this study, the relatively complex nucleophilic S_N2 displacement reaction of chloride with isopropylbromide has been studied in nitrogen buffer gas at 640 Torr between 20 and 185 °C by ion mobility - mass spectrometry. Under the conditions existing within the IM-MS, a prior clustering reaction between the two reactants occurs sufficiently rapidly that a state near that of the true clustering equilibrium condition is continuously maintained. This allows the energetics of this process to be accurately characterized while a slower S_N2 displacement reaction is simultaneously occurring. As a result, both processes can be quantitatively characterized from reaction-modified IM-MS spectra. Analysis of the present IMS results are greatly facilitated by the fact that reaction intermediates, as well as reactants, tend to be maintained in a state of physical equilibrium with the buffer gas medium when unusually high buffer gas pressures are used.

It has been shown that under these conditions the S_N2 nucleophilic displacement reaction probably occurs by the following distinctly two-step mechanism

$$Cl^- + i-PrBr \underset{}{\overset{K_{eq,1}}{\rightleftharpoons}} Cl^-(i-PrBr) \overset{k_1}{\rightleftharpoons} Br^- + i-PrCl \qquad (57)$$

in which a thermalized ion complex, $Cl^-(i\text{-PrBr})$, is maintained in a state of chemical equilibrium with the reactants. An S_N2 displacement reaction then occurs within the cluster ion by its unimolecular decomposition to Br^--containing product ions. By measurements of the

associated equilibrium constants, $K_{eq,1}$, and rate constants, k_1, as a function of temperature, the enthalpy changes associated with each of the two steps have been determined and place the energy of the S_N2 transition state for this reaction at 2.4 kcal mol^{-1} above that of the reactants.

The experimental method demonstrated here for the study of gas phase ion-molecule reactions is made additionally significant by recent theoretical treatments of gas phase S_N2 displacement reactions in which the association complexes resulting from the attachment of chloride ion to methyl chloride (33) and to methyl bromide (31) were predicted to behave in very complex and distinctly non-statistical manners. Such behavior would greatly complicate all attempts to interpret rate constants for ion-molecule reactions of this type if the rate constants were measured under conditions of relatively low pressure where the association complexes are isolated during their lifetimes. Therefore, techniques such as described here, where very high buffer gas pressure causes all reaction intermediates to be brought into a state of thermal equilibrium with the medium, might provide the only means of obtaining macroscopic rate constants that can be reliably interpreted in terms of the potential energy surfaces for dynamically complex ion-molecule reactions of this type.

SUMMARY

Despite the rapid instrumental and theoretical advances taking place within the gas phase ion chemistry community in the past three decades, very little attention has been devoted to the development of instrumental methods operating under conditions of very high buffer gas pressure. This is understandable in terms of the instrumental difficulties encountered at these pressures. However, this lack of resource is becoming more of a liability as theoretical and analytical techniques progress and as the limitations of low pressure instrumental methods become evident. In response to this need, a hyphenated analytical method, IM-MS, composed of Ion Mobility Spectrometry (IMS) and Mass Spectrometry (MS) has been developed that is designed to operate between 300 and 1100 Torr buffer gas pressure. The expanded utility of this instrument has been demonstrated by measuring the rate constants for thermal electron detachment from azulene$^-$ and for the reaction of Cl^- with CH_3Br as a function of pressure and by characterizing the reaction coordinate for the reaction of Cl^- with *i*-PrBr.

The first of these investigations was intended not only to demonstrate the utility of IM-MS in the area of unimolecular applications, but also to investigate recent observations of an apparent pressure dependence in the unimolecular thermal electron detachment (TED) reaction of the azulene anion (Az^-). This reaction has been studied extensively over the past three decades to obtain electron attachment rate constants and also to determine the electron affinity (EA) of azulene, whereas only two measurements have been made of the TED rate constant of Az^-. These experiments by Kebarle et al. (47) using a pulsed high pressure mass spectrometer (PHPMS) and by Mock et al. (46) using a photo-detachment modulated electron capture

detector (PDM-ECD), resulted in the measurement of two very different TED rate constants. The experiment utilizing PHPMS resulted in TED rate constants some three times greater than those measured using the PDM-ECD. The most significant difference in these two methods, and to which the difference in TED rate constants can likely be attributed, is the pressure range within which they operate. The PHPMS operates between 2 and 5 Torr pressure (CH_4) while the PDM-ECD operates between 1 and 2 atmospheres pressure (N_2). This difference in rate constants as a function of pressure motivated the use of IM-MS to investigate the thermal electron detachment of Az^-. Rate constants for the TED of Az^- were measured using IM-MS over the pressure range 300 to 1100 Torr and over the temperature range 82 to 174 °C. These rate constants were about midway between those measured using the PHPMS and the PDM-ECD. It was suggested in the discussion of these results that the likely cause for the reduced rates of thermal electron detachment at higher pressures was the formation of $Az^-(x)$ adducts, where x is a buffer gas species. Ions attributed to the Az_2^- dimer were detected in the study of Az^- TED using IM-MS, but conclusive evidence of the $Az^-(N_2)$ adduct was not obtained. While these measurements provided additional evidence for the existence of a negative pressure dependence for the TED reactions of Az^-, and that this might be due to adduct formation, conclusive evidence to support this assumption has yet to be obtained. Further work using IM-MS involving extensive mass spectrometric investigations as a function of pressure could help resolve this issue.

The second application of IM-MS was designed to utilize its VHP operating capabilities to investigate theoretical predictions and experimental observations regarding the

rate of reaction of Cl^- with CH_3Br as a function of pressure. Predictions by a number of ion-molecule reaction rate theoreticians indicated that reactions of this type, involving halide substitutions with small alkyl halides, probably are not amenable to treatment using statistical reaction rate theories. Wang et al. (31) has predicted very short lifetimes (less than 3 ps) of these reaction intermediates due to barriers to energy randomization. Lifetimes of this duration are less than one-tenth of the time between buffer gas collisions at atmospheric pressure which implies that thermalization of these intermediates is not likely even at this very high pressure. Also, measurements by various workers using low pressure methods resulted in discrepancies with statistical reaction rate predictions. Viggiano et al. (38) measured rates of reaction vs reactant internal energy and found non-statistical behavior while Graul and Bowers (36) found translationally cold products of reaction which also indicated non-statistical behavior. In order for the kinetics of these types of S_N2 reactions to be unambiguously interpreted in terms of their potential energy surfaces, thermalization of these reaction intermediates is necessary. Methods operating at VHP, such as IM-MS, provide the tools to investigate whether or not a reaction is at, or nearing its, HPL of kinetic behavior. The investigation of the Cl^-/CH_3Br system using IM-MS indicated that it is not yet in its HPL of kinetic behavior. However, the observed changes in rate as a function of pressure imply that the reaction system is moving towards this HPL and that pressures in excess of 1100 Torr are needed to reach this limit.

The third application of IM-MS reported in this thesis work was the investigation of the slow S_N2 reaction of Cl^- with *i*-PrBr. Previous investigations using IM-MS revealed ion mobility waveforms that were distinctly different in form than those recorded for faster

reactions such as Cl^- with methyl, ethyl, or n-propyl halides. The difference in waveforms was due to the apparent dependence of the ionic mobility (drift time) of the reactant and product ions on the extent of reaction at low temperatures; these changes in mobility were not observed in the other reactions mentioned. Mass spectrometric investigations, and consideration of possible reaction mechanisms, led to the conclusion that the increase in drift time (decrease in ion mobility) was due to the formation of a relatively long-lived reaction intermediate, Cl^-(*i*-PrBr), in equilibrium with the reactants. The fast forward and reverse reactions of this intermediate with reactants at equilibrium, relative to transport through the drift tube, increased the observed drift time of the Cl^- reactants in proportion to its occurrence as a reaction intermediate. Relating the observed change in drift time (relative to the unclustered Cl^- ion) to neutral *i*-PrBr concentration made it possible to determine the equilibrium constant for this clustering reaction. Repeating this procedure over a range of temperature led to the determination of the enthalpy of association of Cl^- with *i*-PrBr and thus to the experimental determination of the depth of the entrance channel in its reaction coordinate diagram. The same procedure applied to the reaction of Br^- with *i*-PrCl allowed the determination of the depth of the exit channel in the reaction coordinate.

Further characterization of this reaction coordinate diagram was possible by determination of the height of the central barrier, i.e. the transition state, by measuring the rate of reaction as a function of temperature. The usual methods of kinetic analysis using IM-MS were not applicable here due to the existence of the relatively high concentration of reaction intermediates. This meant that the reaction rate was controlled by the rate of unimolecular

dissociation of the entrance channel ion-complex (intermediate), rather than by the usual direct bi-molecular rate observed at higher temperatures and in low pressure instruments. Allowing for the equilibrium concentration of entrance channel complexes and measuring the change in area under the IM waveforms (progress of reaction) as a function of reaction time, rather than of neutral reagent (*i*-PrBr) concentration, allowed the kinetics of this reaction to be determined. The resulting activation energy determined from Arrhenius plots placed the height of the central barrier 2.4 kcal mol^{-1} above the reactants. With the calculation of the energy of the reactants and products, this investigation resulted in the characterization of the major points of the reaction coordinate for the reaction of Cl^- with i-PrBr. It was also revealed that the mechanism which is operative at higher buffer gas pressures, and especially at lower temperatures, is probably an indirect mechanism, proceeding through the dissociation of a thermalized reaction intermediate, rather than via a direct mechanism as in most fast bimolecular reactions.

The application of IM-MS to these investigations of unimolecular and bimolecular reactions has demonstrated the utility of IM-MS as a reliable method for investigating a wide range of IM reactions in the gas phase under conditions of very high pressure.

LITERATURE CITED

1. Bowers, M.T. Gas Phase Ion Chemistry; Academic: New York, **1979**; Vol. 1.

2. Bowers, M.T. Gas Phase Ion Chemistry; Academic: New York, **1979**; Vol. 2.

3. Bowers, M.T. Gas Phase Ion Chemistry; Academic: New York, **1979**; Vol. 3.

4. Adams, N.G.; Babcock, L.M. Advances in Gas Phase Ion Chemistry; JAI Press: London, **1996**; Vol. 1.

5. Adams, N.G.; Babcock, L.M. Advances in Gas Phase Ion Chemistry; JAI Press: London, **1996**; Vol. 2.

6. Collins, C.B.; Lee, F.W. J. Chem. Phys. **1978**, **68**, 1391.

7. Collins, C.B.; Lee, F.W. J. Chem. Phys. **1970**, **71**, 184.

8. Collins, C.B.; Lee, F.W. J. Chem. Phys. **1978**, **72**, 5381.

9. Gylys, V.T.; Jahani, H.R.; Collins, C.B.; Lee, F.W.; Pouvesle, J.M.; Stevefelt, J. J. Quantum Electron. **1986**, **22**, 47.

10. Giles, K.; Grimsrud, E.P. J. Phys. Chem. **1992**, **96**, 6680.

11. Giles, K.; Grimsrud, E.P. J. Phys. Chem. **1993**, **97**, 1318.

12. Knighton, W.B.; Bognar, J.A.; O'Connor, P.M.; Grimsrud, E.P. J. Am. Chem. Soc. **1993**, **115**, 12079.

13. Strode, K.S.; Grimsrud, E.P. Int. J. Mass Spectrom. Ion Proc. **1994**, **130**, 227.

14. Sahlstrom, K.E.; Grimsrud, E.P. J. Phys. Chem. **1997**, **101**, 1501.

15. Matsuoka, S.; Nakamura, H.; Tamura, T. J. Chem. Phys. **1981**, **75**, 681.

16. Matsuoka, S.; Nakamura, H.; Takaaike, T. J. Chem. Phys. **1983**, **79**, 825.

17. Matsuoka, S.; Nakamura, H. J. Chem. Phys. **1988**, **89**, 5663.

18. Matsuoka, S.; Ikesoe, Y. J. Phys. Chem. **1988**, **92**, 1126.

19. Ikezoe, Y.; Shimizu, S.; Onuki, K.; Matsuoka, S.; Makamura, H.; Tagawa, S.; Tabata, Y. J. Phys. Chem. **1989**, **93**, 1193.

20. Sahlstrom, K.E.; Grimsrud, E.P. J. Phys. Chem. **1997**, in print.

21. Carrol, D.I.; Dzidic, I.; Horning, E.C.; Stillwell, R.N. Appl. Spectros. Rev. **1981**, **17**, 337.

22. Eiceman, G.A.; Karpas, Z. Ion Mobility Spectrometry; CRC Press, Boca Raton, FL, **1994**.

23. Zlatkis, A.; Poole, C.F. Electron Capture, Theory and Practice in Chromatography; Elsevier, New York, **1986**.

24. Olmstead, W.M.; Brauman, J.I. J. Am. Chem. Soc. **1977**, **99**, 4219.

25. Forst, W. Theory of Unimolecular Reactions, Academic Press, New York, **1973**.

26. Laidler, W. Chemical Kinetics, Elsevier, New York, **1986**.

27. Pilling, M.J.; Smith, I.W.M, ed. Modern Gas Kinetics, Blackwell Scientific, London, **1987**.

28. Wladkowski, B.D.; Lim, K.F.; Allen, W.D.; Brauman, J.I. J. Am. Chem Soc. **1992**, **114**, 9136.

29. Moylan, C.R.; Brauman, J.I. Advances in Classical Trajectory Methods, Hase, W.L., ed., Vol. 2., JAI Press, Greenwich, CT, **1993**.

30. Vande Linde, S.R.; Hase, W.L. J. Am Chem Soc., **1989**, **111**, 2349.

31. Wang, H.; Peslherbe, G.H.; Hase, W.L. J. Am Chem Soc., **1994**, **116**, 9644.

32. Cho, Y.J.; Vande Linde, S.R.; Zhu, L.; Hase, W.L. J. Chem. Phys. **1992**, **96**, 8275.

33. Vande Linde, S.R.; Hase, W.L. J. Phys. Chem. **1990**, **94**, 6148.

34. Vande Linde, S.R.; Hase, W.L. J. Am Chem Soc., **1995**, **117**, 9347.

35. Basilevsky, M.V.; Ryaboy, V.M. Chem. Phys. Lett., **1986**, **129**, 71.

36. Graul, S.T.; Bowers, M.T. J. Am. Chem. Soc. **1991**, **113**, 9696.

37. Graul, S.T.; Bowers, M.T. J. Am. Chem. Soc. **1994**, **116**, 3875.

38. Viggiano, A.A.; Morris, R.A.; Paschkewitz, J.S; Paulson, J.F. J. Am. Chem. Soc. **1992**, **114**, 10477.

39. Speranza, M. Int. J. Mass Spec. Ion Proc. **1992**, **118/119**, 395

40. Bartmess, J.E. in *Ion Molecule Chemistry: The Roles of Intrinsic Structure, Solvation and Counterions*; Advances in Gas Phase Ion Chemistry; JAI Press: London, **1996**; Vol 2..

41. Sauer, J.; Sustman, R. Angew. Chem. Int. Ed. Engl. **1980**, **19**, 779.

42. McIver, R.T. Sci. Amer. **1981**, 186.

43. Bohme, D.K.; Raksit, A.B. Can. J. Chem. **1985**, **63**, 3007.

44. Hase, W.L.; Zhu, L.; Wang, H. J. Phys. Chem. **1994**, **98**, 1608.

45. Knighton, W.B.; Zook, D.R.; Grimsrud, E.P. Am. Soc. Mass Spec. **1990**, **1**, 372.

46. Mock. R.S.; Grimsrud, E.P. J. Am. Chem. Soc. **1989**, **111**, 2861.

47. Grimsrud, E.P.; Chowhury, S.; Kebarle, P. J. Chem. Phys. **1985**, **83**, 3983.

48. Eiceman, G.A.; Shoff, D.B.; Harden, C.S.; Snyder, A.P. Int. J. Mass Spec. Ion Proc. **1988**, **85**, 265.

49. Preston, J.M.; Rajadhyax, L. Anal. Chem. **1988**, **60**, 31.

50. Kemper, P.R.; Bowers, M.T. in *Ion Cyclotron Resonance Spectroscopy*; Techniques for the Study of Ion Molecule Reactions; Vol. XX in the Techniques of Chemistry Series, John Wiley & Sons: New York, **1988**; Vol 2.

51. Freiser, B.S. in *Fourier Transform Mass Spectrometry*; Techniques for the Study of Ion Molecule Reactions; Vol. XX in the Techniques of Chemistry Series, John Wiley & Sons: New York, **1988**; Vol 2.

52. Viggiano, A.; Masahiro, T.; Matsuoka, S.; Ikezoe, Y. Gas-Phase Ion-Molecuel Rate Constants Through 1986; Maruzen Company, Ltd., Tokyo, Japan, **1986**.

53. Dunbar, R.C.; J. Am. Chem. Soc. **1970**, **93**, 4354.

54. Dunbar, R.C.; Weddle, G.H. J. Chem. Phys. **1988**, **92**, 5706.

55. Bowers, M.T.; Kemper, P.R. J. Chem. Phys. **1986**, **90**, 477.

56. Bowers, M.T.; Kemper, P.R.; Jarold, M.F.; Redeker-Wagner, W. J. Chem. Phys. **1985**, **83**, 1121.

57. Brauman, J.I.; Craig, S.L.; Science **1997**, **276**, 1536.

58. Adams, N.G.; Smith, D. in *Flowing Afterglow and Sift;* Techniques for the Study of Ion Molecule Reactions; Vol. XX in the Techniques of Chemistry Series, John Wiley & Sons: New York, **1988**; Vol 2.

59. Adams, N.G.; Smith, D. Adv. At. Mol. Phys., **24**, 1988.

60. Adams, N.G.;. Smith, D.; in Ausloos, P., ed., Kinetics of Ion-Molecule Reactions, Plenum: New York, **1979**. pp. 345-376.

61. Barlow, S.E.; Van Doren, J.M.; Bierbaum, V.M.; J. Am. Chem. Soc. **1988**, **110**, 7240.

62. Viggiano, A.A.; Morris, R.A.; Dale, F.; Paulson, J.F.; Giles, K.; Smith, D. J. Chem. Phys. **1990**, **93**, 1149.

63. Kebarle, P. in *Pulsed Electron High Pressure Mass Spectrometer;* Techniques for the Study of Ion Molecule Reactions; Vol. XX in the Techniques of Chemistry Series, John Wiley & Sons: New York, **1988**; Vol 2.

64. Meot-ner, M; Field, F.H. J. Am. Chem. Soc. **1977**, **99**, 998.

65. Bohme, D.K.; Stone, J.A.; Mason, R.S.; Stradling, R.S.; Jennings, K.R. Int. J. Mass Spec. Ion Proc. **1981**, **37**, 283.

66. Stone, J.A.; Splinter, D.A.; Kong, S.Y.; Can. J. Chem. **1982**, **60**, 910.

67. Hiraoka, K.; Morise, K.; Shoda, T. Int. J. Mass Spec. Ion Proc. **1985**, **67**, 11.

68. Grimsrud, E.P.; Caldwell, G.; Chowdhury, S.; Kebarle, P. J. Am. Chem. Soc. **1985**, **107**, 4627.

69. Grimsrud, E.P. in *Gas Phase Ion Molecule Chemistry Under Conditions of Very High Pressure*; Advances in Gas Phase Ion Chemistry; JAI Press: London, **1996**; Vol 2., pp 236.

70. Cacace, F. Science, **1990**, **250**, 392.

71. Speranza, M. Mass Spec. Rev., **1992**, **11**, 73.

72. Lubman, D.M.; Kolaitis, L.; Huang, S. Appl. Spec., **1987**, **41**, 1371.

73. Lawrence, A.H. Anal. Chem., **1986**, **58**, 1269.

74. Fox, D.L. Anal. Chem., **1991**, **63**, 292R.

75. Saferstein, R.; Brettell, T.A. Analy. Chem., **1991**, **63**, 148R.

76. Lawrence, A.H. Anal. Chem., **1989**, **61**, 343.

77. Tou, J.C.; Boggs, G.U. Anal. Chem., **1976**, **48**, 1351.

78. Eiceman, G.A.; Leasure, C.S.; Vandiver, V.J. Anal. Chem., **1986**, **58**, 76.

79. Clement, R.E.; Langhorst, M.L.; Eiceman, G.A. Anal. Chem., **1991**, **56**, 270R.

80. Eiceman, G.A.; Blyth, D.A.; Shoff, D.B.; Snyder, A.P. Analy. Chem. **1990**, **62**, 1374.

81. Karasek, F.W. Anal. Chem., **1971**, **43**, 1982.

82. Karasek, F.W.; Denney, D.W. J. Chromat., **1974**, **93**, 141.

83. Ketkar, S.N.; Penn, S.M.; Fite, W.L. Anal. Chem., **1991**, **63**, 457.

84. Lawrence, A.H.; Barbour, R.J.; Sutcliffe, R. Anal. Chem., **1991**, **63**, 1217.

85. Roehl, J.E. Appl. Spec. Rev., **1991**, **26**, 1.

86. Karasek, F..W.; Cohen, M.J. J. Chromat. Sci., **1970**, **8**, 330.

87. Hill, H.H. Jr.; Balm, M.A. Anal. Chem., **1982**, **54**, 38.

88. Hill, H.H. Jr.; Siems, W.F.; St. Louis, R.H. J. Chromat., **1989**, **479**, 221.

89. Chesler, S.N.; Cram, S.P. J. Chromat. Sci., **1973**, **11**, 391.

90. Hill, H.H. Jr.; Siems, W.F.; Shumate, C.B.; Kinzer, J.A.; McMinn, D.G. J. Microcol. Sep., **1990**, **2**, 188.

91. Widmer, H.M.; Morrissey, M.A. J. Chromat., **1991**, **552**, 551.

92. Hill, H.H. Jr.; Siems, W.F.; St. Louis, R.H. J. Microcol. Sep., **1990**, **2**, 138.

93. Eiceman, G.A.; Vandiver, V.J.; Leasure, C.S.; Anderson, G.K.; Tiee, J.J.; Danen, W.C. Anal. Chem., **1986**, **58**, 1690.

94. Gormally, J.; Phillips, J. Int. J. Mass Spec. Ion Proc., **1992**, **112**, 205.

95. Gormally, J.; Phillips, J. Int. J. Mass Spec. Ion Proc., **1991**, **107**, 441.

96. Hill, H.H. Jr.; Baim, M.A.; Eatherton, R.L. Anal. Chem., **1983**, **55**, 1761.

97. Eiceman, G.A.; Leasure, C.S.; Anderson, G.K.; Fleischer, M.E. Anal. Chem., **1986**, **58**, 2142.

98. Foulger, B.E.; corbin, R.; Begley, P.; Simmonds, P.G. J. Chromat., **1991**, **588**, 239.

99. Carrico, J.P.; Sickenberger, D.W.; Spangler, G.E.; Vora, K.N. J. Phys. B: Sci. Instrum., **1983**, **16**, 1058.

100. Roehl, J.E. Optical Engineering, **1985**, **24**, 985.

101. Carrico, J.P.; Roehl, J.E.; Spangler, G.E.; Davis, A.W.; Sima, G.R.; Vora, K.N.; White, R.J. American Laboratory, **1986**, **2**, 154.

102. Carrico, J.P.; Spangler, G.E.; Vora, K.N. J. Phys. B: Sci. Instrum., **1986**, **19**, 191.

103. Spangler, G.E.; Cohen, M.J. Plasma Chromatography, Plennum Press: New York, **1984**.

104. Hill, H.H. Jr.; Siems, W.F.; St. Louis, R.H.; McMinn, D.G. Anal. Chem., **1990**, **62**, 1201A.

105. Carrico, J.P.; Spangler, G.E.; Vora, K.N.: Cambell, D.N. ISA Transactions, **1984**, **23**, 17.

106. Keller, R.A.; Metro, M.M. Separation Science, **1974**, **9**, 521.

107. Carr, T. Anal. Chem., **1979**, **51**, 705.

108. Todd, J.F.J.; Proctor, C.J. Analy. Chem., **1984**, **56**, 1794.

109. Horning, E.C.; Stillwell, R.N.; Dzidic, I.; Carroll, D.I Anal. Chem., **1975**, **47**, 1956.

110. Spangler, G.E.; Collins, C.I. Anal. Chem., **1975**, **47**, 393.

111. Revercomb, H.E.; Mason, E.A. Anal. Chem., **1975**, **47**, 970.

112. Bevington, P.R. Data Reduction and Error Analysis for the Physical Sciences, McGraw Hill, New York, **1969**.

113. Skoog, D.A.; West, D.M. Fundamentals of Analytical Chemistry., Saunders College Publishing, New York, **1982**.

114. Kebarle, P.; Chowdhury, S.; Chem. Rev., **1987**, **87**, 513.

115. Kebarle, P.; Chowdhury, S.; Heines, T.; Grimsrud, E.P. J. Phys. Chem., **1986**, **90**, 2747.

116. Kebarle, P.; Chowdhury, S.; Caldwell, G.; Grimsrud, E.P. J. Am. Chem. Soc., **1985**, **107**, 4629.

117. Briegleb, G. Angew. Chem. internat. Edit., **1964**, **3**, 617.

118. Christophorou, L.G. Adv. Elect. Electron. Phys., **1978**, **46**, 55.

119. Foldiak, G.; Wojnarovits, L. J. Chromat., **1981**, **206**, 511.

120. Pack, J.L.; Phelps, A.V.; J. Chem. Phys., **1966**, **44**, 1870.

121. Christophorou, L.G.; Chaney, E.L.; Collins, P.M.; Carter, J.G. J. Chem. Phys., **1970**, **52**, 4413.

122. Scott, L.T. J. Org. Chem., **1984**, **49**, 3021.

123. Tanaka, K.; Mackay, G.I.; Payzant, J.D.; Bohmé, D.K. Can. J. Chem., **1976**, **54**, 1643.

124. Caldwell, G.; Magnera, T.F.; Kebarle, P. J. Am. Chem. Soc., **1984**, **106**, 959.

125. Ingeman, S.; Nibbering, N.M.M. Can. J. Chem., **1984**, **62**, 2273.

126. Depuy, C.H.; Gronert, S.; Mullin, A.; Bierbaum, V.M. J. Am. Chem. Soc., **1990**, **112**, 8650.

127. Viggiano, A.A.; Morris, R.A.; Paschkewitz, J.S; Paulson, J.F. J. Am. Chem. Soc. **1991**, **113**, 9404.

128. Cyr, D.; Posey, L.A.; Bishea, G.A.; Han, C.C.; Johnson, M.A. J. Am. Chem. Soc., **1991**, **113**, 9697.

129. Depuy, C.H.; Gronert, S.; Bierbaum, V.M. J. Am. Chem. Soc., **1991**, **113**, 4009.

130. Wang, H.; Hase, W.L. J. Am. Chem. Soc., **1995**, **117**, 9347.

131. Seeley, J.V.; Morris, R.A.; Viggiano, A.A.; Wang, H.; Hase, W.L. J. Am. Chem. Soc. **1997**, in press.

132. Ahmed, M.S.; Dunbar, R.C. J. Am. Chem. Soc. **1987**, **109**, 3215.

133. Cace, F.; Acc. Chem. Res. **1988**, **21**, 215.

134. Henchman, M.; Paulson, J.F.; Hierl, P.M. J. Am. Chem. Soc. **1983**, **105**, 5509.

135. Henchman, M.; Paulson, J.F.; Hierl, P.M.; Viggiano, A.A.; Ahrens, A. J. Am. Chem. Soc. **1986**, **108**, 3142.

136. Henchman, M.; Paulson, J.F.; Hierl, P.M. Adv. Chem. Ser., **1987**, **215**, 83.

137. Kebarel, P. Annu. rev. Phys. Chem., **1977**, **28**, 445.

138. Dean, J.A. Langes's handbook of Chemistry, McGraw-Hill: New York, **1992**, p 6.5.

139. Yamdagni, R.; Kebarle, P. Can. J. Chem., **1977**, **52**, 2449.

140. Knighton, W.B.; Grimsrud, E.P. J. Am. Chem. Soc., **1992**, **114**, 2336.

141. Knighton, W.B.; Bognar, J. A.; Grimsrud, E.P. J. Mass Spectrom., **1995**, **30**, 557.

142. Laidler, K.J. Chemical Kinetics, McGraw-Hill: New York, **1965**; p 24.

143. Laidler, K.J. Chemical Kinetics, McGraw-Hill: New York, **1965**; p 123.

144. Weast, R.C.; Astle, M.J.; Beyer, W.H.; CRC Handbook of Chemistry and Physics, CRC Press: Boca Raton, FL, **1988**; p F-198.

145. Weast, R.C.; Astle, M.J.; Beyer, W.H.; CRC Handbook of Chemistry and Physics, CRC Press: Boca Raton, FL, **1988**; p E-64.

146. Dougherty, R.C. Org. Mass Spectrom., **1974**, **8**, 85.